

AD-A121 437

HIGH TEMPERATURE STRENGTH CHARACTERIZATION OF SINTERED
ALPHA SILICON CARBIDE(U) FORD MOTOR CO DEARBORN MI
CERAMIC MATERIALS DEPT R K GOVILA OCT 82

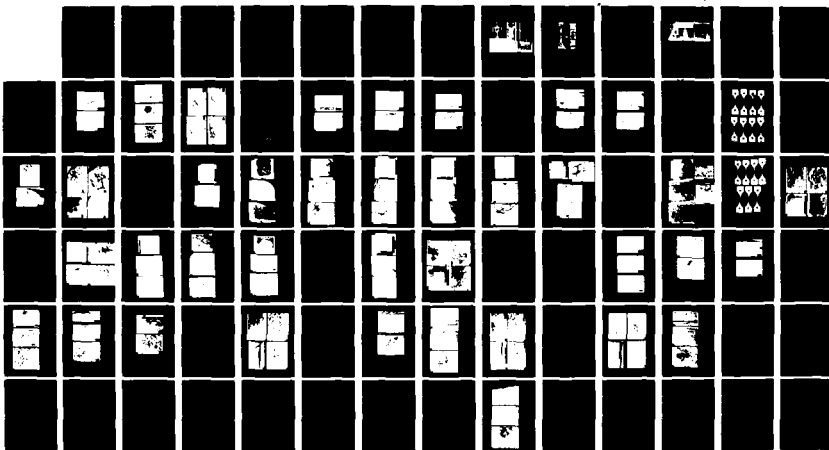
171

UNCLASSIFIED

AMRC-TR-82-51 DRAG46-77-C-0028

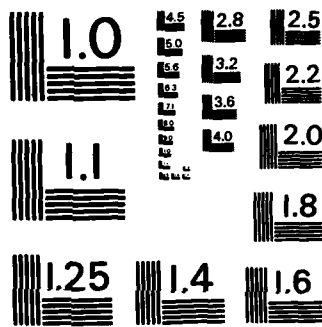
F/G 11/2

NL



END

FILED
BY
DTIC



MICROCOPY RESOLUTION TEST CHART
NATIONAL BUREAU OF STANDARDS-1963-A

Abstract

Uniaxial tensile and flexural stress rupture testing of sintered α -SiC (Carborundum 1980 material) was carried out at 1200° to 1400°C in air at various applied stress levels and the corresponding times-to-failure were measured. Fractographic evidence from uniaxial tensile stress rupture testing at 1200°C revealed limited presence of slow crack growth associated with surface connected porosity failure sites. The extent of slow crack growth increased with increasing temperature and large regions of SCG were observed in tests made at 1300°C. These observations were supported by flexural stress rupture testing at 1300° and 1400°C. Slow crack growth is characterized primarily by intergranular crack propagation while fast fracture (brittle failure) occurs transgranularly. The uniaxial tensile stress rupture testing is much more sensitive in revealing the time-dependent crack growth behavior, especially at lower temperatures such as 1200°C in air, than flexural stress rupture testing.

DTIC
COPY
INSTRUMENT
2

ABSTRACT FOR	
NIS GRAAI	<input checked="" type="checkbox"/>
DTIC ID	<input type="checkbox"/>
DTIC NUMBER	<input type="checkbox"/>
DTIC TITLE	<input type="checkbox"/>

A

1. INTRODUCTION

Sintered α -SiC is currently being investigated for use as structural components for gas turbines and diesel engines. The primary reasons for its use in heat engines are good oxidation resistance and strength at high temperatures ($>1000^{\circ}\text{C}$), high thermal conductivity and possibly better creep resistance relative to other structural ceramics. In general, majority of nitride and carbide ceramics show the presence of sub-critical (slow) crack growth at temperatures of 1000°C and higher.

This study was undertaken primarily to investigate the reliability and durability of sintered α -SiC (Carborundum 1980 material), especially investigating the presence of slow crack growth at 1200°C and higher temperatures in air. Uniaxial tensile stress rupture tests have been carried out at 1200° and 1300°C in air. In addition, flexural stress rupture tests at 1300° and 1400°C , flexural strength tests as a function of temperature (20° to 1400°C) and limited tests of precracked (indentation induced flaw) specimens have been used to evaluate strength of this material. In another independent study, flexural stress rupture strength of this material (Carborundum α -SiC, 1978 and 1980 manufactured) has also been investigated in detail by Quinn^{1,2} and the data are included for comparison in this report.

2. EXPERIMENTAL PROCEDURES

(1) Material and Specimen Preparation

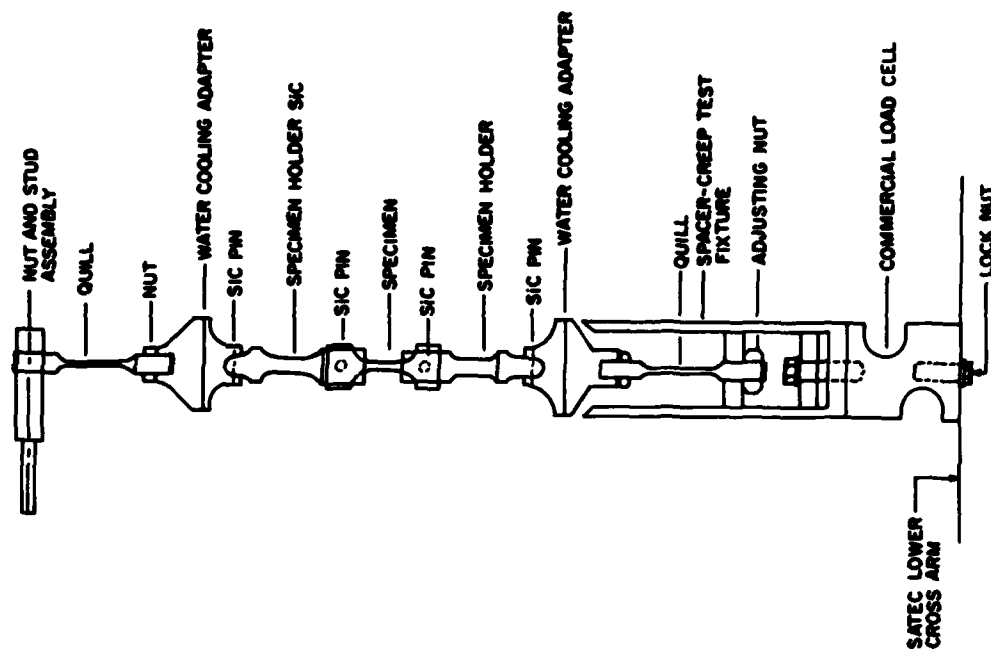
The material used in this study was sintered α -SiC obtained from Carborundum Company in February, 1980 in the form of 12 (twelve) square billets of dimensions 4" (102mm) x 4" (102mm) x 0.375" (9.5mm). The material was prepared by cold pressing α -SiC powder, followed by sintering at high temperatures, producing a dense (98% theoretical) material with equiaxed α -SiC grains with an average size of 7 to 10 microns. The material had extremely fine porosity distributed throughout the microstructure along the grain boundaries as shown in many micrographs later.

From the square billets of α -SiC, rectangular blanks of 4.5" x 1.25" x 0.125" (114mmx32mmx3mm) dimensions were machined diagonally. Each billet produced two blanks and as such a total of 20 rectangular blanks were machined for fabrication of tensile specimens. From the remaining material of the billets, MOR type bend bar specimens were fabricated. For flexural strength evaluation and flexural stress rupture testing, bend bar specimens of dimension (32mm long by 6mm wide by 3mm thick) were machined from these α -SiC billets. All faces were ground lengthwise using 220 grit diamond wheels and the edges chamfered lengthwise to prevent notch effects. Tensile stress rupture specimens were machined in a similar fashion as the bend bar specimens and had the same orientation. In addition, the two contoured sides of the uniaxial tensile test specimens were hand polished with diamond paste to give a smooth finish and thus rounded the edges as well. These specimens were randomly selected from different billets. Prior to testing, each tensile specimen was inspected visually (using optical microscope at 10X magnification), radiographed (X-rays) and examined with fluorescent dye penetrants to determine the presence of any machining (surface) damage. Specimens which did not display surface damage were used for testing.

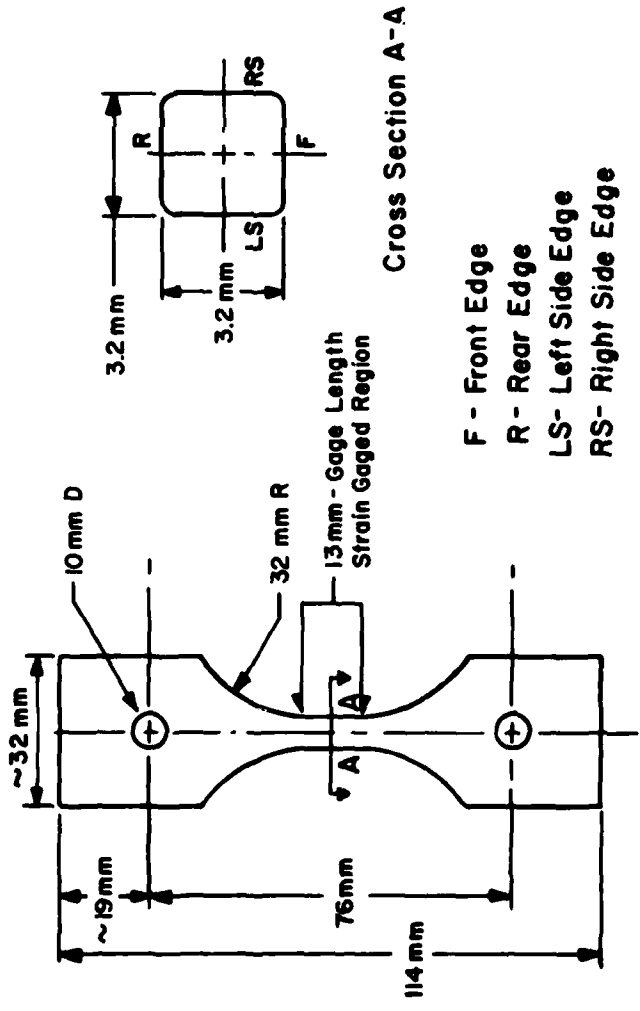
(2) Tensile Specimen Geometry and Load Train design

The tensile stress specimen consisted of a simple rectangular geometry with a narrow cross-section in gage length and large radii at the shoulders necessitated by the sensitivity of ceramic materials to stress concentrations. The specimen geometry and dimensions are shown schematically in Fig. 1(A). This geometry was selected rather than a circular cross-section to facilitate machining. In the gage length, the 90° corners were hand ground (with diamond paste) to a smooth curvature to minimize stress concentrations (as shown in cross-section A-A, Fig. 1(A)). The fracture face of the lower half of each broken specimen was examined metallographically and the edges of the fracture face were identified in a fashion shown in the cross-section A-A, Fig. 1(A). This procedure also helped in identifying whether the fracture initiation sites were random or preferential.

A standard creep testing machine (Satec Systems, Inc., Groove City, PA 16127) with a modified load train assembly was used for tensile stress rupture testing. The test specimen is retained in two slotted SiC holders by large SiC



(B)



(A)

Fig. 1 (A) Geometry and dimensions of tensile stress rupture specimen.
(B) Schematic of load train assembly for tensile stress rupture testing at high temperatures.

pins. The SiC holders are retained in water cooled metal adaptors which in turn are attached to the standard Satec machine head which includes crossed (90°) knife edges. The assembly procedure includes hanging the load train parts from the Satec machine head as influenced by gravity. At this point the lower Satec cross-arm is lowered to load the train in this position. The load train assembly is shown schematically in Fig. 1(B). A high temperature furnace capable of reaching 1400°C is mounted on the side of the Satec machine and encloses the full area between the water cooled metal adaptors, Fig. 2. The temperature is controlled and monitored separately with the use of two Pt - 13% Rh thermocouples placed behind the test specimen. Complete details regarding the load train instrumentation, continuous monitoring of applied stress, test temperature and time are given in an earlier study³ done on hot-pressed silicon nitride (NC-132 Si_3N_4).

Each test specimen contained a total of eight strain gages (two on each face in the gage-length area) which, for each test, were used for custom axial alignment to keep the bending stresses below 5% at full load. Initial alignment of the specimen is done at 20°C with full load. A typical specimen with strain gages attached in the gage section is shown in Fig. 3. After alignment at 20°C , the lead wires of the strain gages are cut and either the gages are left on the specimen to burn out at high temperatures or the strain gages are peeled off the specimen surface. During this time full load is maintained on the specimen.

(3) Flexural Strength and Stress Rupture Measurements

For flexural strength evaluation, all specimens were tested in four-point bending in an Instron machine (Model 1125) at a machine head speed of 0.5mm/min using a specially built self-aligning ceramic fixture³ made from hot-pressed SiC. The outer and inner knife-edges were 0.75" (19mm) and 0.375" (9.5mm) span, respectively. The high temperature bend tests were conducted in air in a furnace (CM Inc., High Temperature Furnaces, Bloomfield, N.J.) attached to the machine head of an Instron machine.

The flexural stress rupture tests at high temperatures (1200° to 1400°C) were also conducted in four-point bending using the aforesaid ceramic fixture and high temperature furnace. The load is applied on the test specimen through



Fig. 2 A partial view of the test set-up showing the furnace, strain-gaged specimen, strain indicator and lower part of the load train assembly.

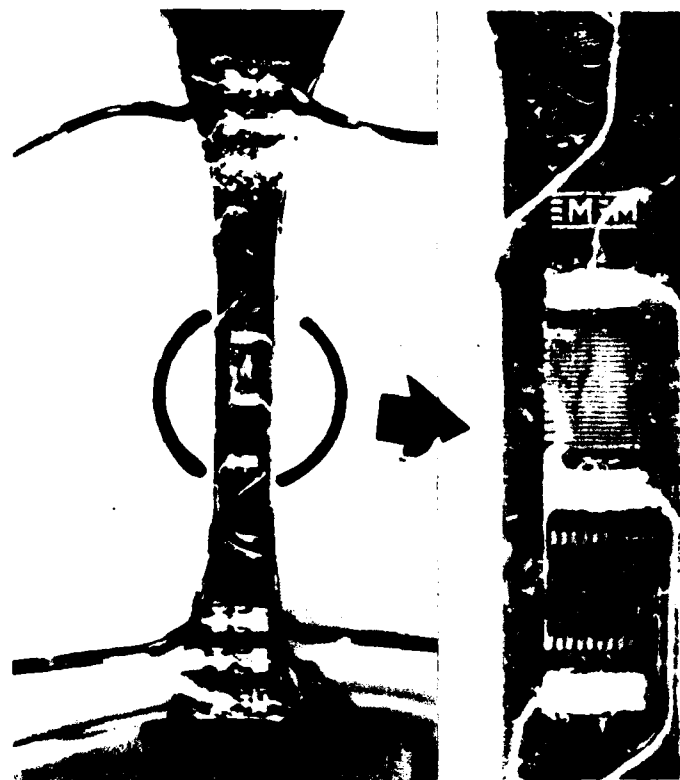


Fig. 3. Typical tensile stress rupture test specimen with strain gages attached to the gage length.

a cantilever arm dead-weight assembly. The experimental set-up is equipped with a microswitch to cut-off power supply to the furnace and the timer at the instant failure of the specimen occurs and the total time-to-failure is recorded through the timer in the power control unit. The temperature is allowed to stabilize for a minimum of 30 minutes before full load is applied to the test specimen. An overall view of the test set-up is shown in Fig. 4. Several tests were also conducted in a partial inert gas (Argon) environment. Argon gas was passed in the high temperature furnace chamber (150mm x 150mm x 200mm) at the rate of 10 CFH (cubic feet per hour) with a positive pressure. This method simply reduces oxidation effect to a lesser degree and does not eliminate completely.

(4) Bend Bar Precracked (Indentation Induced Flaw) Specimens

Several bend bar specimens were precracked using the Knoop indenter with varying loads to establish flexural strength as a function of flaw size (crack depth) and temperature. A limited number of stress-rupture tests and high temperature annealing effects ($\geq 1000^{\circ}\text{C}$) were also investigated using precracked specimens.

3. RESULTS AND DISCUSSION

Before tensile and flexural stress rupture tests can be carried out on sintered α -SiC, it was necessary to know the average flexural strength (4-point bending) and Weibull modulus at room temperature and further determine the inherent flaw size in the material.

3.1 Flexural Strength Vs. Temperature

A large number of bend bar specimens were tested in bending at room temperature (20°C) and the fracture strength data are given in Table 1. Assuming a two-parameter Weibull distribution to be representative of the test results, one can use a maximum likelihood estimator (MLE) method of statistical analysis to determine the Weibull modulus, m , and the characteristic (MOR) strength, σ_{θ} , using a Fortran computer program⁴. The characteristic (MOR) strength, σ_{θ} , refers to that value of fracture strength at which 63.2



Fig. 4 An overall view of the flexural stress rupture test set-up.

TABLE I. FLEXURAL (4-POINT BENDING) STRENGTH DATA FOR AS MACHINED SINTERED ALPHA SiC (CARBORUNDUM 1980) VS. TEMPERATURE

Specimen No.	Test Temp.	Fracture Stress (MPa)	Failure Origin
1	20°C	308	Failed in 3 pieces, porosity, Fig. 6.
2	"	315	" " "
3	"	306	" " "
4	"	371	Failed in 2 pieces, porosity.
5	"	347	Failed in 3 pieces, porosity, Fig. 7.
6	"	334	Failed in 4 pieces, porosity.
7	"	339	Failed in 3 pieces, porosity.
8	"	382	" " "
9	"	342	" " "
10	"	289	Failed in 2 pieces, multiple sites, Fig. 8.
11	"	360	Failed in 2 pieces, porosity.
12	"	390	" " "
13	"	314	" " "
14	"	379	" " "
15	"	306	" " "
16	800°C	312	Failed in 3 pieces, surface porosity.
17	"	343	" " , not visible.
18	1000°C	308	Failed in 2 pieces, surface porosity.
19	"	347	Failed in 4 pieces, " "
20	1200°C	328	Failed in 4 pieces, surface porosity.
21	"	343	Failed in 2 pieces, surface porosity, Fig. 10.
22	"	381	Failed in 4 pieces, not visible.
23	1300°C	305	Failed in 2 pieces, surface porosity, Fig. 11.
24	"	310	" " "
25	"	371	" " "
26	1400°C	310	Failed in 3 pieces, surface porosity, Fig. 12.
27	"	336	" " , Fig. 13.
28	"	410	Failed in 2 pieces, sub-surface porosity, Fig. 14.

All the above specimens were tested at a machine head speed of 0.5 mm/min. and failed in fast fracture mode.

percent of the population (specimens) will fail and the Weibull modulus, m , is a measure of shape and distribution of flaws in the material. The statistical variation in fracture strength (σ_F) (Weibull Probability Plot) at 20°C is shown in Fig. 5. A large scatter in σ_F is evident as indicated by a low value of Weibull modulus $m \approx 11$. The σ_F varied from a minimum of 289 MPa to a maximum of 390 MPa with a distribution mean of 337 MPa and a standard deviation of 37 MPa. Two types of porosity was observed in the bulk material on the fracture faces of specimens, Fig. 6; (i) Fine pores usually of the size 0.5 to $3\mu\text{m}$ distributed uniformly along the grain boundaries. (ii) Large pores usually of the size 20 to $80\mu\text{m}$. Majority of the failures showed surface related failure initiation sites as typically shown for test specimen #5 in Fig. 7, but occasionally sub-surface failure origins were also observed as seen later. Occasionally, multiple failure origins along the tensile edge of the fracture face (where maximum stress occurs) were also observed, Fig. 8. It is possible that the small pores in the material opened-up due to surface machining damage. In room temperature tests, all fracture faces showed a smooth appearance characteristic of fast fracture similar to cleavage of ionic single crystals and this type of failure is characterized by transgranular crack propagation.

Flexural strength was also evaluated at higher temperatures (800° to 1400°C) in order to determine if any plastic deformation accompanied the fracture process and if any of these flaws seen in fast fracture (20°C) grow slowly or subcritical (slow) crack growth (SCG) occurs. The data are given in Table I and the variation in fracture strength as a function of temperature is shown in Fig. 9. There is some scatter in the data but the fracture strength, σ_F , for as-machined specimens essentially remains constant and independent of temperature from 20° to 1400°C . The constancy of σ_F suggests that no change in fracture mechanism occurs and indicates the absence of plastic deformation and slow crack growth. This was confirmed by the appearance of the fracture surfaces at higher temperatures (1200° to 1400°C) similar to that observed at 20°C . Typical fracture surfaces in which failure origin was located at the tensile surfaces at 1200° , 1300° and 1400°C are shown in Figs. 10, 11, 12, respectively. Note the random distribution of fine porosity along the grain boundaries in the bulk material (Figs. 10(b), 11(b), 12(b)) and the fracture face appearances are similar to that observed at 20°C (cf. Figs. 10-12 and Figs. 6-8). Also, the failure origin sites in every case (especially true for fast fracture)

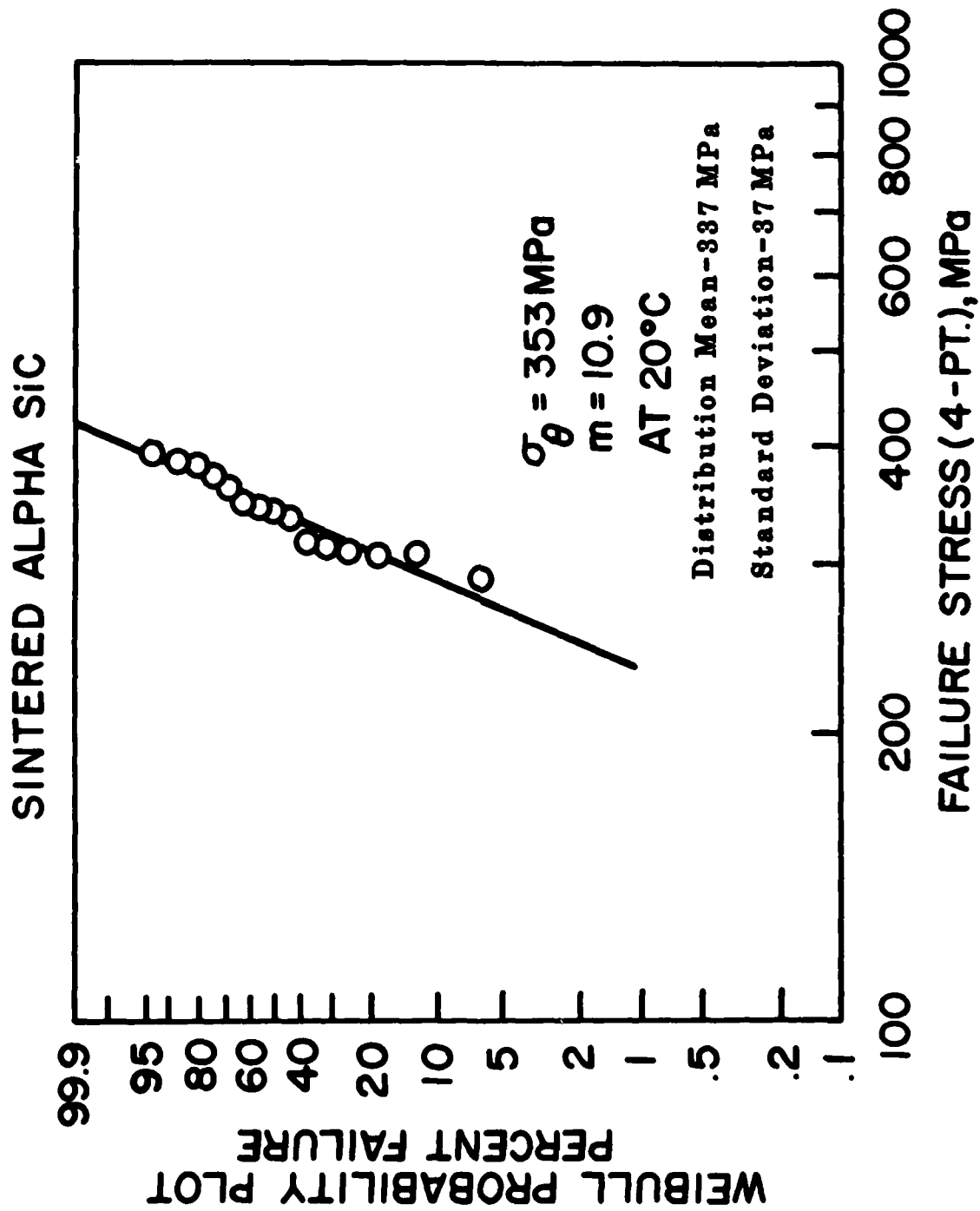


Fig. 5 Statistical variation in fracture strength.

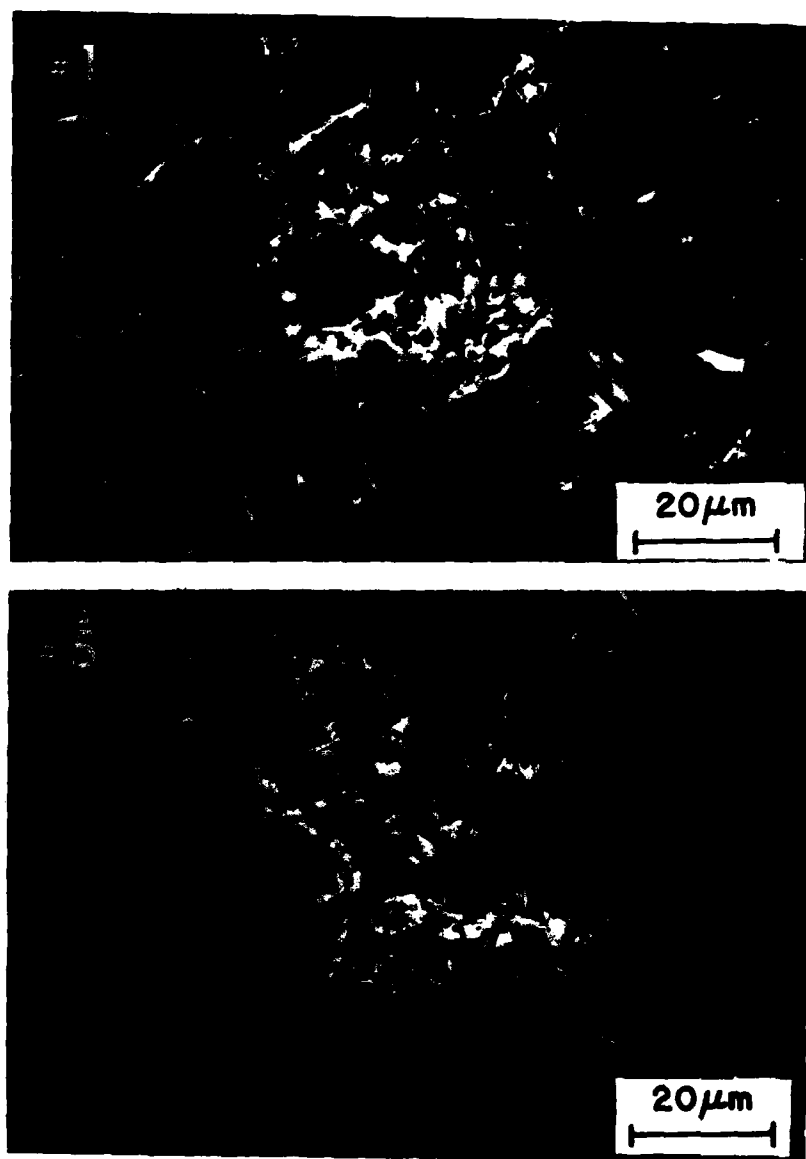


Fig. 6 Typical porosity as seen (in SEM) on the fracture faces of sintered α -SiC specimen (#1 and #5, Table I) tested in flexure at 20°C. Note the fine porosity usually of the size 0.3 to 3 μm distributed uniformly along the grain boundaries.

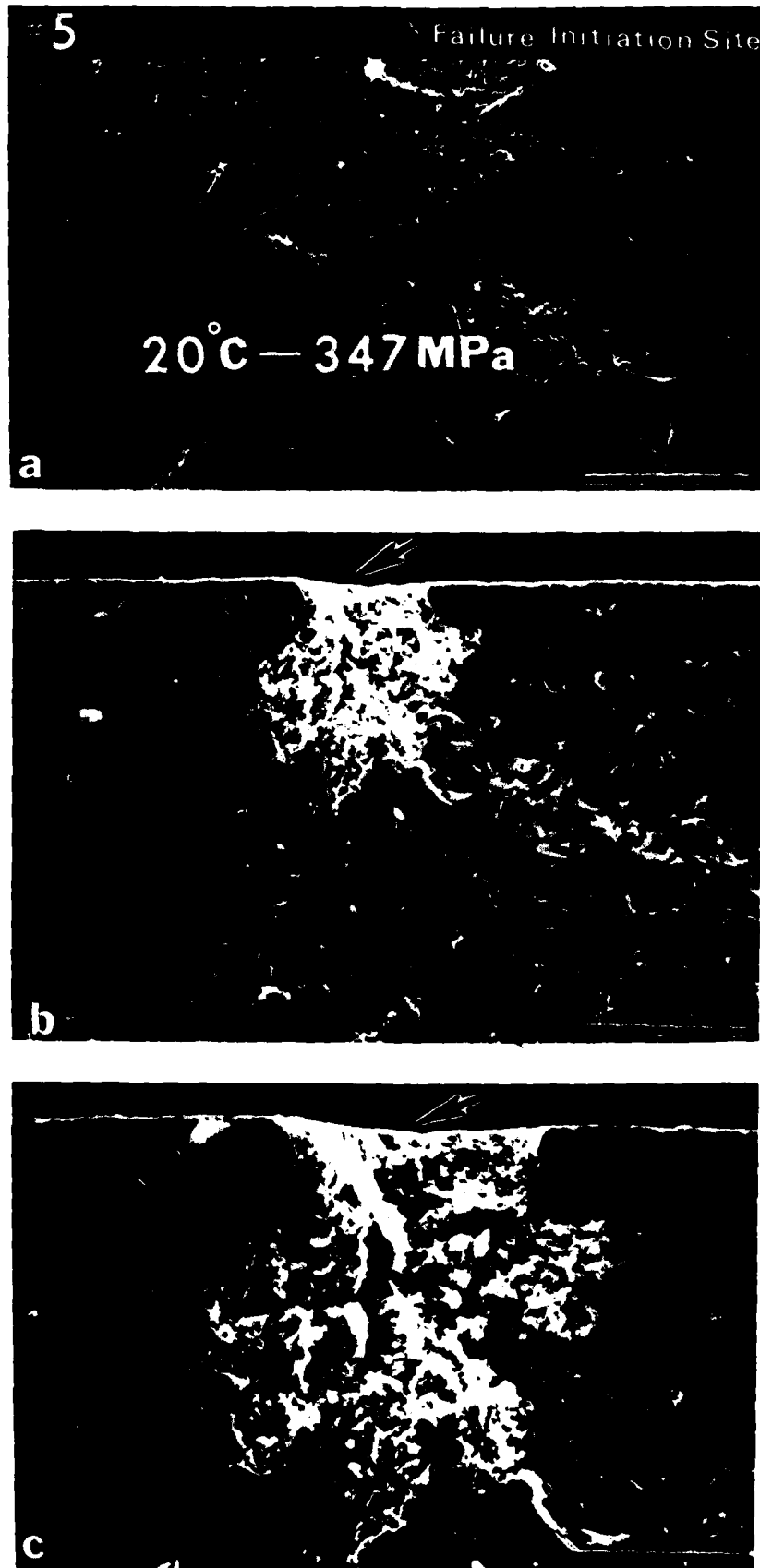


Fig. 7 Typical failure site (as seen in SEM) along the tensile edge of the sintered α -SiC specimen tested in 4-pt. bending.

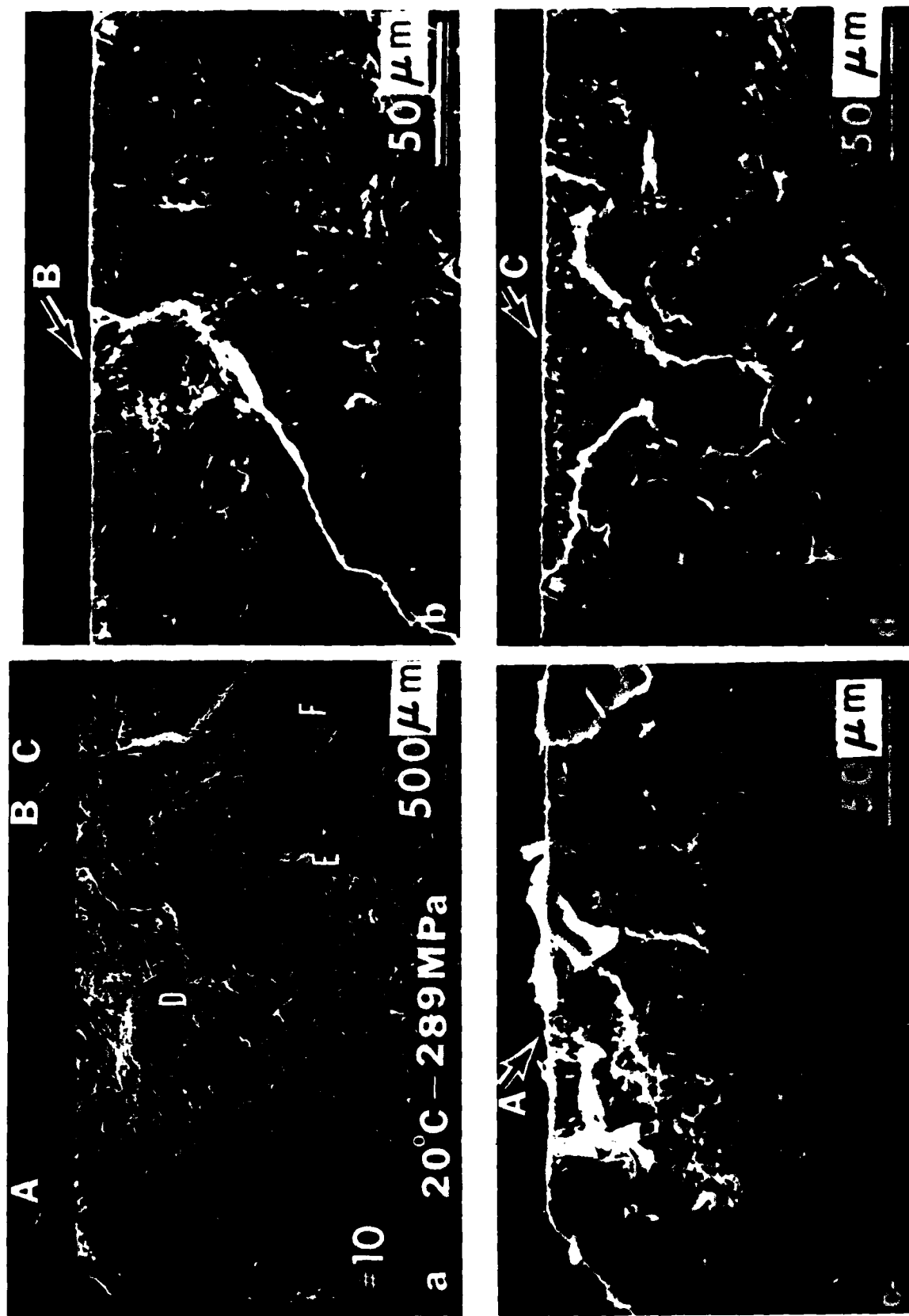
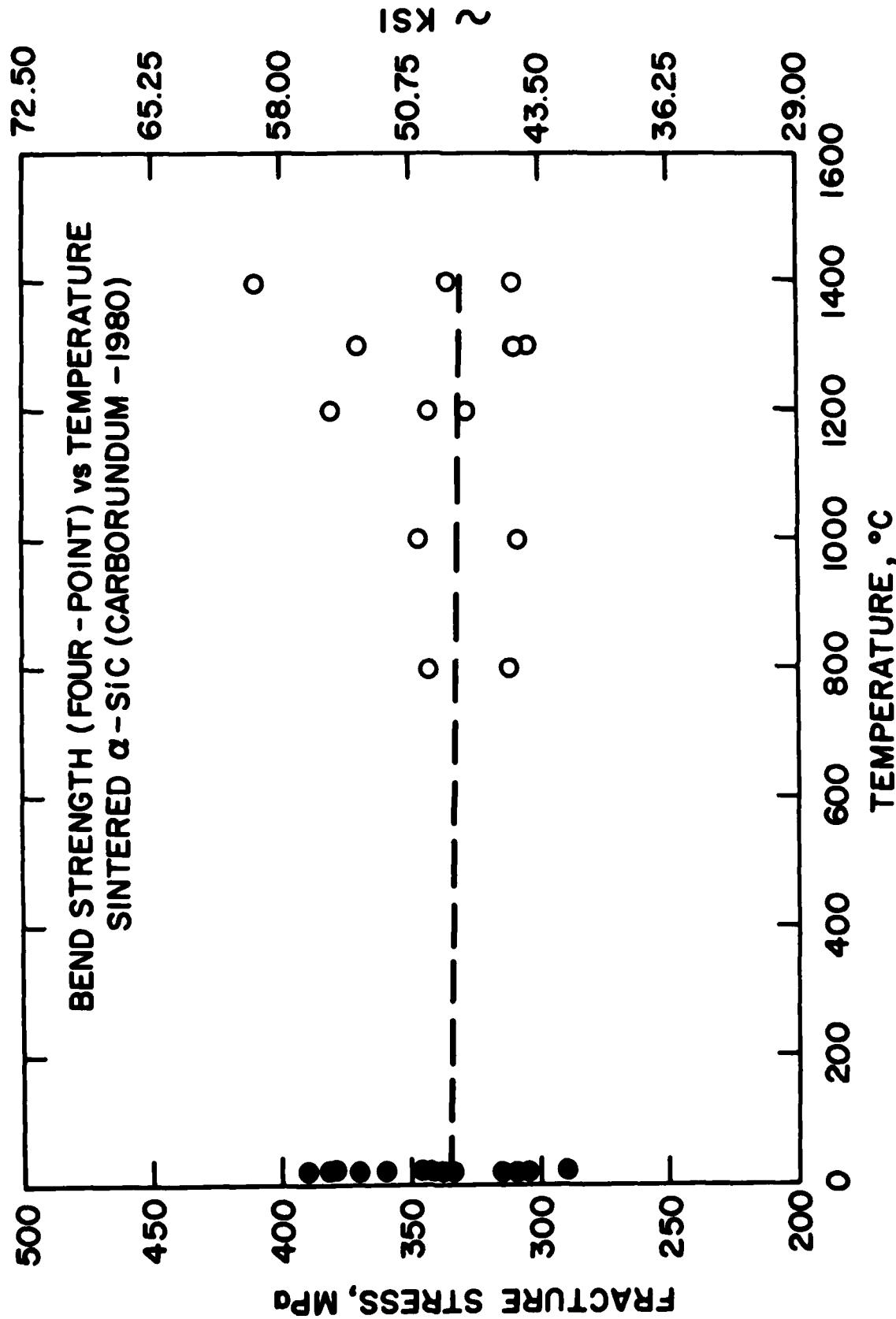


Fig. 8 Multiple failure sites (as seen in SEM) along the tensile edge of a α -SiC specimen tested in 4-pt. bending. (a) Failure sites along A,B, and C. Typical porosity at D,E and F. (b-d) Enlarged view of the failure sites along B, A and C.



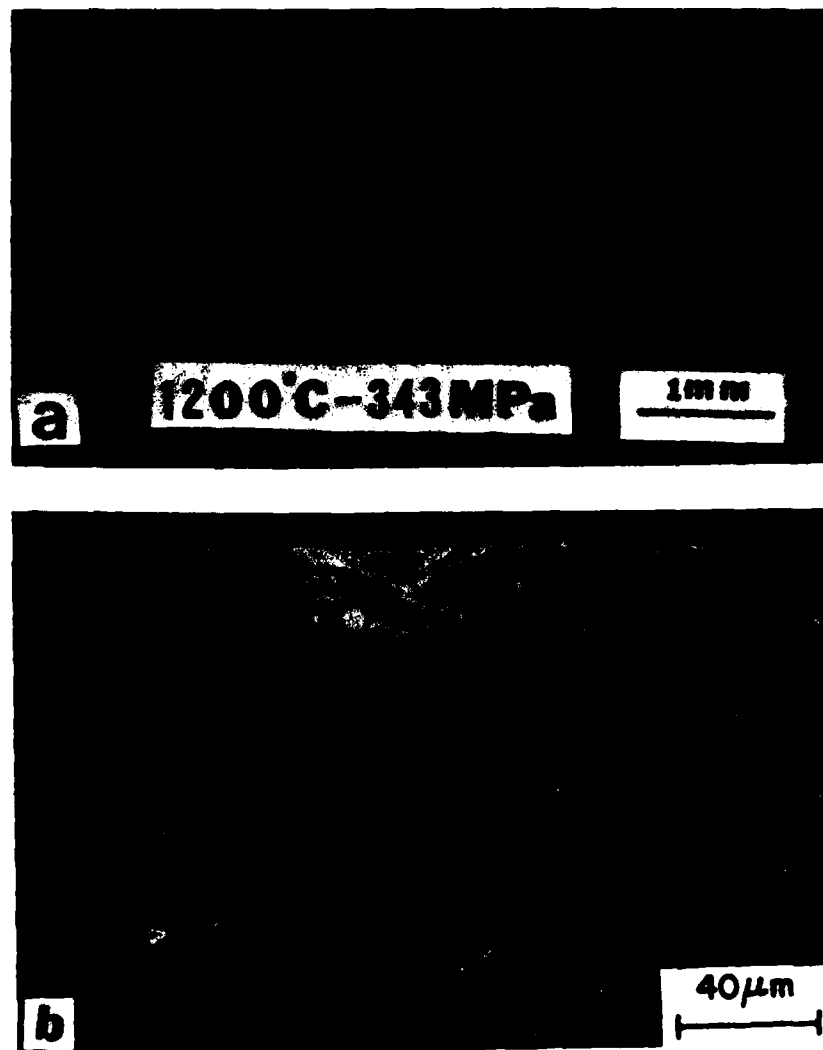


Fig. 10 SEM micrographs of the fracture surface of a specimen (sintered α -SiC) tested in 4-pt. bending at 1200°C in air showing surface associated failure site. Note the uniform distribution of fine porosity throughout the material.

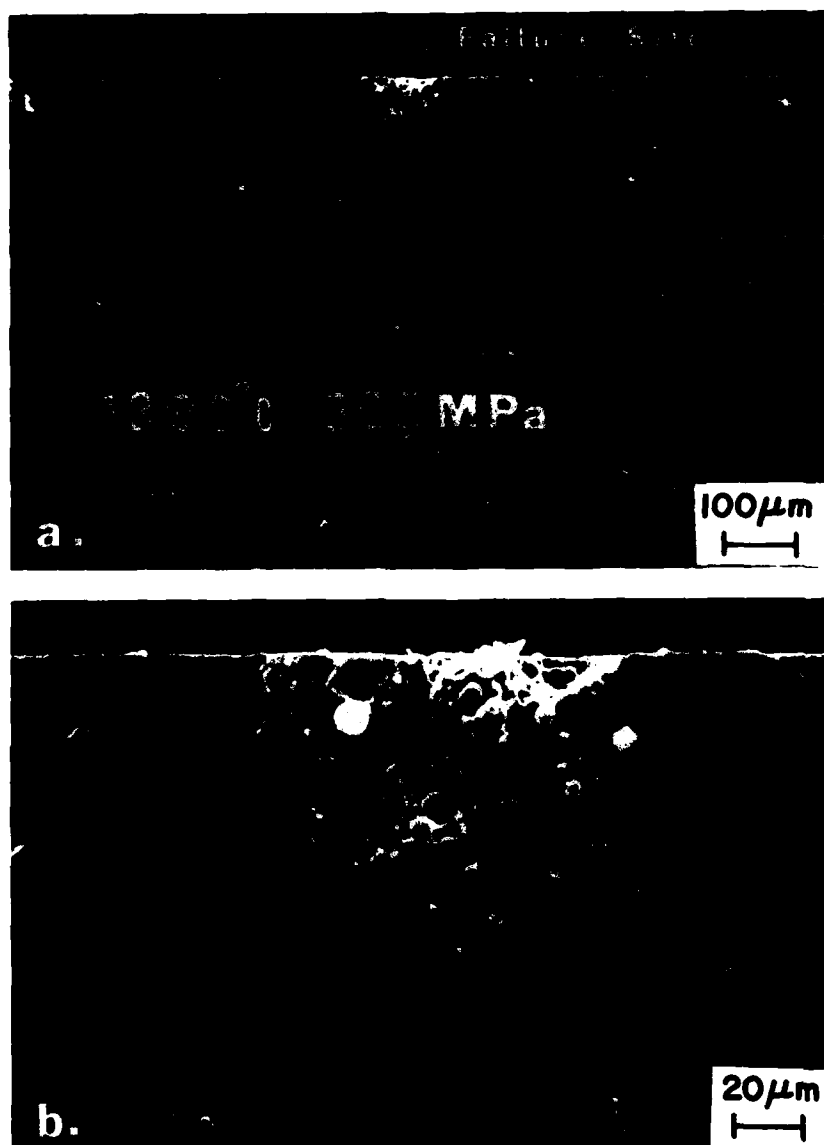


Fig. 11 SEM micrographs of the fracture surface of a specimen (sintered α -SiC) tested in 4-pt. bending at 1300°C in air showing surface associated failure site. Note the uniform distribution of fine porosity throughout the material.

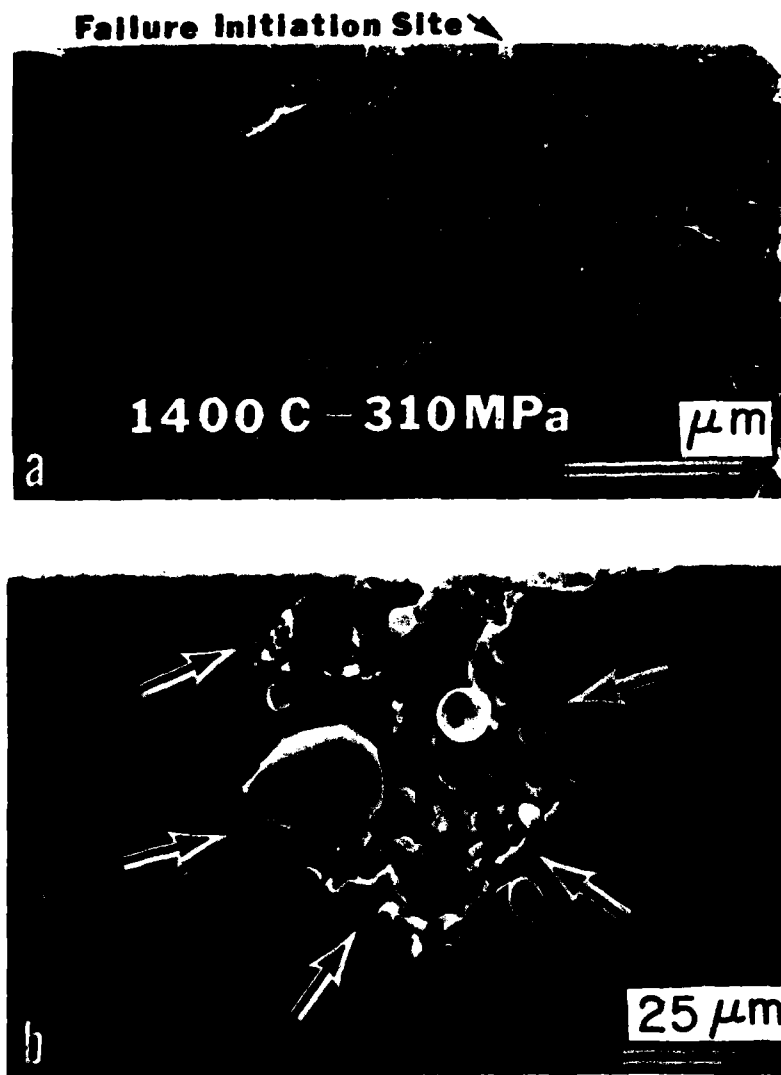


Fig. 12 SEM micrographs of the fracture surface of a specimen (sintered α -SiC) tested in 4-pt. bending at 1400°C in air showing surface associated failure site. Fracture mode is primarily transgranular and no sign of any slow crack growth.

display large porosity made up of loose grains instead of a single void. Another example of surface initiated failure site at 1400°C is shown in Fig. 13. Occasionally, failure occurred at subsurface flaws (pore with loose grains) and a typical example of such failure is shown in Fig. 14. Note the loosening (debonding) of grains in the failure initiating flaw. In short, the flexural strength evaluation indicates the absence of slow crack growth up to about 1400°C and primary mode of fracture during crack propagation is transgranular.

3.2 Uniaxial Tensile Stress Rupture at 1200°C

Twelve (12) tensile stress rupture specimens of sintered α -SiC (Carborundum 1980) were tested at 1200°C in air at applied stresses varying from 100 to 240 MPa. Out of these, four (4) specimens failed during axial alignment at 20°C and as such they were considered premature failures and eight failed as desired, in a time-dependent manner. Complete results are given in Table II. Some specimens failed in the center of the gage length (see #1 and #4, Fig. 15) while others failed at the upper or lower end of the gage length (see #2 and #7, Fig. 15). All of the eight specimens tested successfully at 1200°C are shown in Fig. 15. In addition to the failure in gage length, some specimens showed failure at the tensile pin supports (see #1, #5, #6, #7 and #8, Fig. 15). This results due to impact effect with furnace openings after failure in gage length. All specimens are numbered (Table II) and the corresponding numbers also appear on micrographs to identify the particular test specimen. The first specimen tested in this temperature series #1 was subjected to 103 MPa (15,000 psi) and it survived 1500 hrs. at 1200°C in air with no signs of early failure. It was then decided to test the specimen in a stepped stress rupture series (SSRS) fashion as shown in Fig. 16. The applied stress was increased in increments of ~ 7 MPa (1000 psi) after sustaining some time and when the stress reached 200 MPa (29,000 psi), the specimen survived for 7 hrs. and failed. The total time to failure was 2035 hrs. The specimen (#1) broke in the center of the gage length (Fig. 15) and the fracture surface for the bottom half of the specimen as examined in SEM (Scanning Electron Microscope) is shown in Fig. 17. The failure initiation site or region is in the vicinity of rear right corner and consists of a small zone marked by arrows (Fig. 17(B)). The upper half (matching piece) of this broken specimen was also examined in SEM, Fig 18, and showed clearly the failure initiation region, Fig. 18(B), which consisted of some porosity (primarily along grain boundaries) and separation of grains (Fig. 18(C))

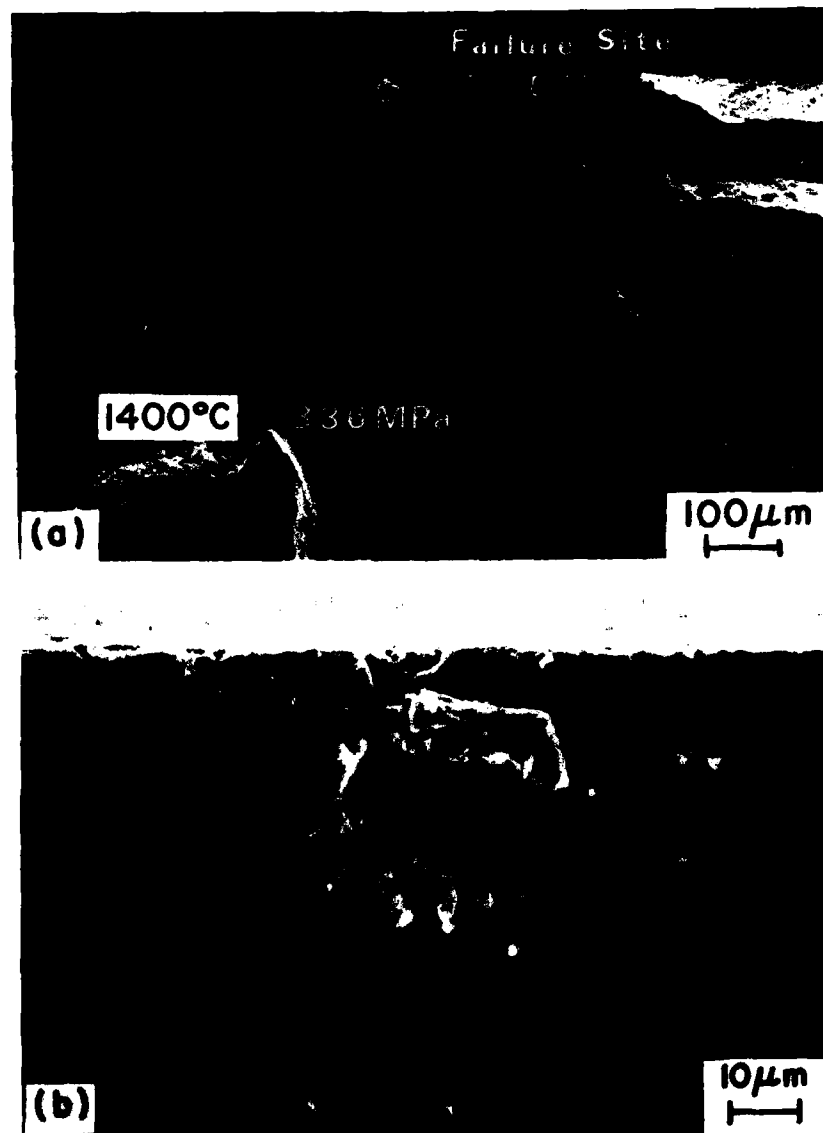


Fig. 13 SEM micrographs of the fracture surface of a specimen (sintered α -SiC) tested in 4-pt. bending at 1400°C in air showing subsurface porosity failure site. Fracture mode is primarily transgranular and no sign of any slow crack growth.

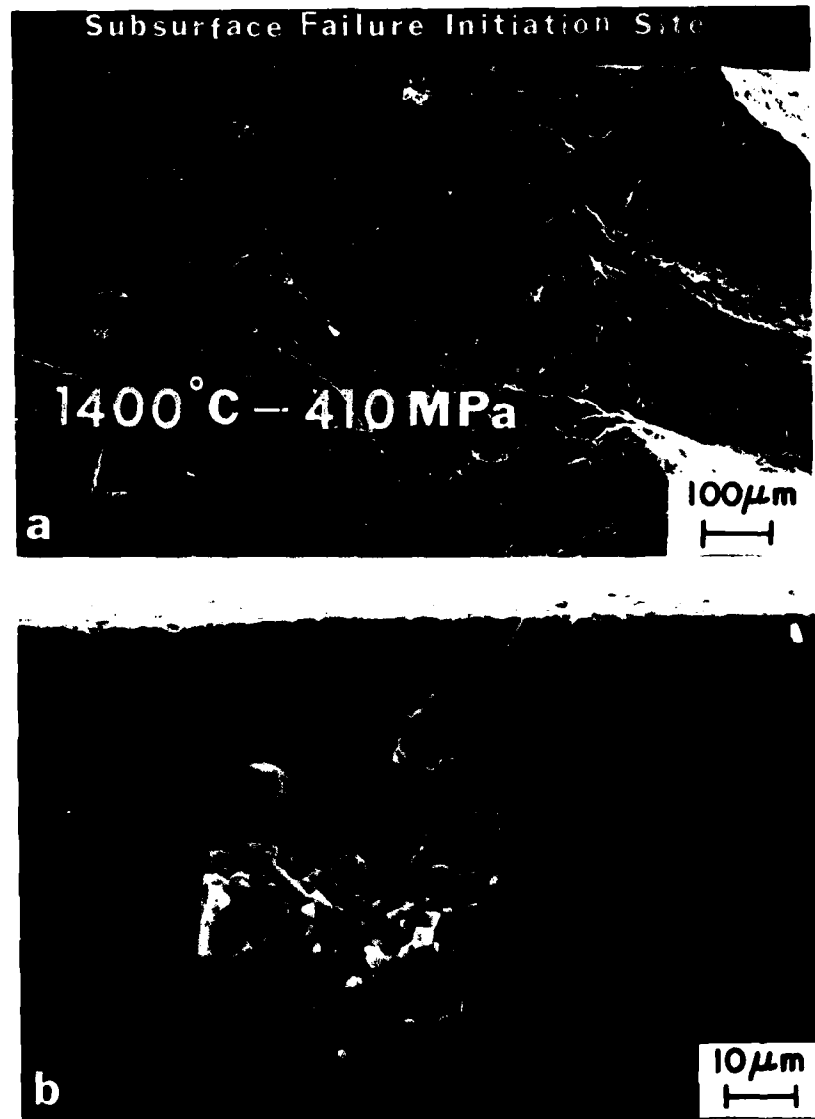


Fig. 14 SEM micrographs of the fracture surface of a specimen (sintered α -SiC) tested in 4-pt. bending at 1400°C in air showing subsurface porosity failure site. Fracture mode is primarily transgranular and no sign of any slow crack growth.

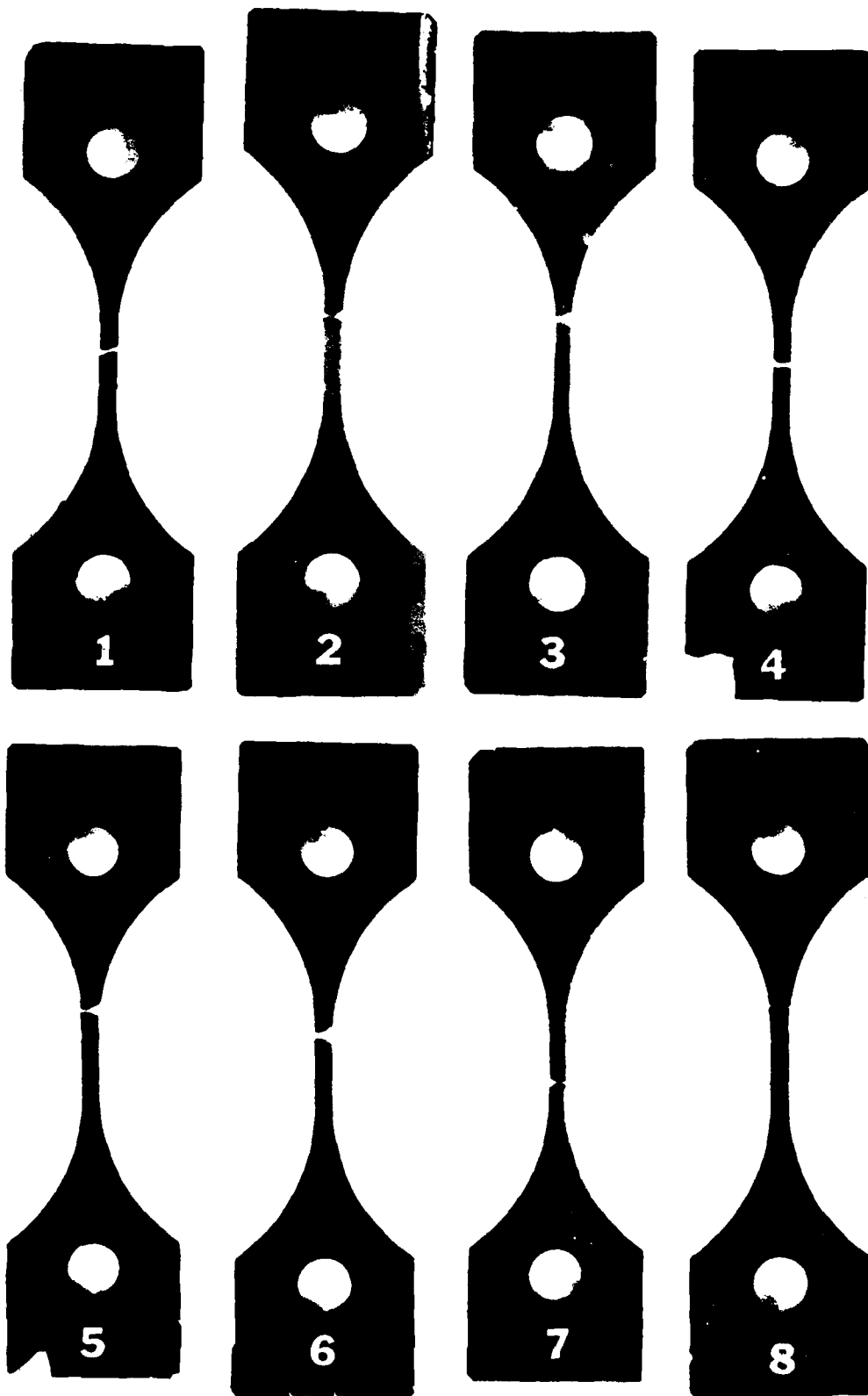
TABLE II. UNIAXIAL TENSILE STRESS RUPTURE RESULTS FOR SINTERED α -SiC (CARBORUNDUM 1980)

Specimen No.	Applied Stress		Time-to-Failure(h)	Approximate Flaw Size,* mm	Failure Proximity
	psi	MPa			
Testing Temperature: 1200°C in Air					
1**	15,000	103	2035 [†]	0.10-0.15	Rear right corner, limited SCG (Figs. 17-18).
2**	25,000	172	1900	-	Unable to identify failure site, no SCG (Figs. 19-20).
3	"	"	100	0.060-0.080	Rear left corner, porosity and machining damage. No SCG (Fig. 21).
4	30,000	207	447	0.10-0.30	Front right corner, porosity and limited SCG (Fig. 22).
5	32,000	220	0.33	0.080-0.090	Internal failure site (near rear left corner) due to an inclusion or foreign particle. No SCG (Fig. 23).
6	35,000	241	0.75	0.075-0.095	Porosity and machining damage. No SCG (Fig. 24).
7	"	"	4	0.070-0.120	Rear edge, machining damage and porosity. No SCG (Fig. 25).
8**	30,000	207	1500 [†]	-	Front surface edge & no visible SCG (Fig. 26).
Testing Temperature: 1300°C in Air					
9	25,000	172	171	AB \approx 0.20 CO \approx 0.15	Internal (0.064 mm long) pore and large SCG region (Fig. 28).
10	"	"	833	AB \approx 0.250 CO \approx 0.130	SCG region along right surface edge (Fig. 29).
11	27,000	186	1	-	Machining damage near front right corner (Fig. 30).
12	"	"	23	0.125	Limited SCG region along left side edge (Fig. 31).
13	"	"	27	0.130	Small SCG region near rear left corner (Fig. 32).
14	30,000	207	0.5	-	Machining damage near front left corner and porosity (Fig. 33).
15	"	"	7.5	AB = 0.175 CO = 0.100	Large region of SCG along front edge (Fig. 34).

[†] Stepped stress rupture test and as such not plotted in Fig. 49.

* These do not take into account the shape of the flaw but simply represent its length or width.

** During these long tests, the SiC heating elements burned out several times, replaced at room temperature while the test specimen maintained full load and, subsequently, the furnace was restarted.



1200 C

Fig. 15 Typical appearance of the broken specimens of sintered α -SiC tested at 1200°C in air in uniaxial tensile stress rupture model (see Table II for results).

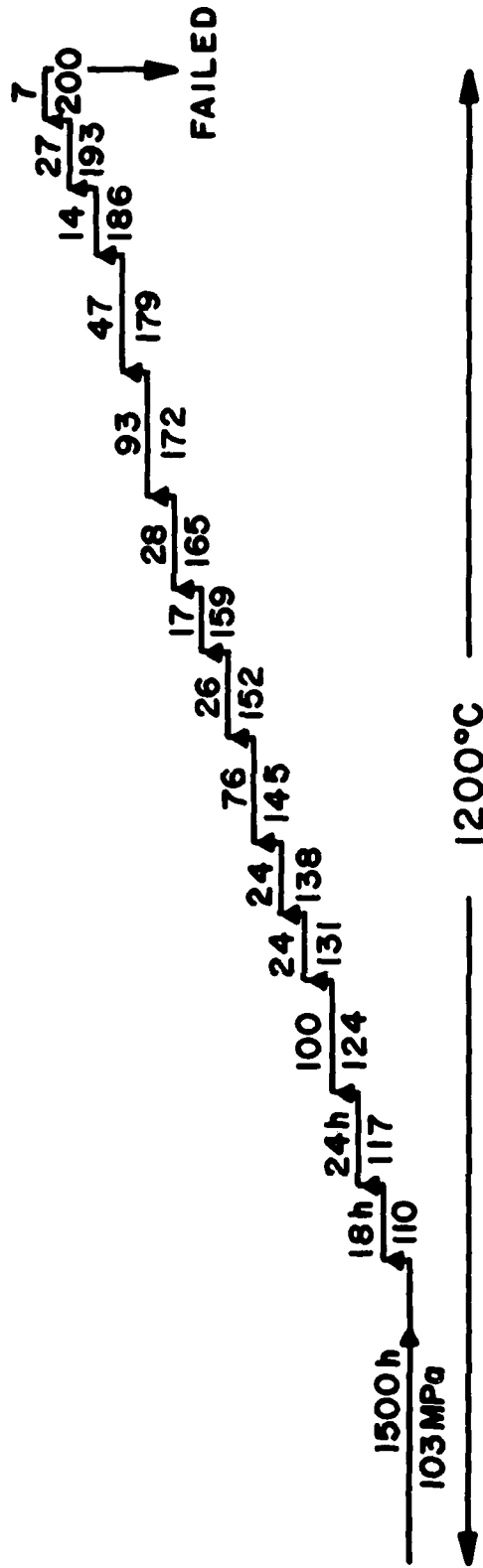


Fig. 16 Schematic illustration of the stepped stress rupture testing in uniaxial tension for sintered α -SiC specimen #1 (Table II). Initially the specimen was subjected to an applied stress of 103 MPa and sustained the stress for 1500 hrs. without failure. The applied stress was increased gradually as shown above and finally the specimen failed after 7 hrs. at 200 MPa. Fracture surfaces of both (bottom and upper) halves are shown in Figs. 17 and 18, respectively.

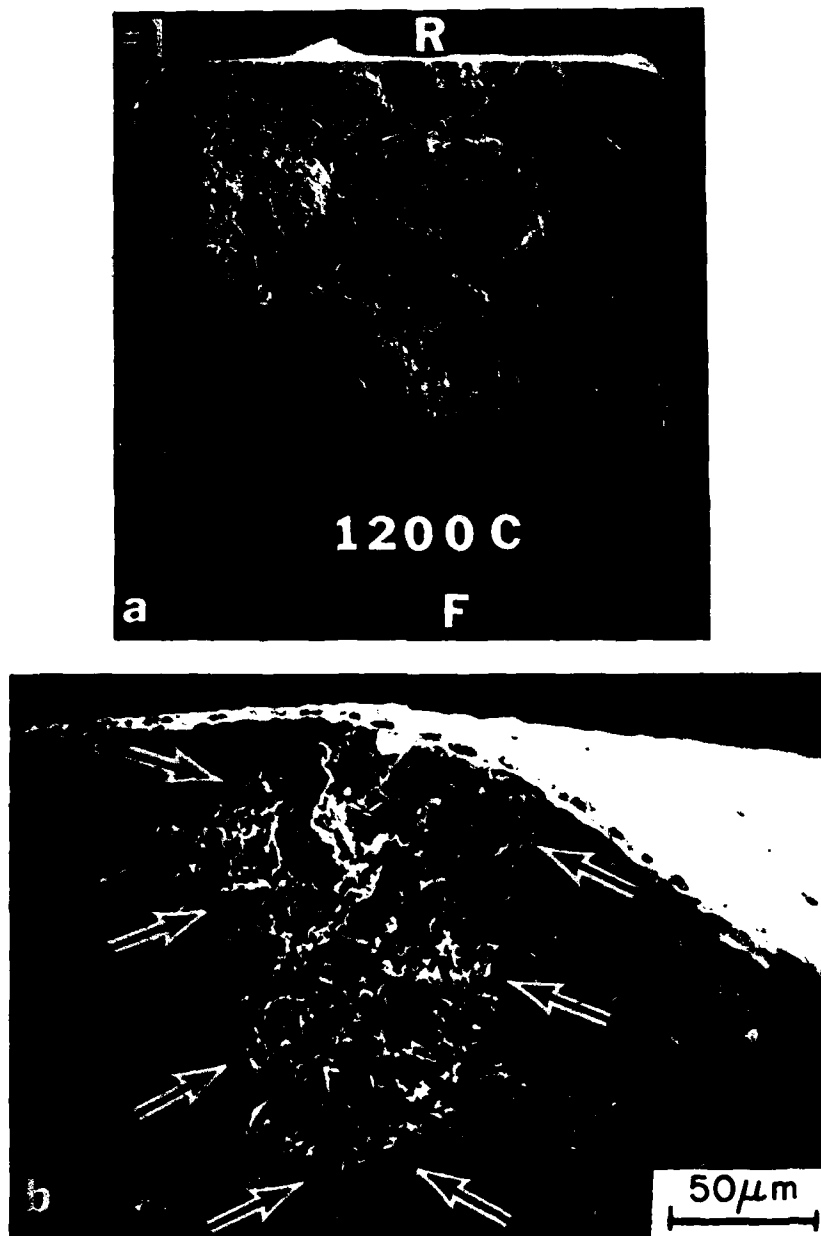


Fig. 17 Overall view of the fracture surface (bottom half) as seen in SEM of tensile stress rupture specimen (#1, Table II) of sintered α -SiC tested at 1200^oC in air. (a) Failure site as indicated. (b) Failure region is distinct in appearance from the remainder of the fracture surface and shows limited slow crack growth. Separation of grains due to intergranular crack propagation is visible.

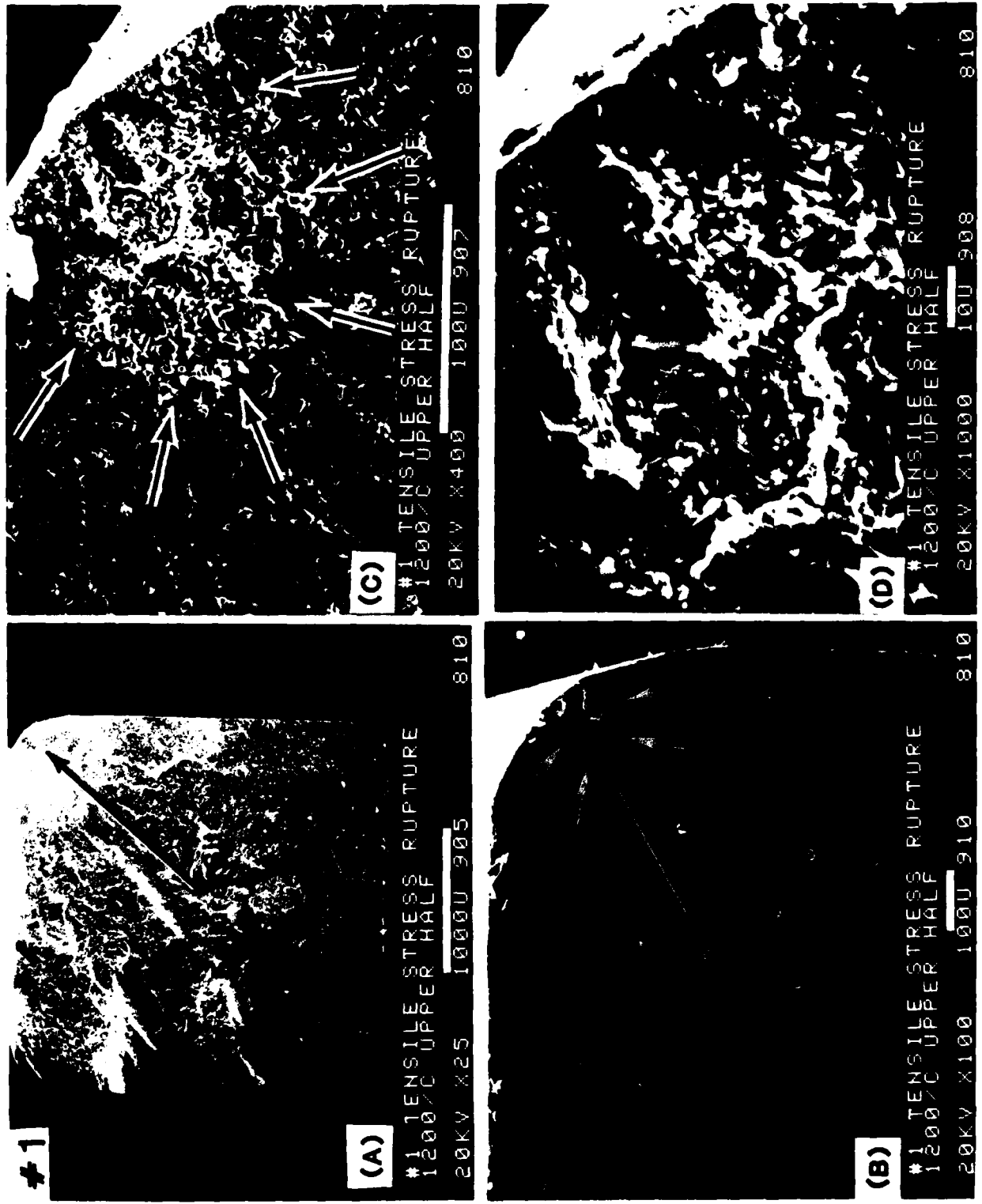


Fig. 18 SEM micrographs of the fracture surface (upper half of failed specimen) of specimen #1 showing failure site and the associated region of slow crack growth. Note the separation of grains along the grain boundaries inside the subcritical crack growth region clearly indicates that crack propagation during slow crack growth is primarily intergranular.

and (D)). The failure site is essentially a small slow crack growth (SCG) region surrounded by fast fracture region, Fig. 18(B). Since the specimen survived for a considerable long time, it is unlikely that failure started due to any machining damage around the rear right corner.

The next specimen #2 was subjected to a higher stress, 172 MPa (25 ksi) and failed after 1900 hrs. Both halves of the fractured specimen were examined in SEM, Figs. 19-20, and did not show the presence of SCG and localized failure initiation region similar to the one observed in specimen #1 (Figs. 17-18). To confirm the lack of significant SCG region, especially when the specimen survived for such a long time, another specimen (#3) was tested at the same applied stress (172 MPa) and temperature (1200°C) and failed after 100 hrs. The fracture face showed clearly the failure initiation site, Fig. 21 in which considerable porosity was evident. It is believed that the early failure relative to specimen #2, was due to some machining damage occurred around the rear left corner and opened up few grains (by joining up fine pores along grain boundaries) in the material. Under applied stress, the pores spread out, reach a critical size and led to sudden fast failure in short time. The same phenomenon occurs under higher stress more clearly and the time-to-failure is reduced drastically (see specimens #5-7, Table II).

The next specimen was tested at an applied stress of 207 MPa (30,000 psi) and failed after 447 hrs., Fig. 22. The failure region is clearly visible as shown in Figs. 22(A-B) and limited SCG is also evident inside the failure region, Fig. 22(C). Occasionally, failure occurring at an inclusion or foreign particle was observed, Fig. 23, and in such cases the time-to-failure was short (< 1 hr.) and fracture surface showed smooth appearance characteristic of fast fracture (transgranular crack propagation), Fig. 23(C).

The evidence of machining damage leading to early failure (short time-to-failure) was clearly evident in specimens #6 and #7, subjected to an applied stress of 241 MPa (35,000 psi) which failed in 45 mins. and 4 hrs., respectively. The fracture faces are shown in Figs. 24 and 25, respectively. Specimen #6, Fig. 24, shows clearly a notch effect (localized stress concentration) possibly produced by machining which opened up porosity (loosening of grains), Fig. 24(C) and led to early failure (fast fracture). Specimen #7, Fig. 25, basically



1200 C-172 MPa-1900 Hrs.

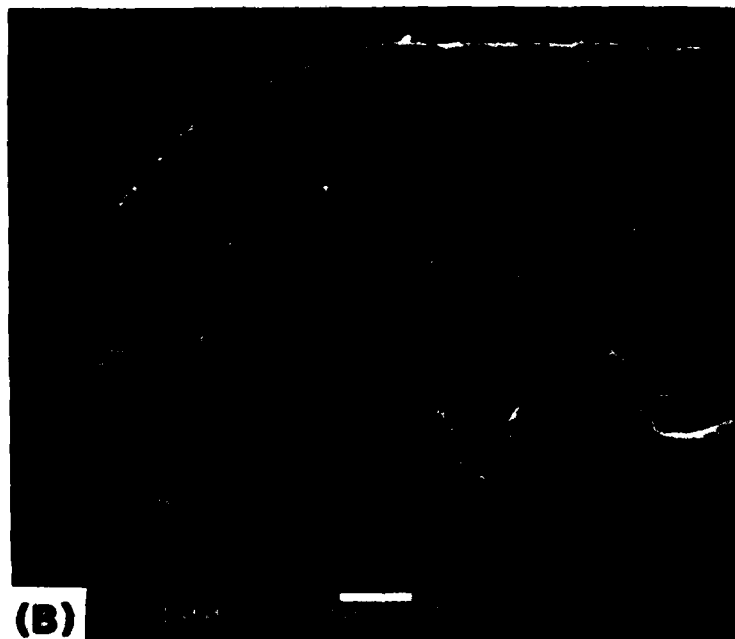


Fig. 19 (A) Overall view of the fracture surface (bottom half) as seen in SEM for tensile stress rupture specimen #2. Failure appears to have originated near the corner as indicated by the arrow. (B) Higher magnification view (SEM) around the corner. Failure origin is not visible and no sign of any slow crack growth.

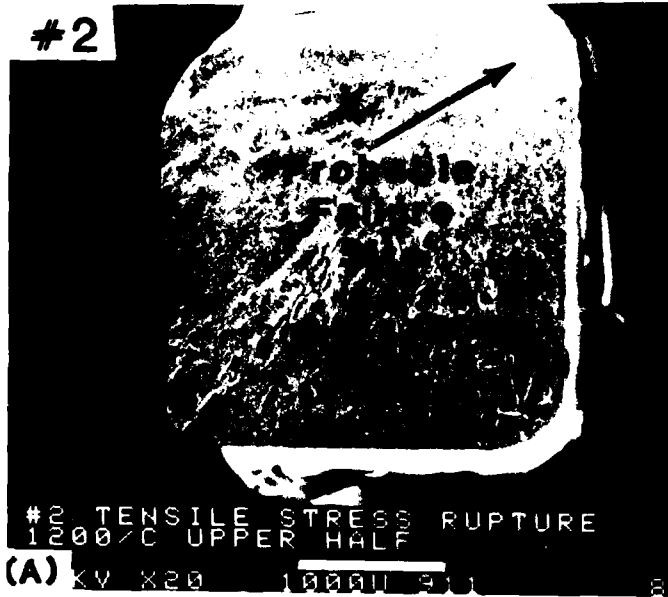
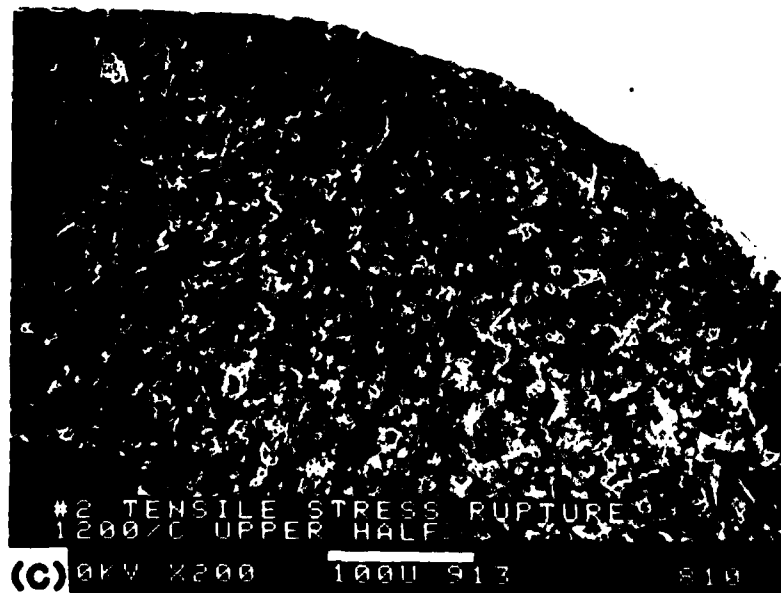


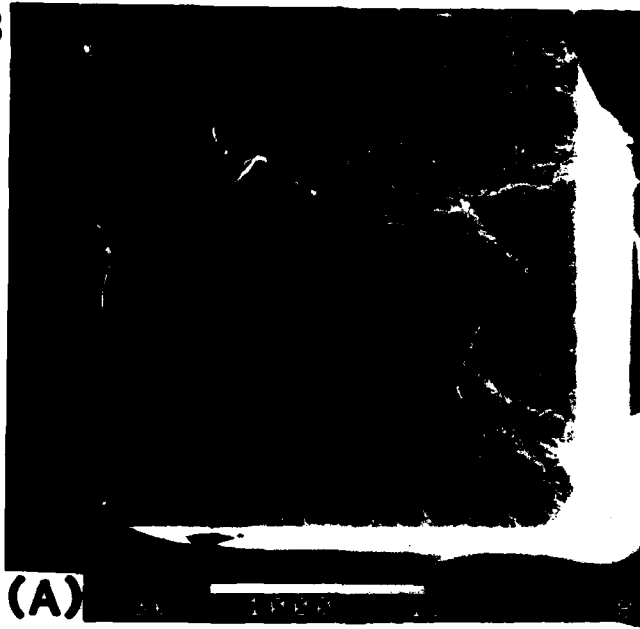
Fig. 20

Upper half of the fracture surface of failure specimen #2 as examined in SEM. Fracture surface shows smooth appearance indicating fast fracture and does not show any SCG region.

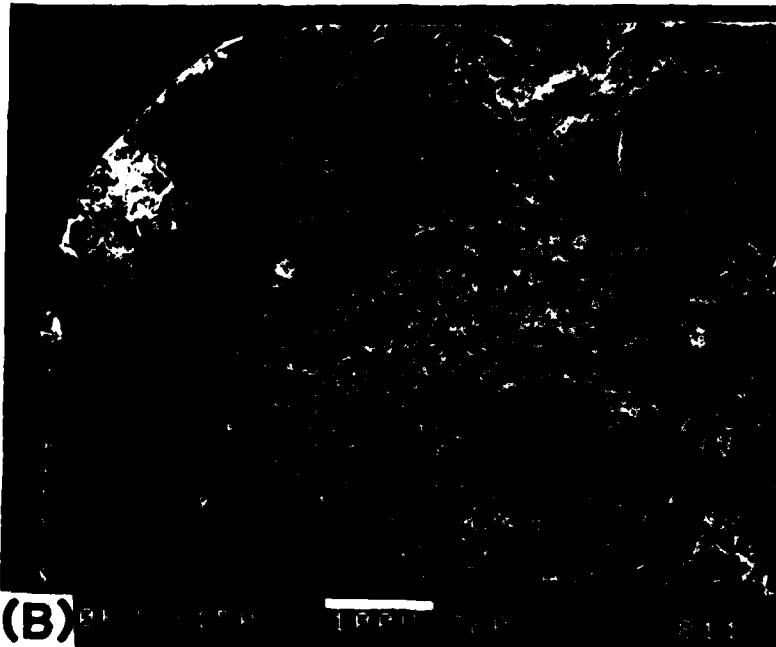


#3

-30-



(A)



(B)



(C)

Fig. 21

SEM micrographs of the fracture surface of tensile stress rupture specimen #3 showing failure site and the associated damage surrounding it.

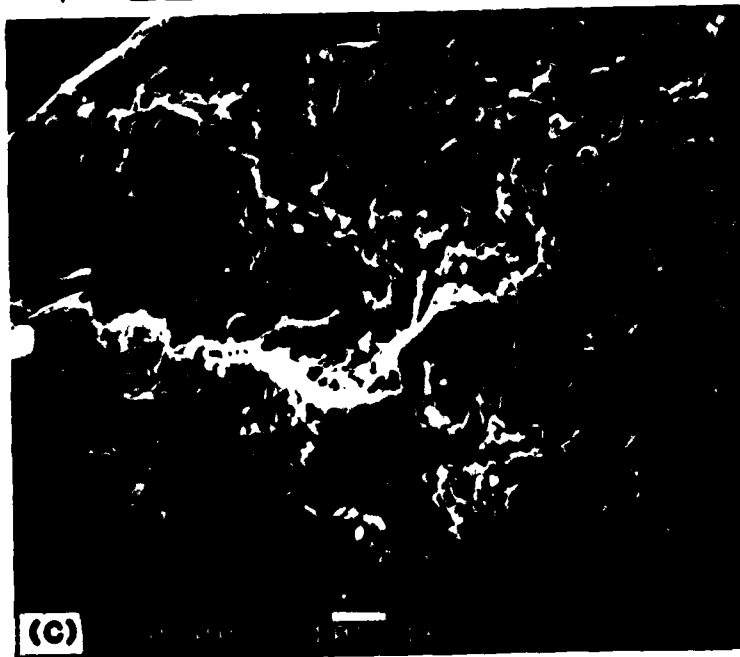
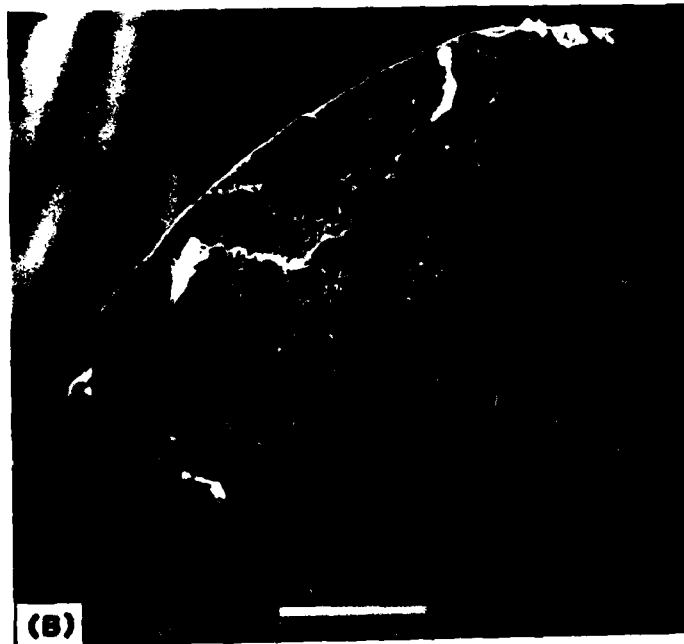
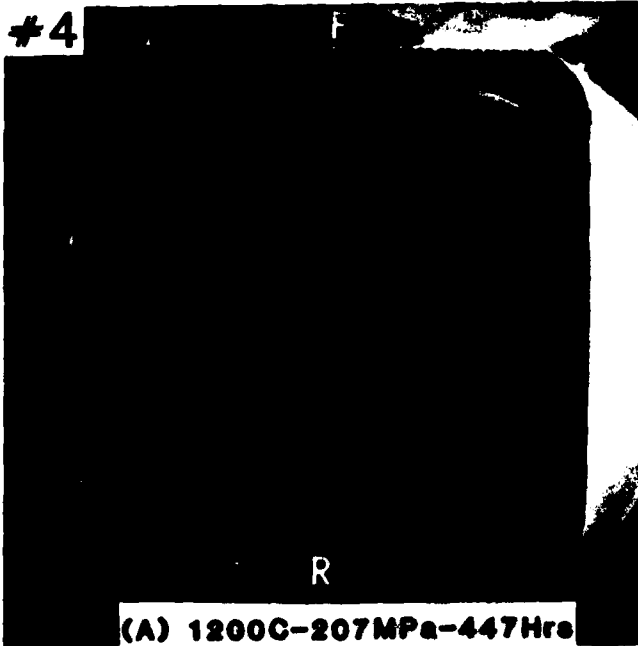


Fig. 22
SEM micrographs of the fracture surface of tensile stress rupture specimen # 4 showing failure initiation site, porosity and limited slow crack growth.

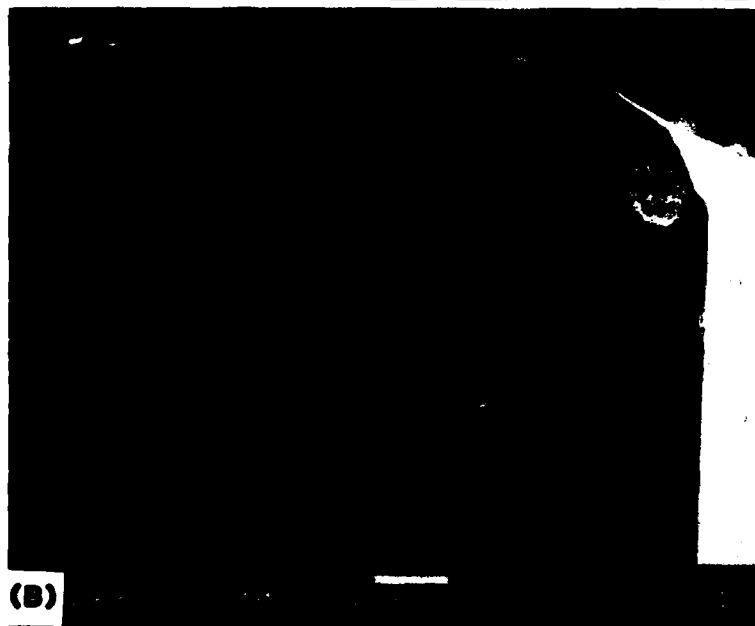
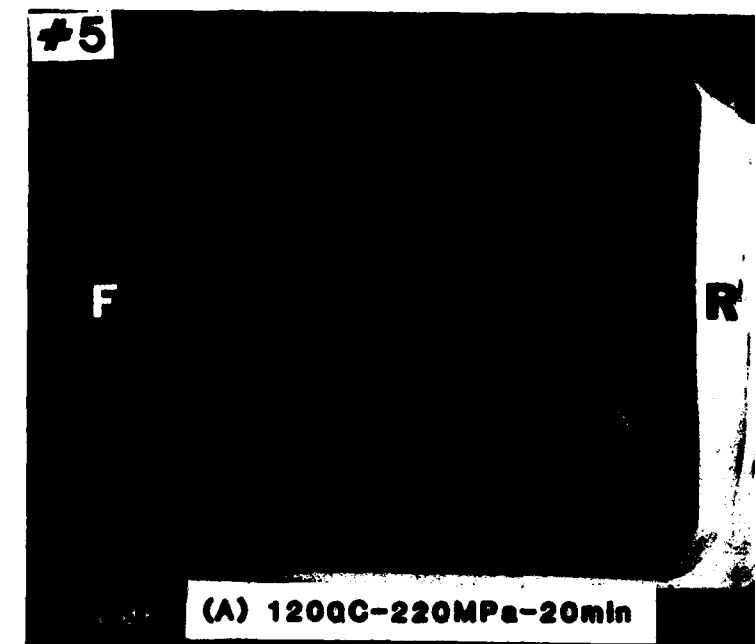
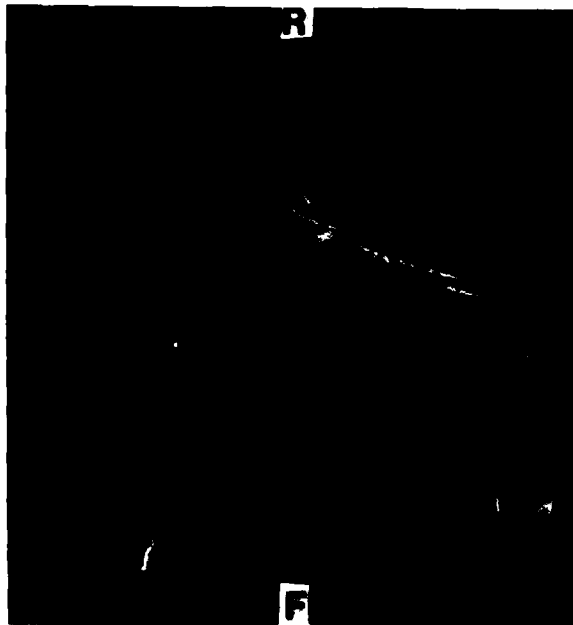


Fig. 23
SEM micrographs of the fracture surface of tensile stress rupture specimen # 5 showing internally occurring failure initiation site possibly due to an inclusion or foreign particle. No visible slow crack growth.

#6



(A) 1200C-24 1MPa-45min

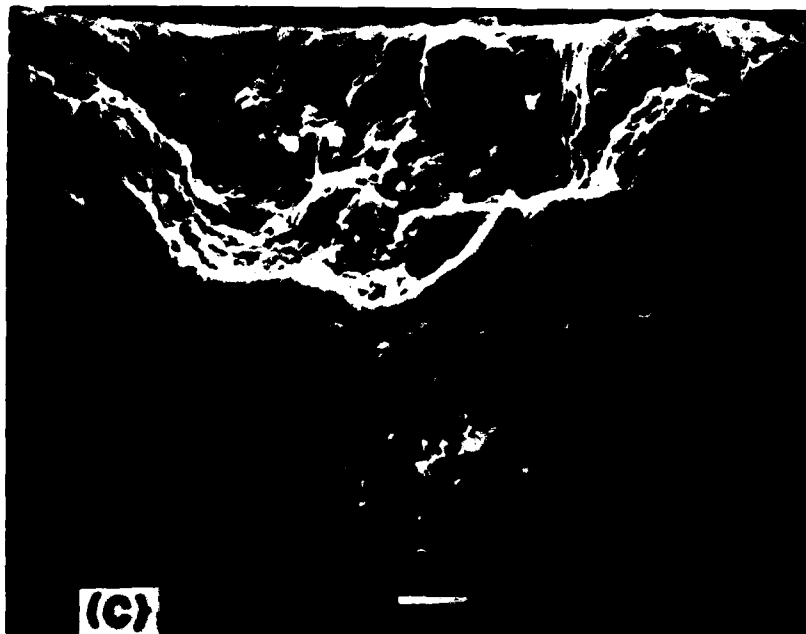
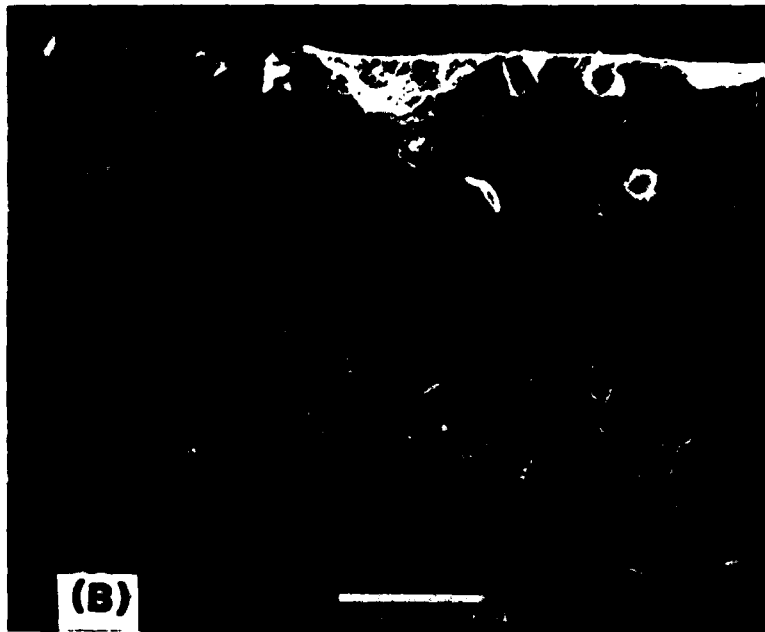
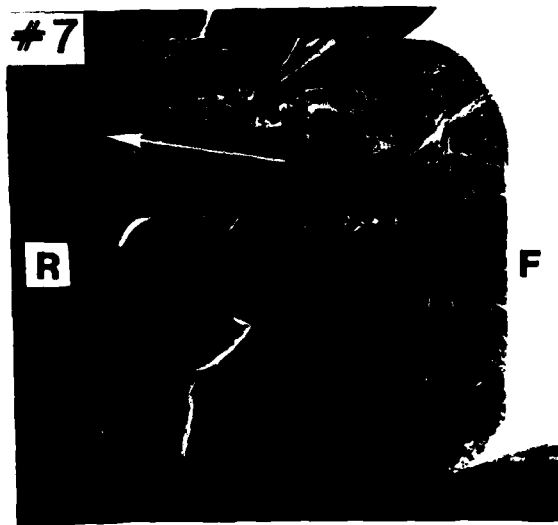


Fig. 24

SEM micrographs of the fracture surface of tensile stress rupture specimen #6 showing possible machining damage leading to fast failure. No visible SCG.



(A) 1200C-241MPa-4Hrs

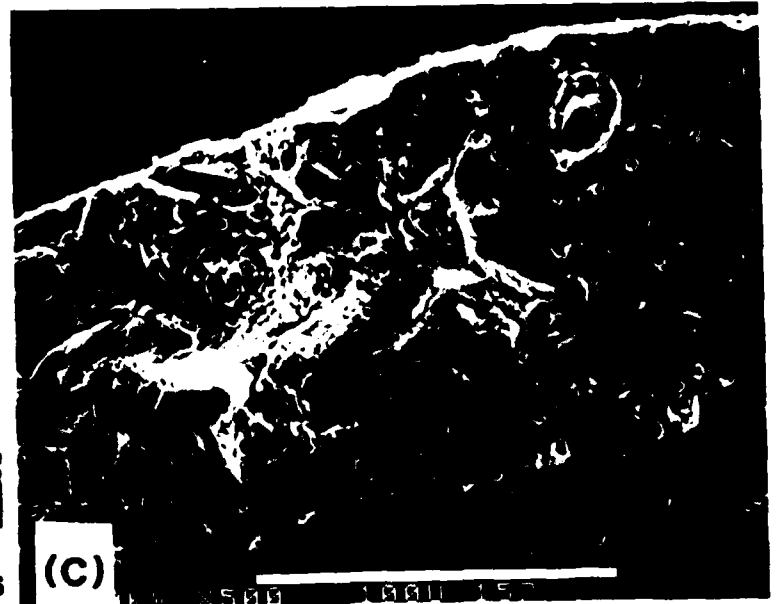


Fig. 25 SEM micrographs of the fracture surface of tensile stress rupture specimen #7 showing possible machining damage leading to early failure. No visible SCG.

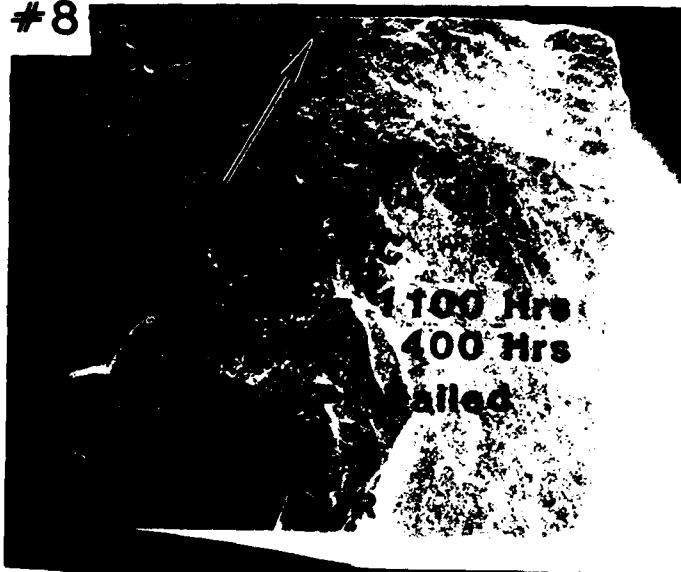
showed the same behavior as #6 (Fig. 24) except machining damage does not appear to be as severe, (cf. Figs. 24(C) and 25(C)), and therefore the time-to-failure was slightly longer (4 hrs.). Both specimens showed the absence of SCG.

The last specimen #8 in this series was tested in a stepped stress rupture fashion similar to specimen #1 except that the initial stress was much higher, 207 MPa (30,000 psi), and the test specimen survived 1100 hrs. without failure. The applied stress was increased to 241 MPa (35,000 psi) and the specimen survived for 400 hrs. without failure. The applied stress was increased to 276 MPa (40,000 psi) and the test specimen failed instantly. We had hoped that the specimen will show significant SCG because of sustaining higher stresses for long periods but it broke outside the gage length area, Fig. 15. The fracture surface is shown in Fig. 26 and the failure initiation site was clearly visible but did not show any evidence of SCG. From these tests, it is apparent that α -SiC is extremely sensitive to machining damage, especially of curved surfaces. In a recent study⁵ related to machining aspects of α -SiC, it was found that large cuts can be made in this material without introducing flaws. But this was only true for planar surface machining and not for curved surfaces. It should be noted that the average flexural strength of sintered α -SiC (Carborundum 1980) was 337 MPa (48,865 psi) from 20° to 1400°C, Fig. 9, and that this material can withstand tensile stresses of the order of 200 MPa (29,000 psi) for considerable time (100 to 500 hrs.) provided the work pieces or components are free from machining damage and large internal porosity (≥ 0.060 mm).

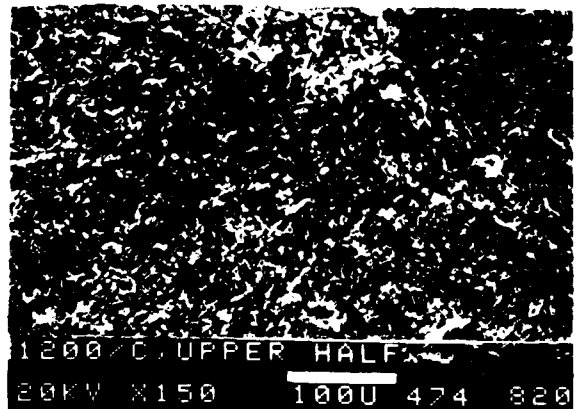
3.3 Uniaxial Tensile Stress Rupture at 1300°C

Eight (8) specimens were tested in uniaxial tensile stress rupture mode at 1300°C in air at various applied stress levels. The results are given in Table II and the broken specimens are shown in Fig. 27. Among these tests, one test specimen failed during axial alignment (at 207 MPa) at 20°C and is therefore, not listed in Table II. The first specimen (#9) tested at 1300°C was subjected to an applied stress of 172 MPa (25,000 psi) and failed in the center of the gage length after 171 hrs. Examination of the fracture face revealed that the failure initiation site consisted of a large semi-circular region of SCG, Fig. 28. The SCG region was surrounded by a mirror region. Inside the SCG zone, a large void (0.080mm long) was present. The large void became the localized stress concentration site and led to early failure. Therefore, another specimen

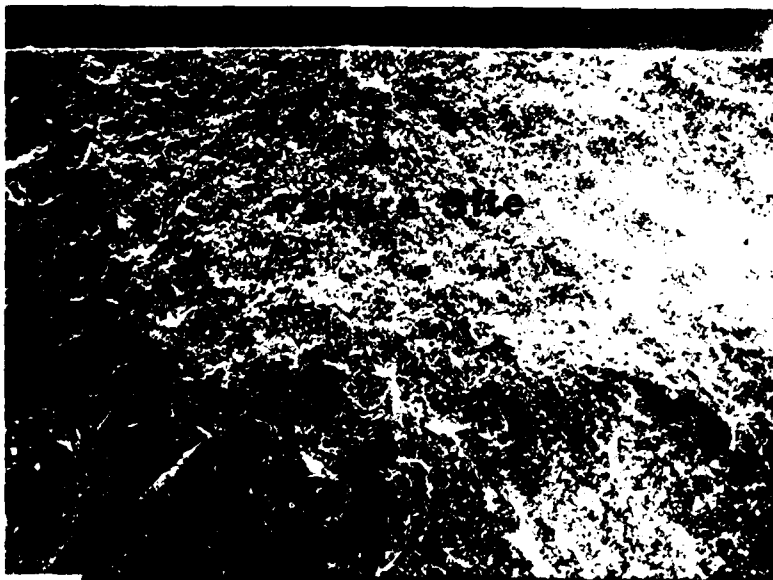
#8



(A) 20KV X28 1000U 723 81



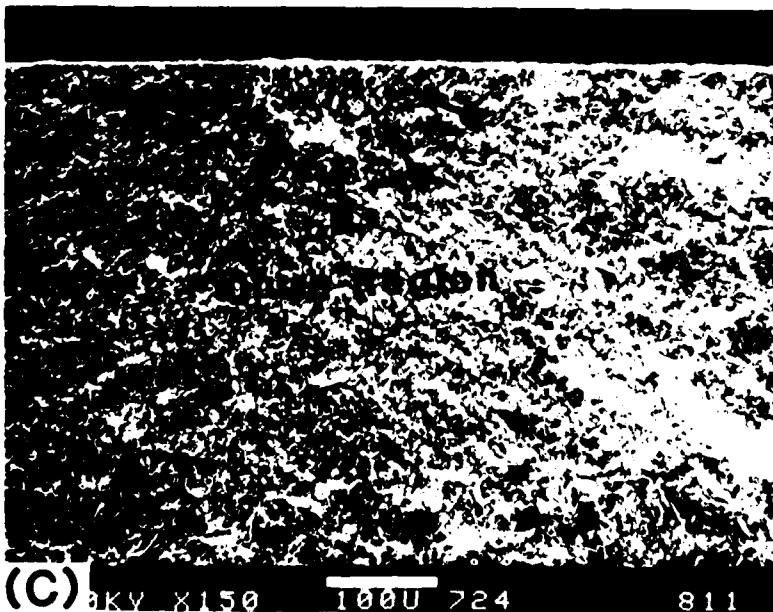
(D)



(B) 20KV X75 1000U 722 811



(E)



(C) 20KV X150 1000U 724 811

Fig. 26

SEM micrographs of the fracture surfaces of specimen # 3 tested in a stepped stress rupture fashion at 1200 C in air. (A-C) Bottom half of the specimen. Failure site is clearly visible as indicated but no slow crack growth. (D-E) Upper half of the fracture surface. Failure site is visible but no slow crack growth.

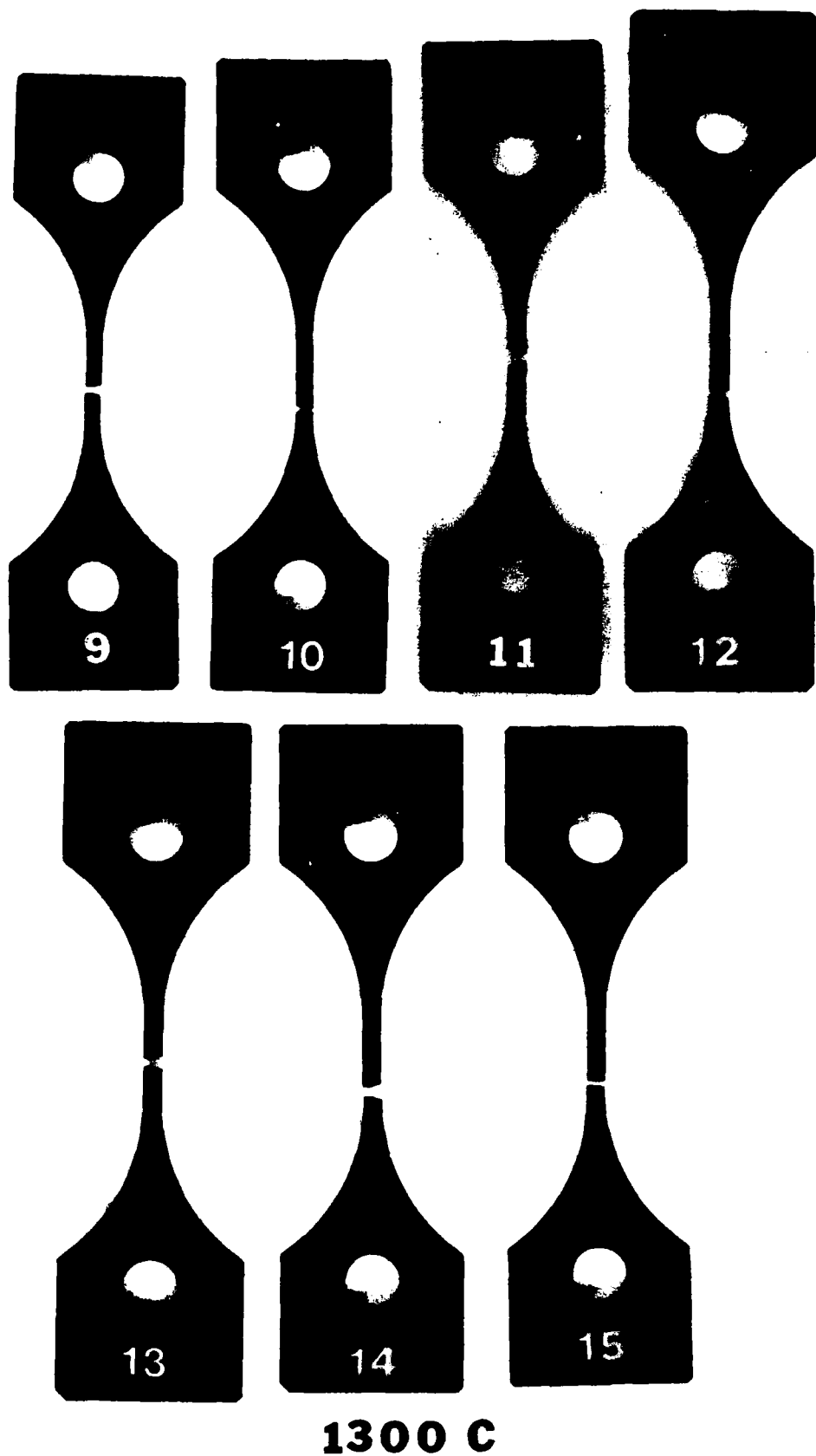


Fig. 27 Typical appearance of the broken specimens of sintered α -SiC tested at 1300°C in air in uniaxial tensile stress rupture mode (see Table II for results).

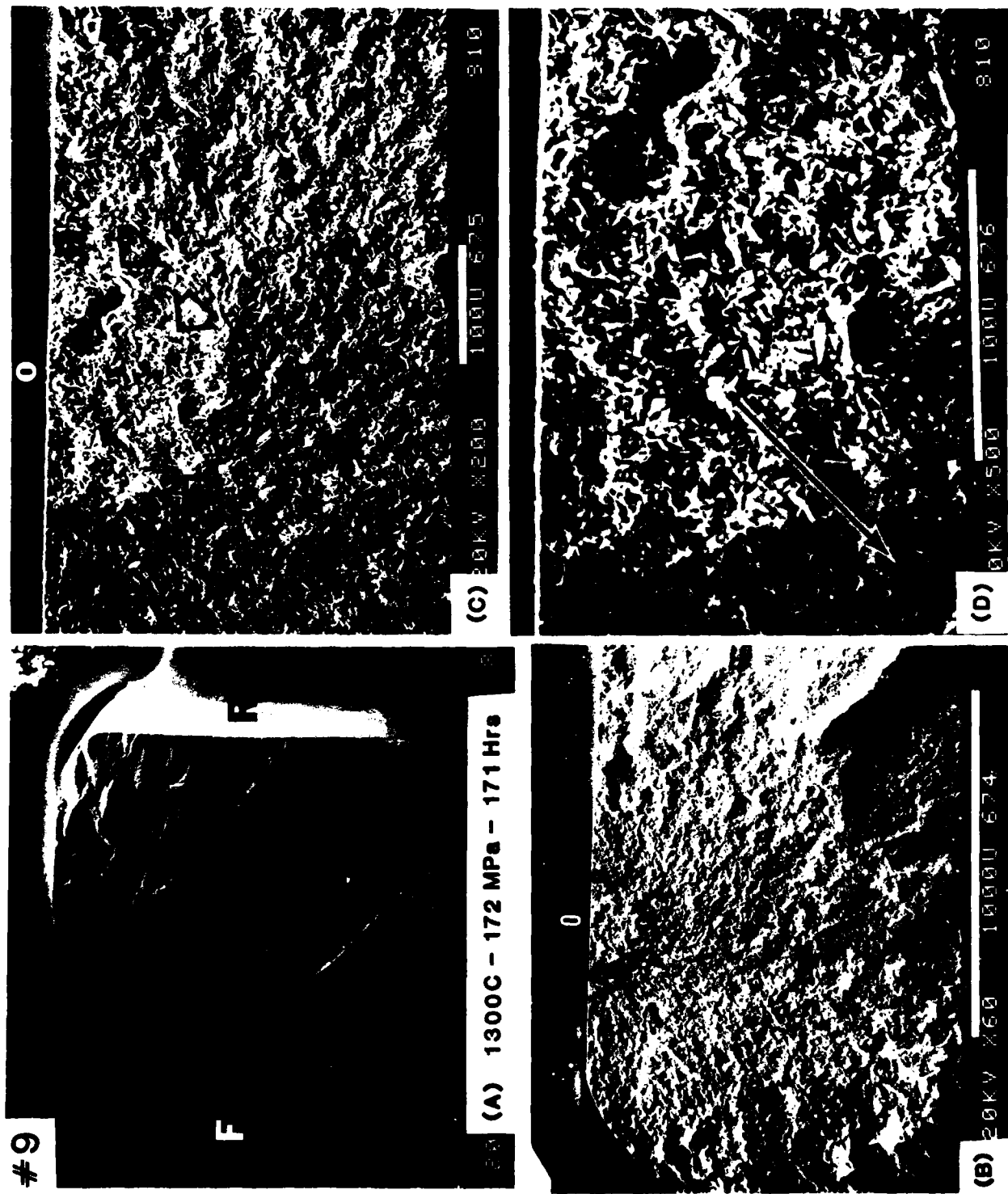


Fig. 28 SEM micrographs of the fracture surface of specimen #9 tested at 1300°C in air at an applied stress of 172 MPa and failed after 171 hrs. (A-B) Failure site is distinct in appearance and appears to be a zone (ACB) of slow crack growth region. (C) Large pore inside the SCC region. (D) Transition from SCC region to fast

(#10) was tested at the same stress (172 MPa) and temperature and failed after 833 hrs. The fracture face showed clearly the failure site, followed by a mirror region, Fig. 29(A). The failure site consisted of a semi-circular region ACB, Fig. 29(B), which was actually a SCG region, Fig. 29(C). Once the crack (flaw) grew to a critical size, catastrophic failure occurred. The nature of crack propagation during SCG is intergranular while the fast fracture occurred by transgranular mode as seen clearly in Fig. 29(D). Arrow (Fig. 29(D)) indicates the transition from SCG to fast fracture. Inside the SCG region, separation of grains characteristic of intergranular crack propagation is clearly visible. No large voids similar to the one observed in Specimen #9, Fig. 28, were observed in the SCG region. Fine porosity was visible. The strong dependence of SCG on temperature should be noted. Specimen (#2, #3) tested at 1200°C and 172 MPa (25,000 psi) did not show the presence of SCG, even though the specimen failed after 1900 hrs. (#2).

The next three specimens, #11-13, were tested at a slightly increased stress (relative to specimens #9-10) of 186 MPa (27,000 psi) and the time-to-failure decreased significantly, Table II. Specimen #11 failed in 1 hr. and the fracture surface of the specimen, Fig. 30, revealed clearly that the early failure was due to machining damage, Fig. 30(C) along the curved surface (corner). The next two specimens (#12 and #13) failed after 23 and 27 hrs, and the fracture faces are shown in Figs. 31 and 32, respectively. In specimen #12, the failure initiation site is along the left side edge (away from the rear left corner), Fig. 31, and shows limited SCG, Fig. 31(C). In specimen #13, the failure site is close to rear left corner, Fig. 32(A), but does not show any obvious machining damage similar to that observed in specimen #11, Fig. 30. Furthermore, separation of grains along grain boundaries inside the failure zone is clearly visible, Fig. 32(C), and characterizes the presence of SCG. Beyond the failure zone, the fast failure region is visible on the fracture face, Fig. 32(C).

The last two specimens, #14 and #15, were tested at a slightly increased stress (relative to specimens # 11-13) of 207 MPa (~30,000 psi) and the time-to-failure was 0.5 and 7.5 hrs., respectively. Examination of the fracture face in specimen #14 revealed the failure initiation site to be associated with a corner, Fig. 33(A), and the failure zone (Fig. 33(B)) showed considerable porosity and loosening of grains, possibly due to some machining damage which led to early

#10

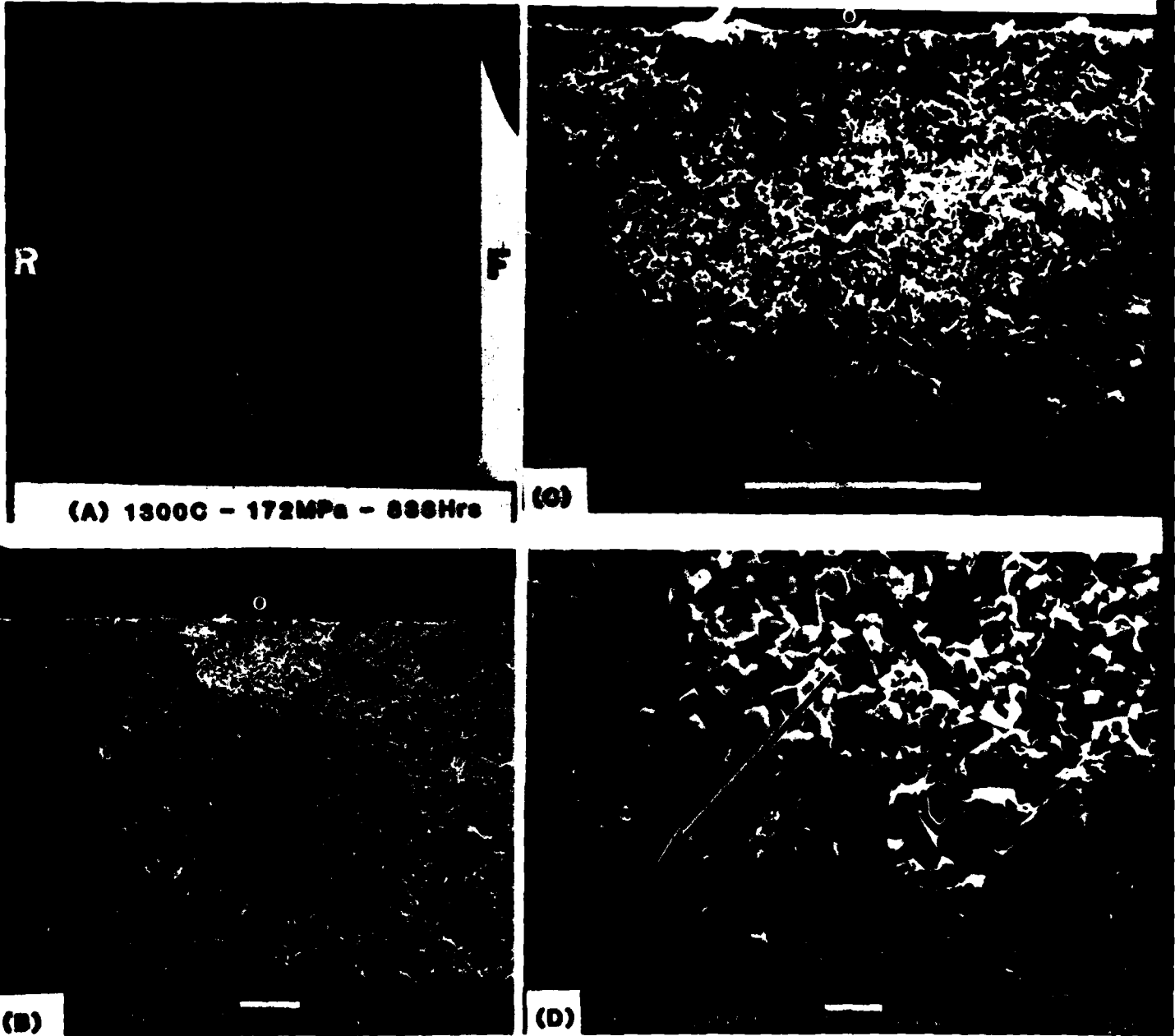


Fig. 29 SEM micrographs of the fracture surface of specimen #10 tested at 1300°C in air at 172 MPa and failed after 833 hrs. (A) Surface associated failure site. (B) ACB is the failure site and represents the slow crack growth region. (C) Higher magnification view of the SCG region ACB. (D) Arrow indicates the transition from slow crack growth (SCG) region to fast failure region. Note, the nature of crack propagation inside the SCG region is primarily intergranular while outside the SCG region, it is transgranular failure.

11



Figure 30

SEM micrographs of the fracture surface showing fast failure due to machining damage No SCG.

12

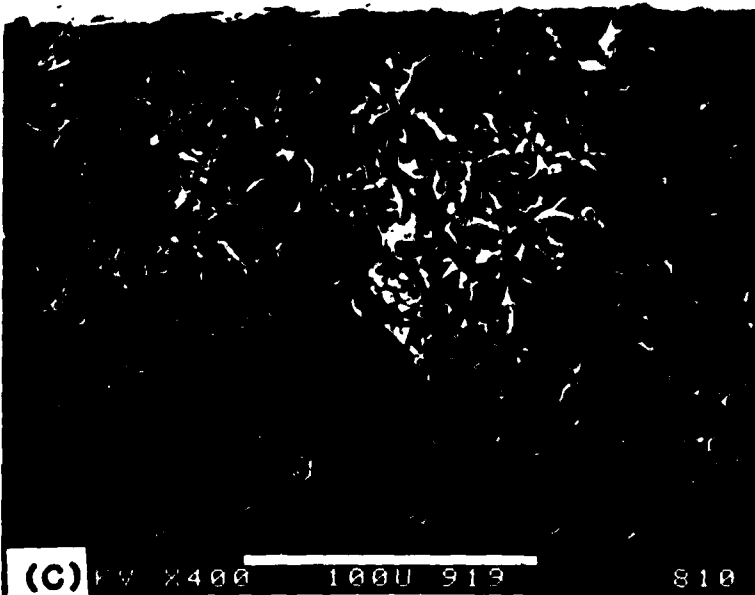
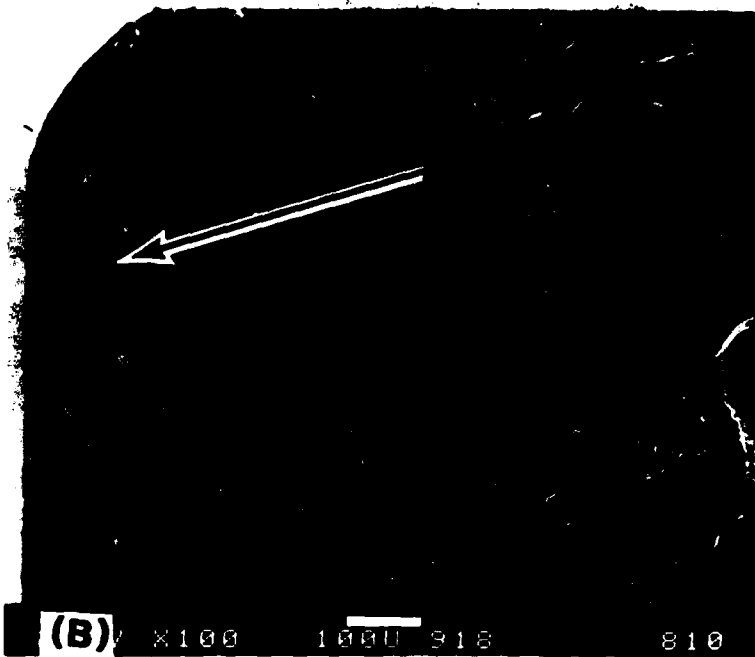


Figure 31

SEM micrographs of the fracture surface showing failure initiation site and the associated region of limited slow crack growth.

13

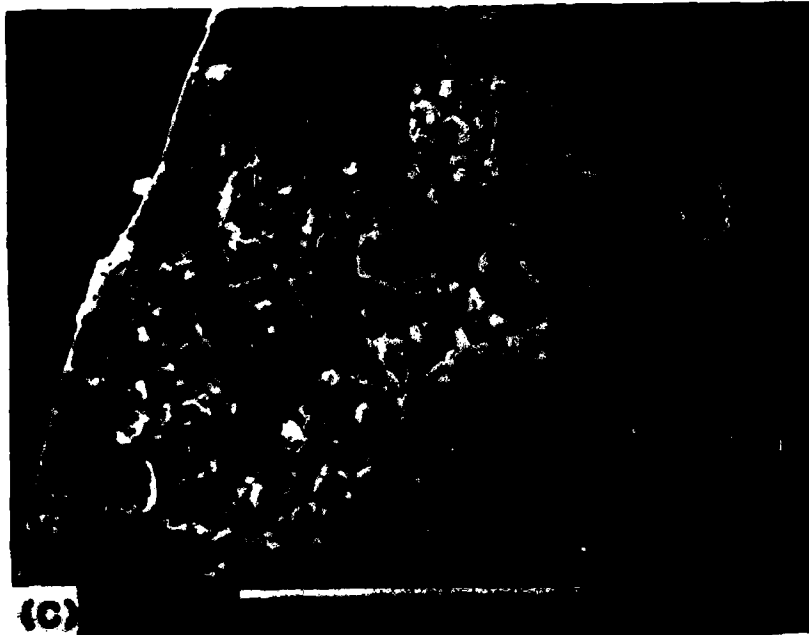
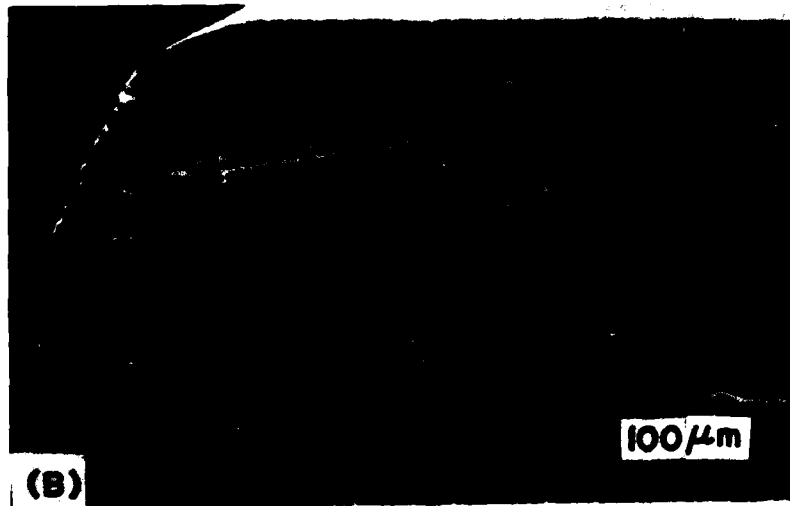


Figure 32

SEM micrographs of the fracture surface showing failure initiation site and the associated slow crack growth region.

and fast failure. It is equally probable that the early failure in this specimen was primarily due to localized porosity inside the failure region and under stress, the pores got interconnected and acted as a single large flaw (crack); thus producing fast fracture. Inside the failure zone, Fig. 33(C), the absence of SCG is clearly visible (cf. Fig. 33(C) and Fig. 32(C)) and the fracture face has the appearance of transgranular failure.

The specimen #15 which failed after 7.5 hrs. showed a large failure initiation site in the front face, Fig. 34(A). The failure site consisted of a large SCG area designated ACB followed by a mirror region, Fig. 34(B). Separation along the grain boundaries was clearly visible, inside the ACB region, Fig. 34(C). Outside the SCG region, the crack propagation mode is transgranular, Fig. 34(D), while inside it is intergranular.

The uniaxial tensile stress rupture tests at 1300°C have clearly demonstrated the extreme influence of applied stress and temperature in revealing the presence of SCG. A small increase in stress of 35 MPa (~5000 psi) decreased the time-to-failure by about two orders of magnitude. Increasing the temperature by 100°C (from 1200° to 1300°C) while maintaining the same stress of 172 MPa (25,000 psi) revealed the presence of large amounts of SCG.

3.4 Flexural Stress Rupture

Sintered α -SiC (Carborundum 1980) material was also examined in flexural stress rupture mode at 1400°C and 1300°C in order to determine the range of applied stress at which slow crack growth (SCG) occurs. From the temperature dependence of the fracture stress (Fig. 9, Table I and section 3.1), the mean flexural strength of the material is about 337 MPa (~48,865 psi) and is essentially independent of temperature. It is important to note that the flexural stress rupture strength of these ceramic materials (in which processing flaws are large and widespread) is usually significantly lower than the mean flexural strength. Therefore, flexural stress rupture tests should be conducted below the mean strength in order to provide meaningful time-to-failure data (≥ 10 hrs.).

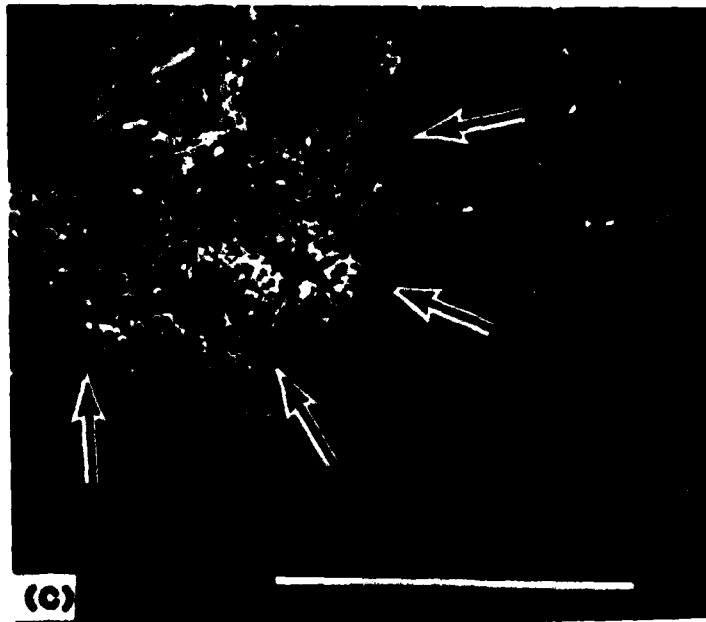
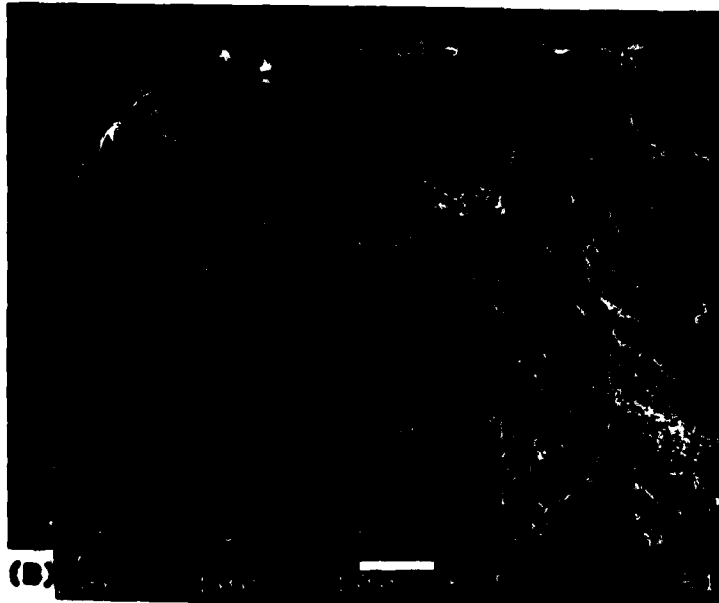
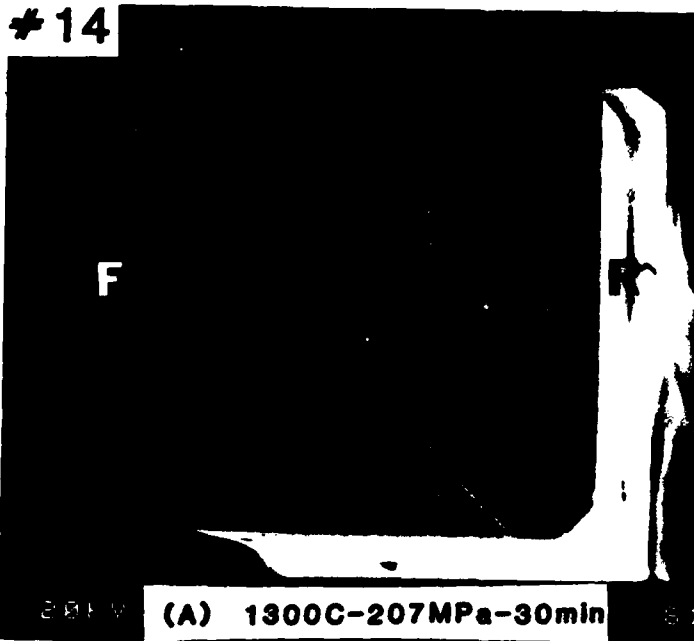


Figure 33

SEM micrographs of the fracture surface showing possible machining damage leading to fast failure.

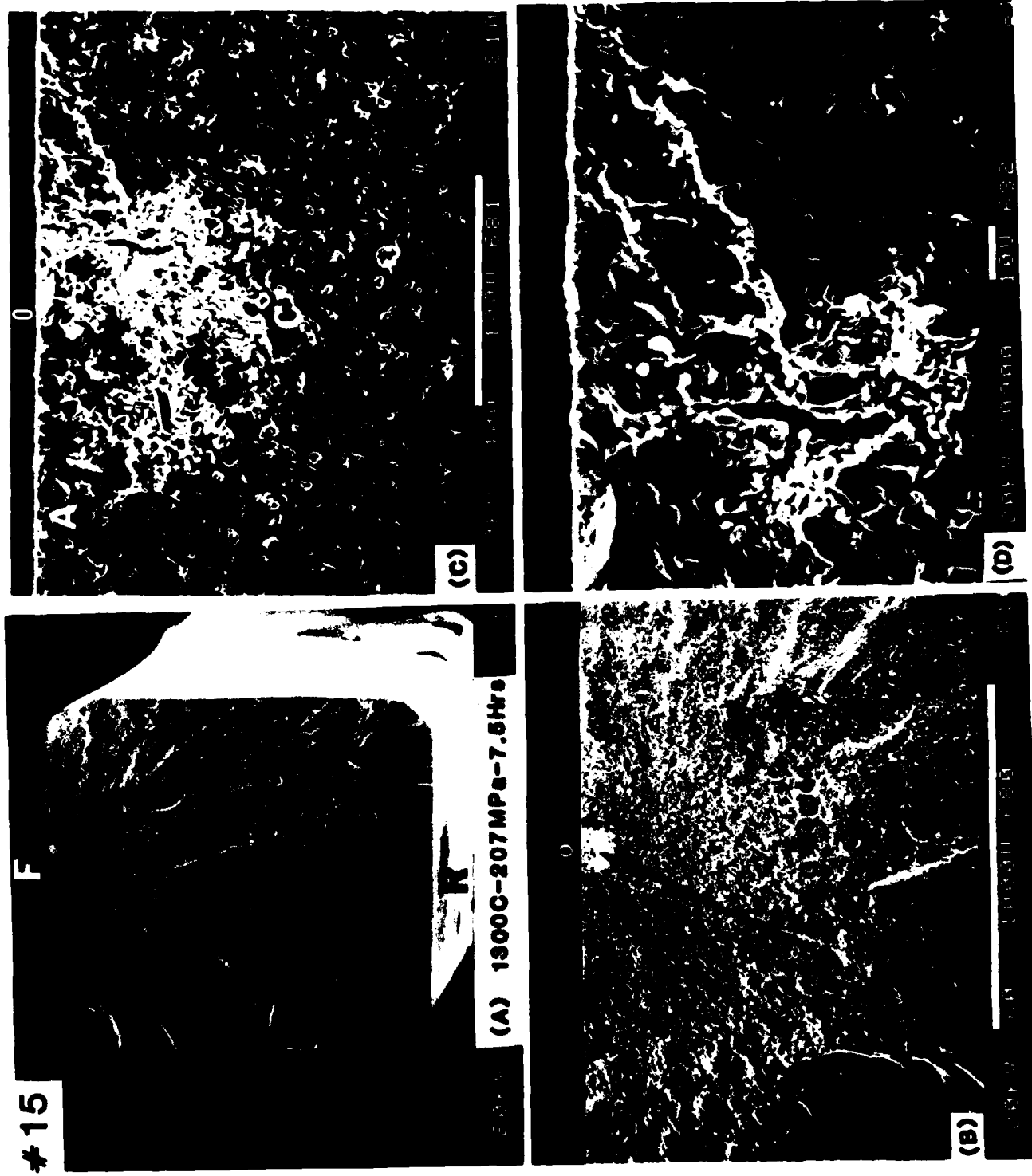


Fig. 34 SEM micrographs of the fracture surface showing the surface associated slow crack growth (SCG) region, separation of grains inside the SCG region and porosity.

At 1400°C

Fourteen (14) bend bar specimens were tested in stress-rupture mode at 1400°C in air at three different stress levels, and two (2) were tested in a partial environment of Argon gas. Complete results are given in Table III.

The first specimen in this series was tested at an applied stress of 283 MPa (~41,100 psi) at 1400°C in air and failed in 18 mins. Failure was associated with surface porosity similar to that seen earlier in Figs. 12-13 and did not show the presence of SCG.

The applied stress was decreased significantly (about 30% relative to mean strength) to a level of 234 MPa (~34,000 psi) and a total of seven (7) specimens were tested and the time-to-failure varied from 6 min. to 320 mins. (Table III). Majority of these (total of 5) failed within 60 mins. and two specimens failed in 110 and 320 min., respectively. Fracture surfaces for specimens failed in 18 min. and 45 min. are shown in Figs. 35 and 36, respectively. The failure origins are associated with sub-surface porosity (Fig. 35) and large grain of α -SiC (Fig. 36) and did not show clear evidence for the presence of SCG. Fracture surface for the specimen which failed in 320 mins. is shown in Fig. 37 and it appears that failure originated at a sub-surface porosity site similar to that observed in Fig. 35 and does not show the presence of SCG. The approximate depth (below tensile edge) of pore or flaw is 100 μm for the specimen which failed in 320 mins. while it is 30 or 40 μm for the specimen which failed in 18 mins. (cf. Fig. 37(B) and Fig. 35(C)). This would probably explain the longer time (320 mins.) achieved or sustained in comparison to significantly shorter time (18 mins.) when both specimens were subjected to the same applied stress of 234 MPa and a temperature of 1400°C.

The introduction of localized stress raisers such as notches, fine cracks residual stresses, and other types of flaws is common in surface machining of ceramic materials⁽⁵⁾ and thus lowering the fracture strength of the material. Annealing at high temperatures in vacuum often blunts the stress raisers and also relieves residual stresses⁽³⁾, thereby improving and restoring the original strength of the material. Therefore, three bend bar specimens were annealed at 2000°C in high vacuum for 10 min., and later were tested in stress rupture mode

TABLE III. FLEXURAL (4-POINT BENDING) STRESS RUPTURE RESULTS AT 1400°C SINTERED α -SiC

Specimen No.	Applied Stress (MPa)	Time to Failure	Failure Origin
Testing Temperature: 1400°C in Air			
1	283	18 min.	Surface pore; no SCG. [†]
2	234	6 min.	Crushed; not visible.
3	"	18 min.	Sub-surface porosity, Fig. 35.
4	"	21 min.	Surface pore; no SCG.
5	"	45 min.	Surface flaw with large grain, Fig. 36.
6	"	48 min.	Crushed; not visible.
7	"	110 min.	" " "
8	"	320 min.	Sub-surface porosity; Fig. 37.
9	"	10 min.*	Crushed; not visible.
10	"	300 min.*	Sub-surface porosity; large SCG; Fig. 38.
11	"	360 min.*	Crushed; not visible.
12	195	15 min.	Surface flaw; porosity; no SCG.
13	"	20 hrs.	Large SCG region; Fig. 39.
14	"	69 hrs.	Large SCG region; Fig. 40.
Testing Temperature: 1400°C in Argon			
15	234	12 min.	From corner; no SCG.
16	210	60 hrs.	Large SCG region and porosity; Fig. 41.

[†] Slow crack growth.

* Specimens annealed at 2000°C in high vacuum for 10 minutes prior to testing.

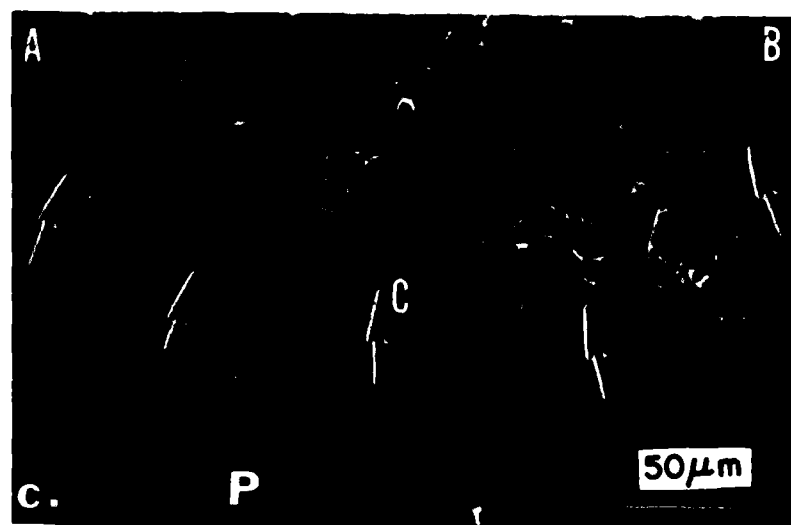
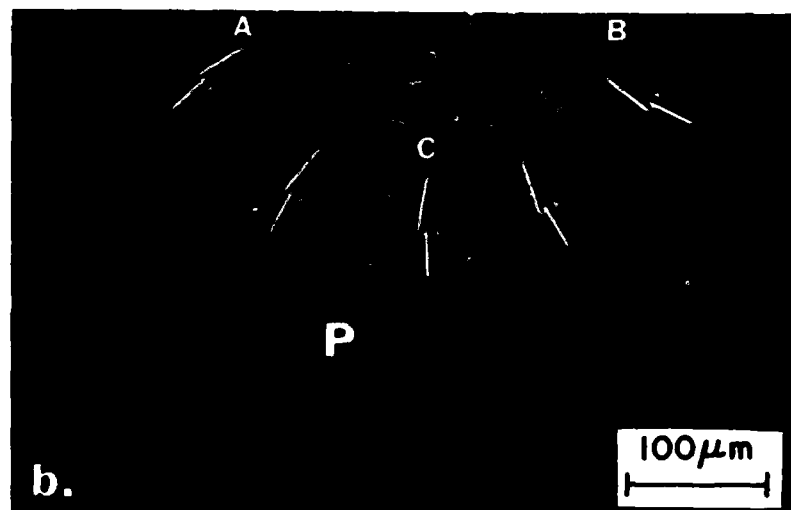
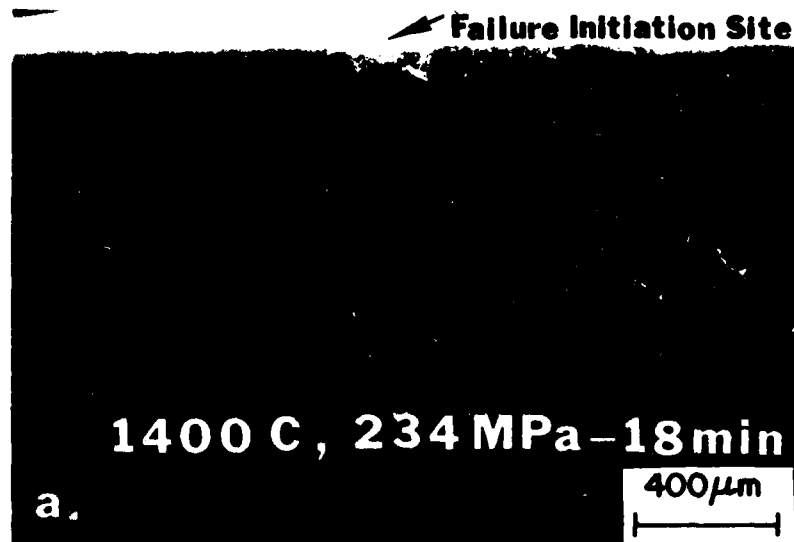


Fig. 35 SEM micrographs of the fracture surface of a specimen tested in 4-pt. bending at 1400 C in air at 234 MPa and failed after 18 mins. Note the presence of porosity (P) inside the failure region led to early failure and no signs of any slow crack growth.

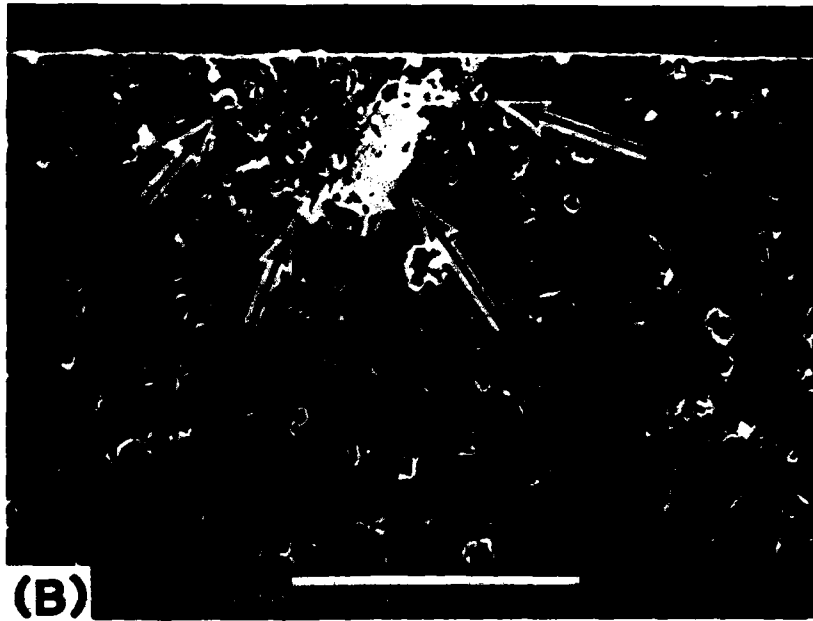
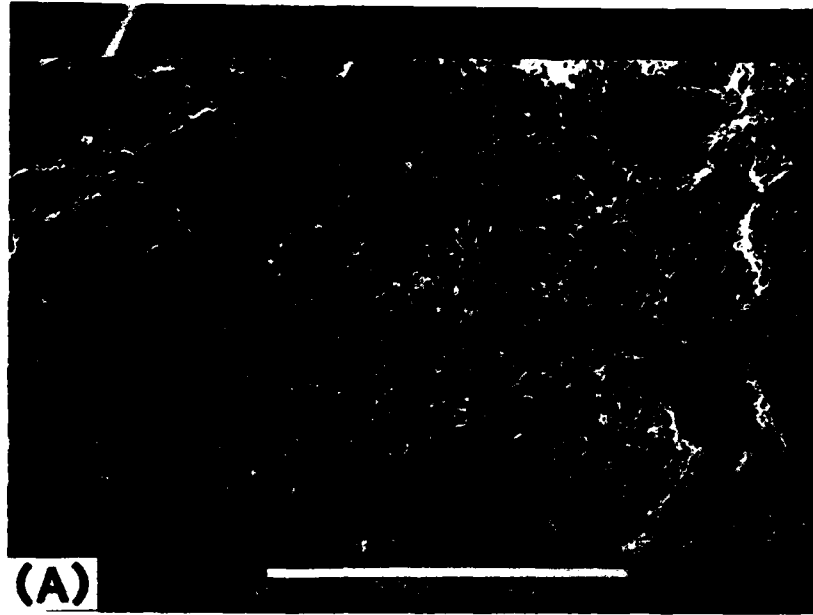


Fig. 36 SEM micrographs of the fracture surface of a specimen tested in 4-pt. bending showing the failure site. Note the presence of a large single α -SiC grain. No visible SCG.

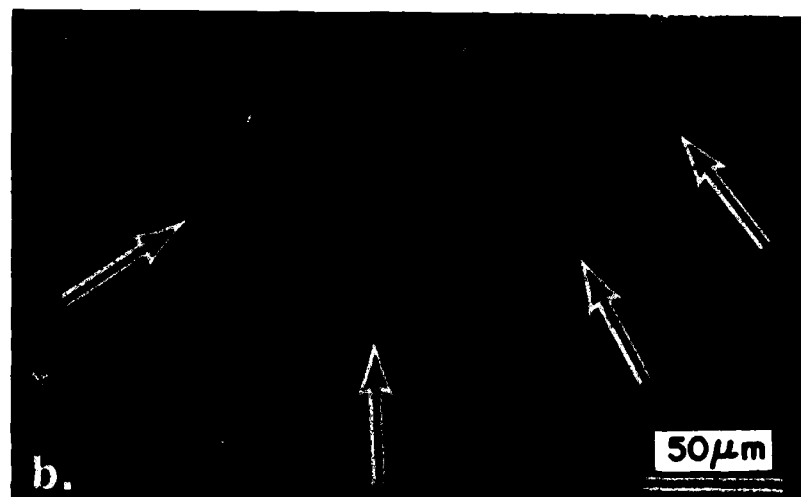
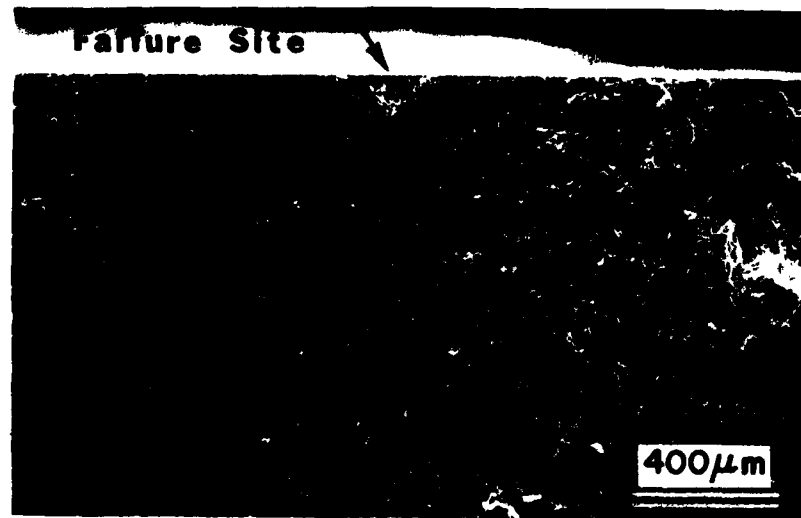


Fig. 37 SEM micrographs of the fracture surface of a specimen tested in 4-pt. bending at 1400°C in air at 234 MPa and failed after 320 mins. Note the presence of subsurface porosity (P) below the tensile edge. Fracture surface appearance is smooth and similar to that seen earlier (Figs. 7, and Figs. 10-14). No visible slow crack growth.

at 234 MPa and 1400°C, Table III. One broke in 10 mins. while the other two broke in 300 and 360 mins., respectively. Examination of the fracture face in SEM revealed a large semi-circular ACB failure initiation site, Fig. 38(A). The failure zone displayed large porosity inside it and a large region of SCG surrounding it, Fig. 38(B). Crack propagation during SCG is exclusively intergranular, Fig. 38(C) while the fast failure region displays transgranular mode of fracture, Fig. 38(C). It should be noted that among the annealed specimens, 2 out of 3 sustained the stress for 300 mins., while among the unannealed as machined specimens, only 1 out of 7 sustained the stress for 300 mins. and 5 failed in less than 60 mins. It appears that annealing at high temperatures in vacuum did have some effect on the flaws, possibly blunting them and thereby improving materials strength. However, this needs further investigation.

The nature and extent of slow crack growth in earlier versions of sintered α -SiC (also made by Carborundum) has been studied at 1400°C by several workers. Kraft and Coppola⁽⁶⁾ used the stress-rate method at 1400°C in air to determine the presence of SCG in α -SiC and concluded little or no SCG. Lack of sensitivity of the stress-rate technique in detecting the presence of SCG compared to stress rupture methods was the prime reason and similar evidence was found in hot-pressed Si_3N_4 ^{3,7}. Coppola et al.⁸ and others^{1,2,9,10} found the presence of SCG at 1400°C in air in their studies of flexural stress rupture in α -SiC similar to that reported in this study.

The applied stress was decreased considerably (about 40% relative to mean strength) to a level of 195 MPa (~28344 psi), three specimens were tested at 1400°C in air and the results are given in Table III. One failed in 15 mins. due to a large pore while the other two failed in 20 and 69 hrs., respectively. Both of these specimen showed large regions of SCG, Figs. 39 and 40, similar to that observed at 1300°C in uniaxial tensile stress rupture tests, Figs. 29 and 34.

In an attempt to find out if slow crack growth also occurs in an inert environment at 1400°C, preliminary studies were done in an Argon gas environment. Two bend bar specimens were tested in stress rupture mode at applied stress levels of 234 MPa (34,000 psi) and 210 MPa (~30,470 psi) and failed in 12 mins. and 60 hrs., respectively, Table III. Specimen tested at the higher stress (234 MPa) basically behaved in the same fashion as those tested in air at the same temperature and stress, and essentially failed in fast fracture

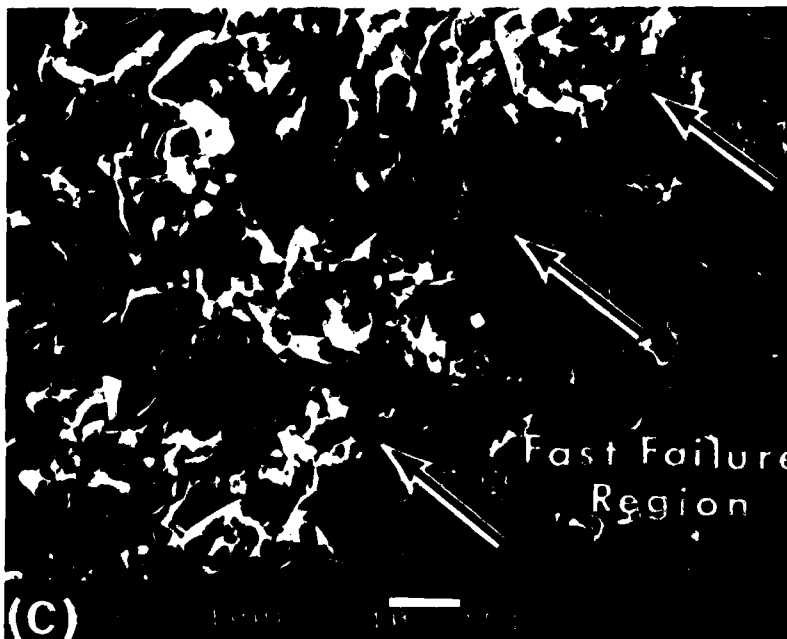
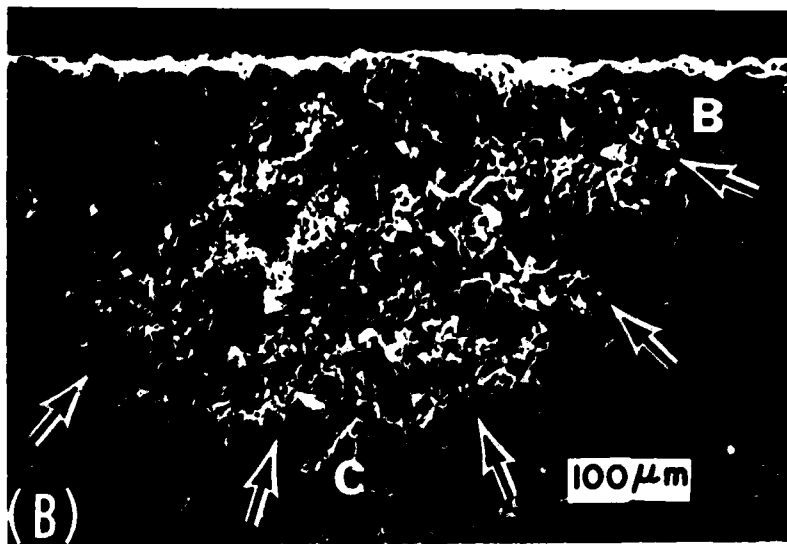
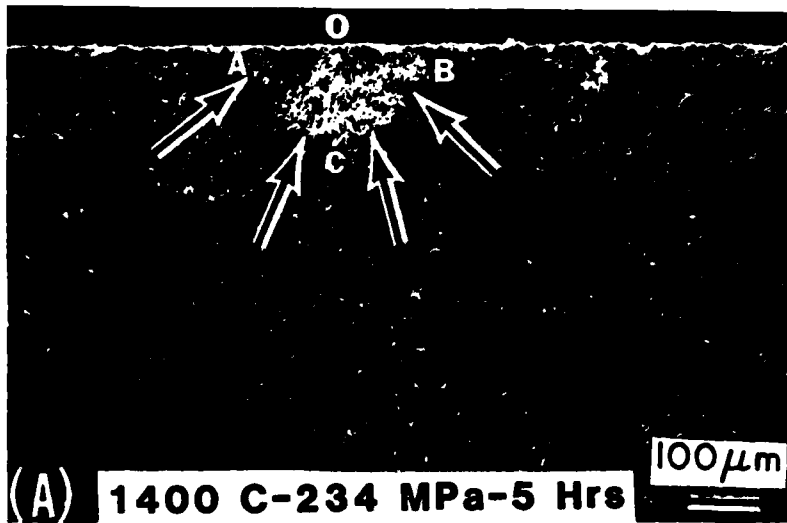


Figure 38

SEM micrographs of the fracture surface of a specimen tested in 4-pt. bending at 1400°C in air at 234 MPa and failed in 300 mins. (A) ACB is the slow crack growth region. (B) Higher magnification view showing porosity associated with SCG region. (C) Higher magnification view along the crack front (SCG region) boundary BC. Arrows separate the transition from slow crack growth to fast fracture region. Note the crack propagation in the SCG region is primarily intergranular while in the fast failure region it is transgranular.

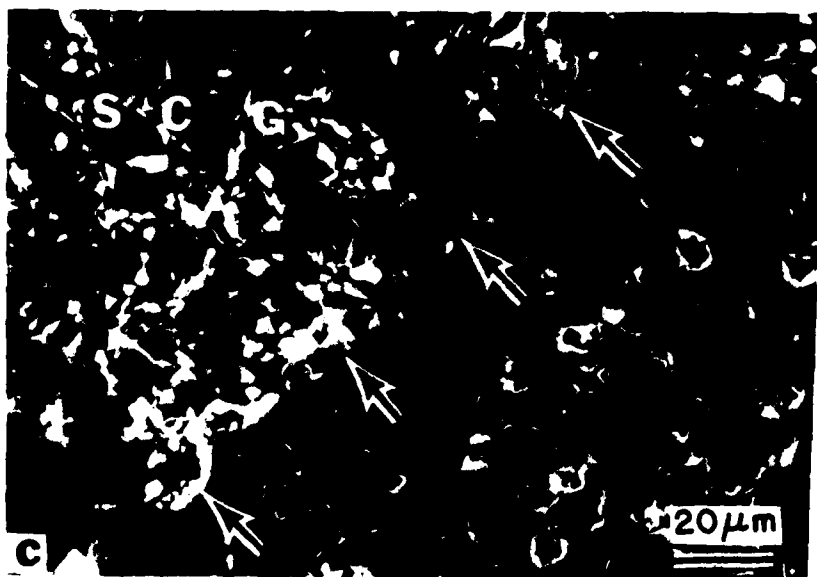
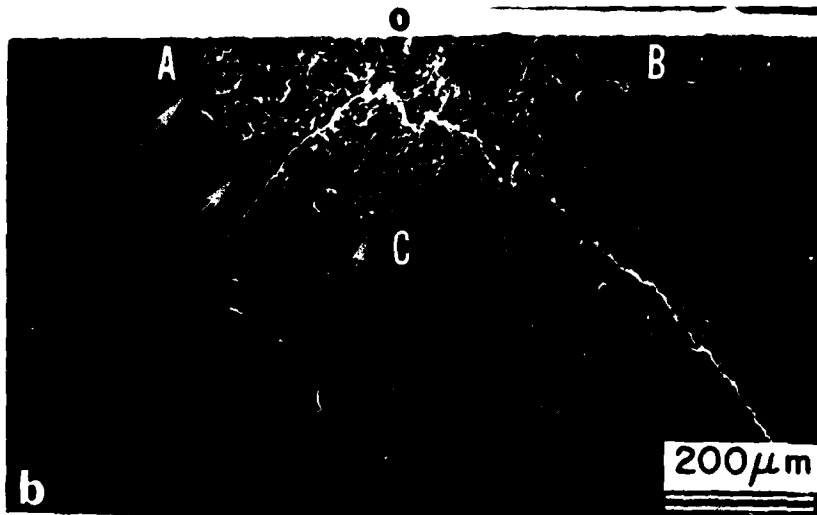
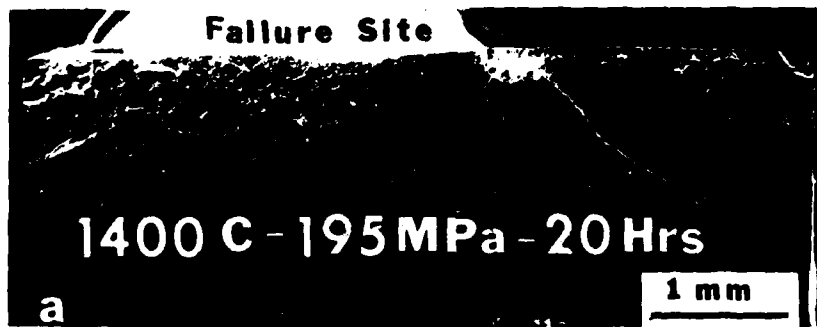


Figure 39

SEM micrograph of the fracture surface of a stress rupture specimen tested in 4-pt. bending. (a) Failure initiation site. (b) ACB is the slow crack growth region. Note the change in morphology of the fracture surface outside the slow crack growth region. (c) Circled area in (b) shown at a higher magnification. Arrows indicate the end of SCG region and start of the fast fracture region.

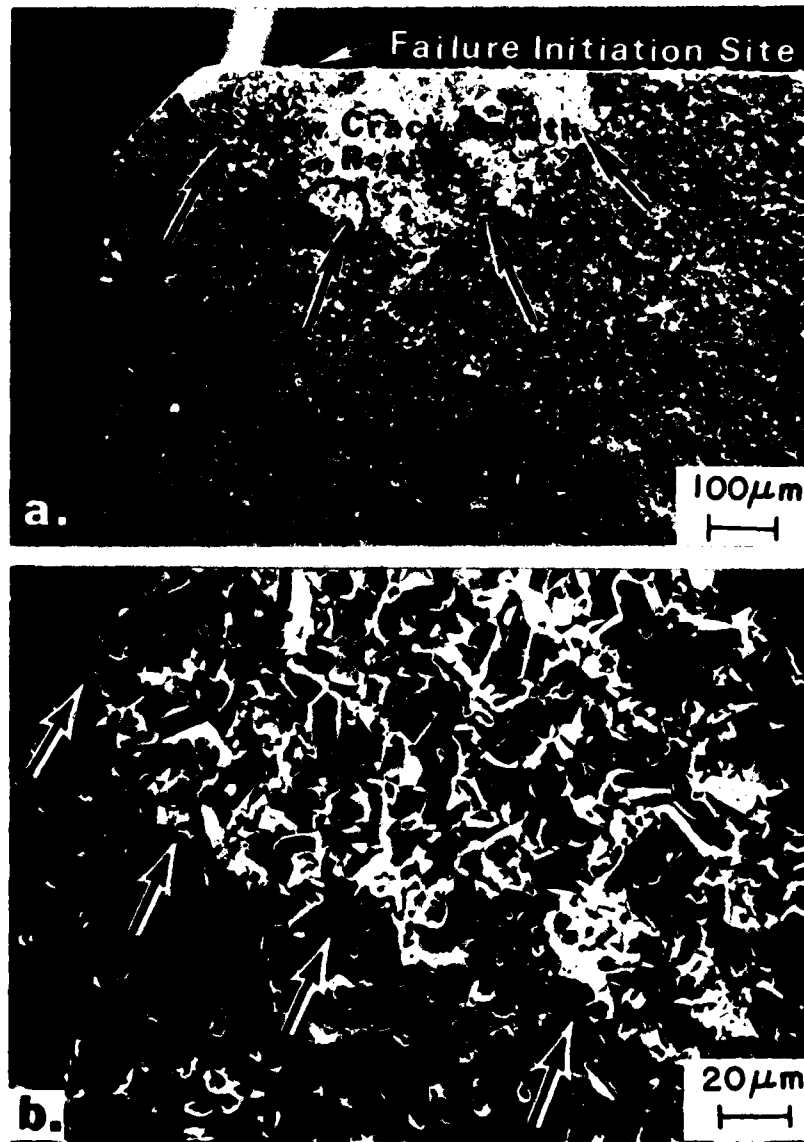


Fig. 40 SEM micrographs of the fracture surface of a stress rupture specimen tested in 4-pt. bending. (a) Failure initiation site and the associated slow crack growth region, ACB. (b) Circled area in (a) seen at a higher magnification. Arrows indicate the boundary of the SCG region.

mode. The specimen which was tested at a slightly lower stress (210 MPa) and sustained the stress for a fair length of time (60 hrs.) showed a large region of SCG, Fig. 41. The nature of crack propagation during SCG and fast fracture was similar to that observed in tests made at 1400°C in air, Figs. 38-40.

At 1300°C

A total of ten (10) bend bar type specimens were tested in flexural stress rupture mode at 1300°C in air and Argon gas environment at applied stresses varying from 327 MPa (~47,500 psi) to 210 MPa (~30,500 psi) and the time-to-failure varied from 18 mins. to 350 hrs., Table IV.

Three specimens were tested in air at applied stress levels of 327 MPa (close to mean strength of 337 MPa) and failed within 4 hrs. in an essentially fast fracture mode (brittle manner).

The applied stress was lowered to 293 MPa (~42,500 psi) and three specimens were tested at 1300°C in air and the times-to-failure were 1.3 hrs., 26 hrs., and 53 hrs., respectively. Fracture surface for the specimen which survived 53 hrs. is shown in Fig. 42 and shows clearly the origin of failure to be associated with subsurface porosity surrounded by a large region of SCG similar to the type seen earlier were visible.

The magnitude of the applied stress was decreased to 244 MPa (~35,400 psi) and a specimen was tested at 1300°C in air. The specimen sustained the stress for a long time and failed after 152 hrs. Examination of the fracture face revealed a large region of failure site associated with surface (tensile edge), Fig. 43(A). The failure site is actually a zone of SCG, distinct in its appearance, surrounded by a fast fracture region, Fig. 43(B). Inside the SCG region grain boundary separation and thus forming zig-zag pores characteristic of creep cavitation in metals were noticeable, Fig. 43(C).

The applied stress was further decreased to 210 MPa (30,500 psi) and the specimen sustained the stress for a significantly longer time, failing after 358 hrs. Fracture face showed a large SCG region, Fig. 44, associated with surface similar to that seen earlier.

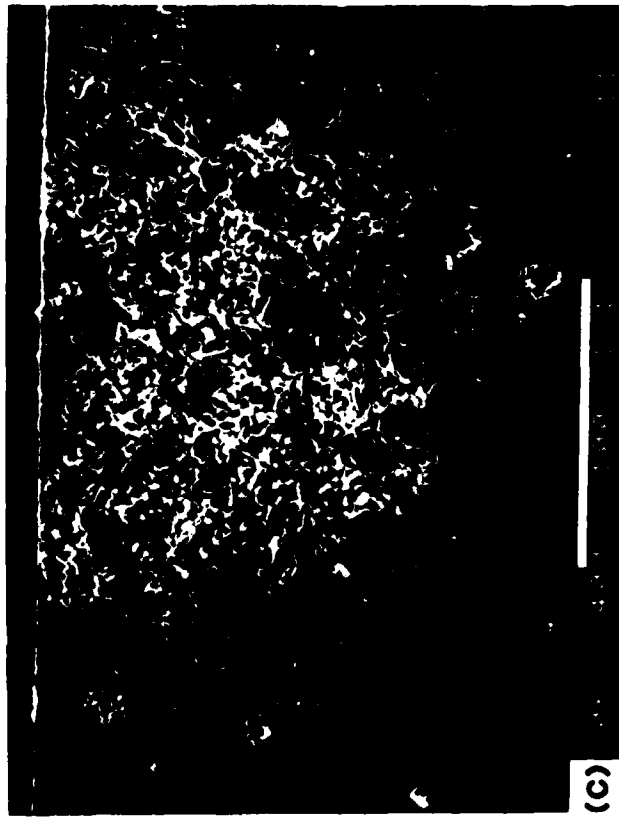
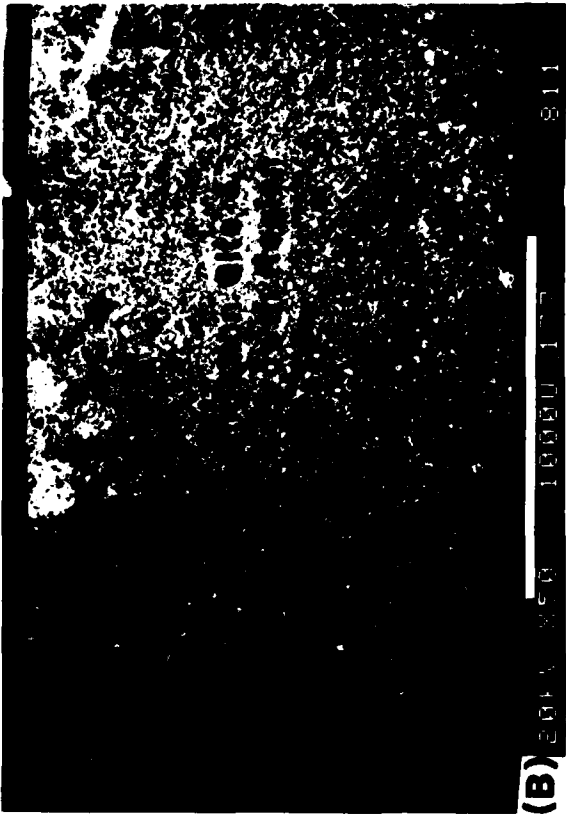


Fig. 41 SEM micrographs of the fracture surface of a flexural stress rupture specimen tested at 1400°C in partial Argon gas environment. (A) Overall view of the fracture surface. (B) Failure initiation site and the associated slow crack growth region. (C) Higher magnification view of the SCG region. (D) Arrow indicates the transition from slow crack growth to fast fracture. Note the separation of grains inside the SCG region indicating intergranular crack propagation while transgranular crack propagation outside it (in the fast fracture region).

TABLE IV. FLEXURAL (4-POINT BENDING) STRESS RUPTURE RESULTS AT 1300°C SINTERED ALPHA SiC

Specimen No.	Applied Stress (MPa)	Time to Failure	Failure Origin
Testing Temperature: 1300°C in Air			
1	327	18 min.	Surface pore; no visible SCG.
2	"	2 hrs.	Crushed; not visible.
3	"	3.5 hrs.	" " "
4	293	1.3 hrs.	Crushed; not visible.
5	"	26 hrs.	Broke in 3 pieces; not visible.
6	"	53 hrs.	Porosity and SCG, Fig. 42.
7	244	152 hrs.	Large SCG region, Fig. 43.
8	210	358 hrs.	Large SCG region, Fig. 44.
Testing Temperature: 1300°C in Argon			
9	293	27 hrs.	Porosity and SCG, Fig. 45
10	244	+81 hrs.	Large SCG region, Fig. 46

+ Stepped Stress Rupture Test.

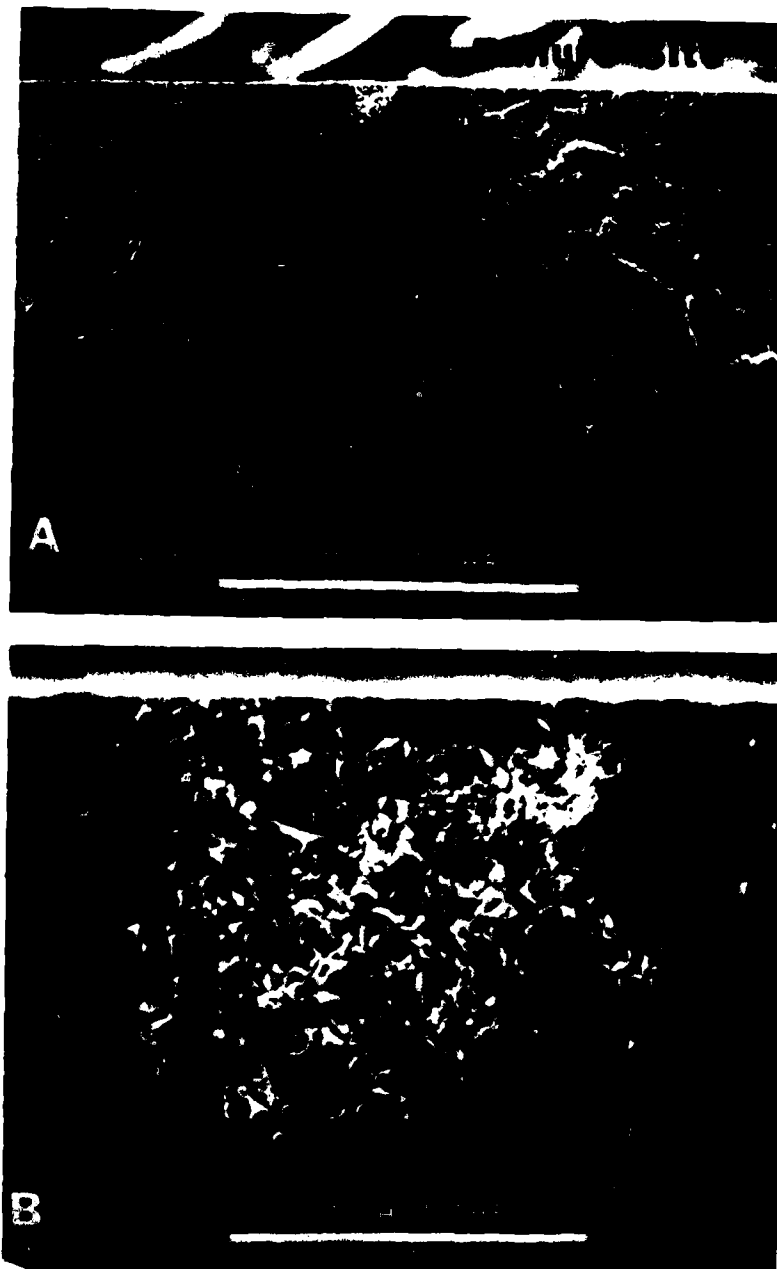


Fig. 42 SEM micrographs of the fracture surface of a flexural stress rupture specimen tested at 1300°C in air. (A) Failure initiation site (B) Porosity and the associated slow crack growth region.

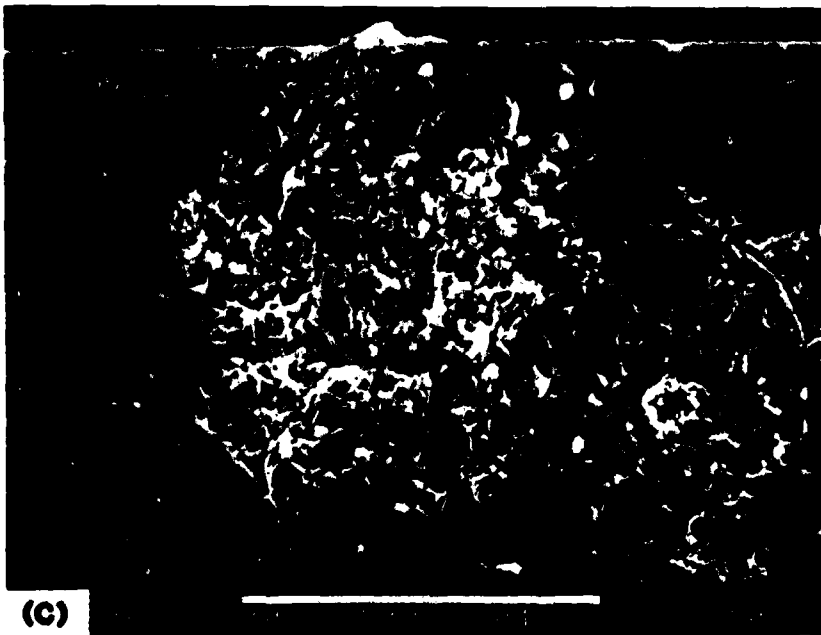
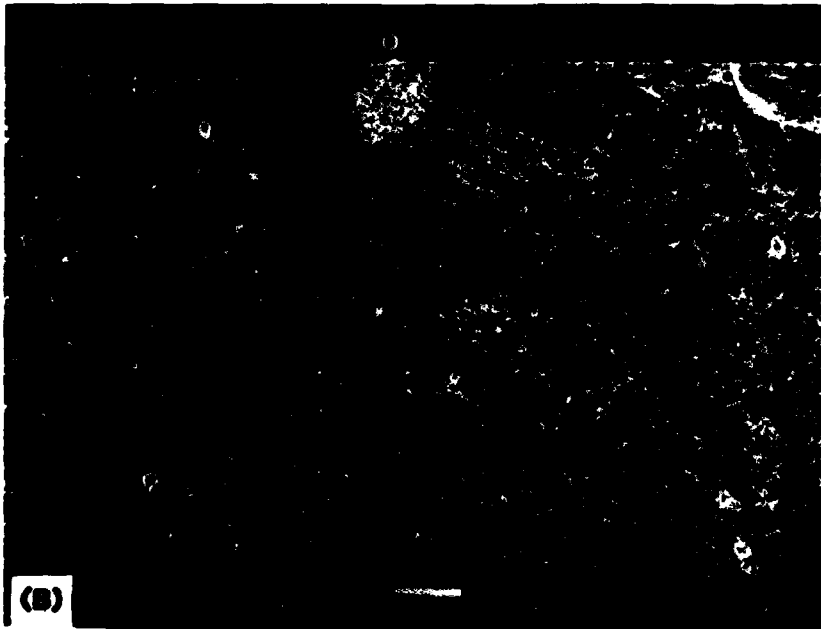
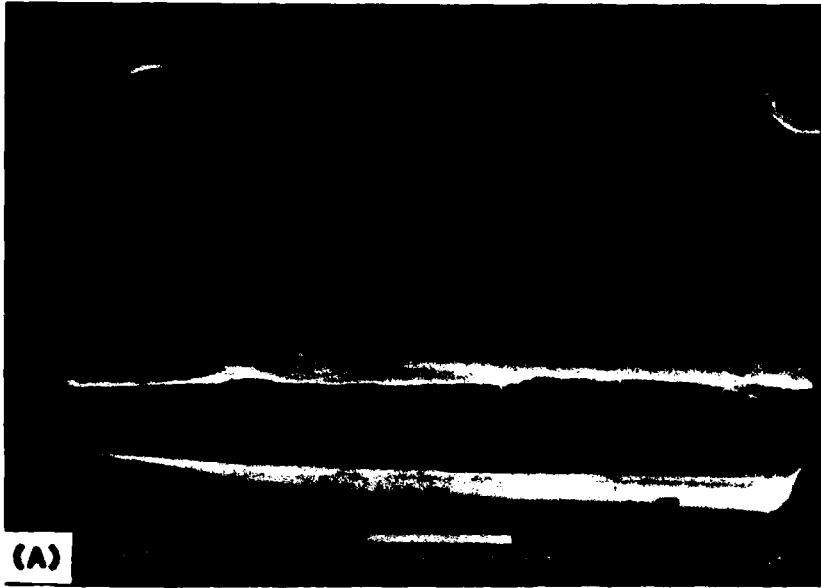


Figure 43

SEM micrographs of the fracture surface of a flexural stress rupture specimen. (A) Overall view of the fracture surface. (B) Failure origin ACB is the slow crack growth region. (C) Higher magnification view of the slow crack growth region. Note the grain boundary openings.

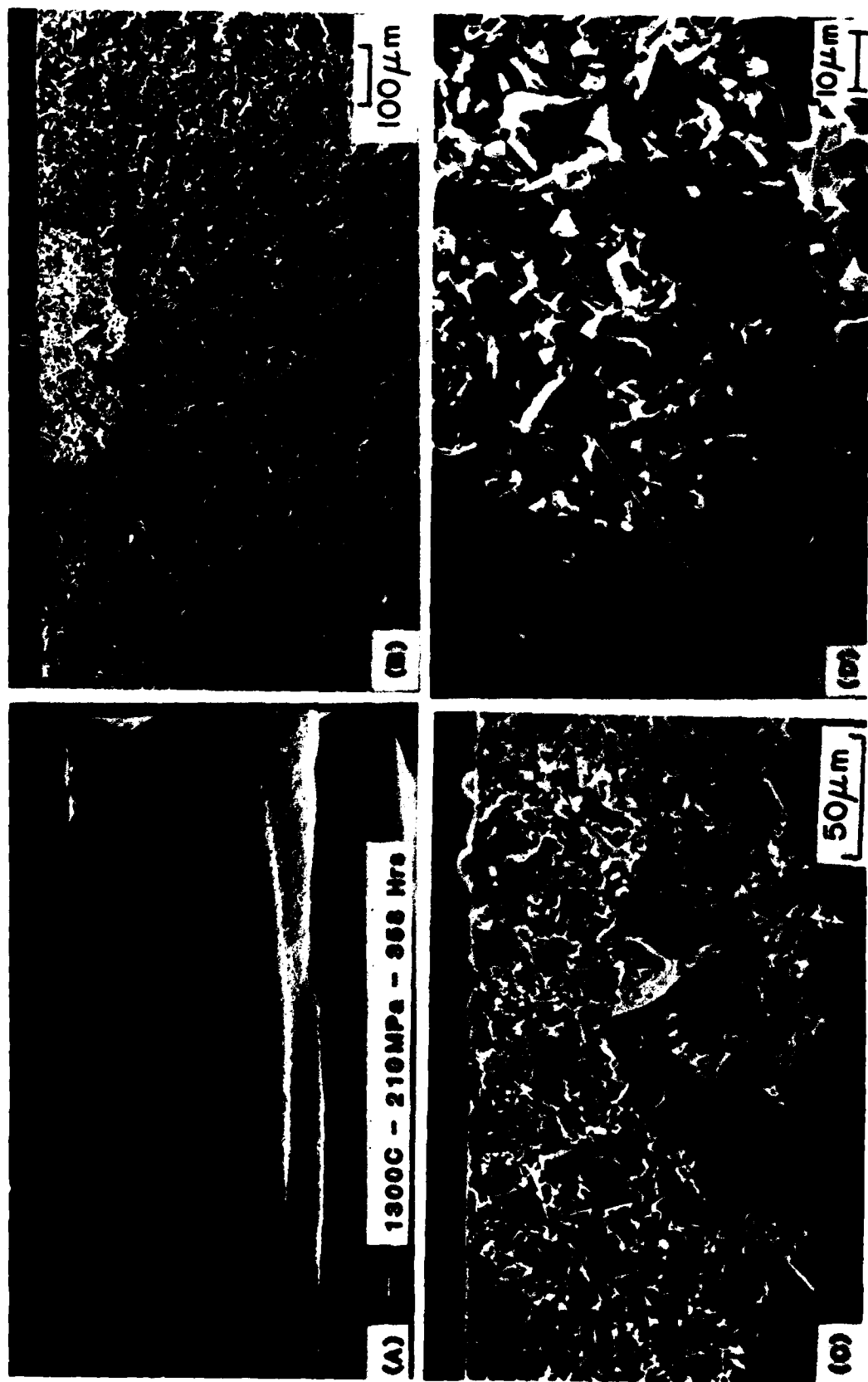


Fig. 44 SEM micrographs of the fracture surface of a flexural stress rupture specimen. (A) Overall view of the fracture surface (B). ACB is the slow crack growth region. (C) Higher magnification view of the SCG region. (D) Arrow indicates the transition from SCG region to fast fracture.

Two specimens were tested at 1300°C in Argon gas environment to determine if the nature of SCG is the same as in air, Table IV. First specimen was tested at the same stress level of 293 MPa as those tested in air and failed in 27 hrs. Examination of the fracture face, Fig. 45, revealed that the surface associated failure region seen consisted of large voids inside the semi-circular failure zone, Fig. 45(C) and showed limited SCG, Fig. 45(D).

Another bend bar specimen was tested in a stepped stress rupture fashion at 1300°C in Argon gas environment. The specimen was first subjected to a stress of 244 MPa and sustained it for 27 hrs. The stress was increased to 293 MPa and sustained it for 48 hrs. Finally, the stress was increased to 327 MPa and the specimen failed after sustaining the stress for 6 hrs. Examination of the fracture face showed localized, surface associated slow crack growth region, Fig. 46, similar to those tested in air.

From the preliminary tests carried out in Argon gas environment at 1400° and 1300°C, it is clear that the localized SCG regions formed under constant stress conditions are not significantly influenced by oxidation of α -SiC.

The oxidation kinetics of sintered α -SiC has been investigated over the temperature range 1200° to 1500°C in air by Costello and Tressler¹¹. McHenry and Tressler¹² conducted stress rate tests on sintered α -SiC in the temperature range 900-1100°C in oxygen partial pressures of 10^{-4} and 10^{-8} atm and found the absence of slow crack growth. However, after oxidation and after oxidation and etching, a stressing rate dependence of the fracture stress was found. The values of the crack velocity exponent, n , at 1000°C were 41 and 25 for oxidized samples and oxidized and etched samples, respectively. The α -SiC after oxidation may contain a borosilicate phase as a result of SiO_2 and B_2O_3 formation during oxidation.

At 1200°C

Flexural stress rupture studies have been made in detail by Quinn^{1,2,9} on two versions of α -SiC (1978 and 1980, sintered α -SiC from Carborundum Co.) at 1200°C in air and as such no efforts were made to carry out similar studies. Quinn has been kind enough to supply this data for inclusion in this report.

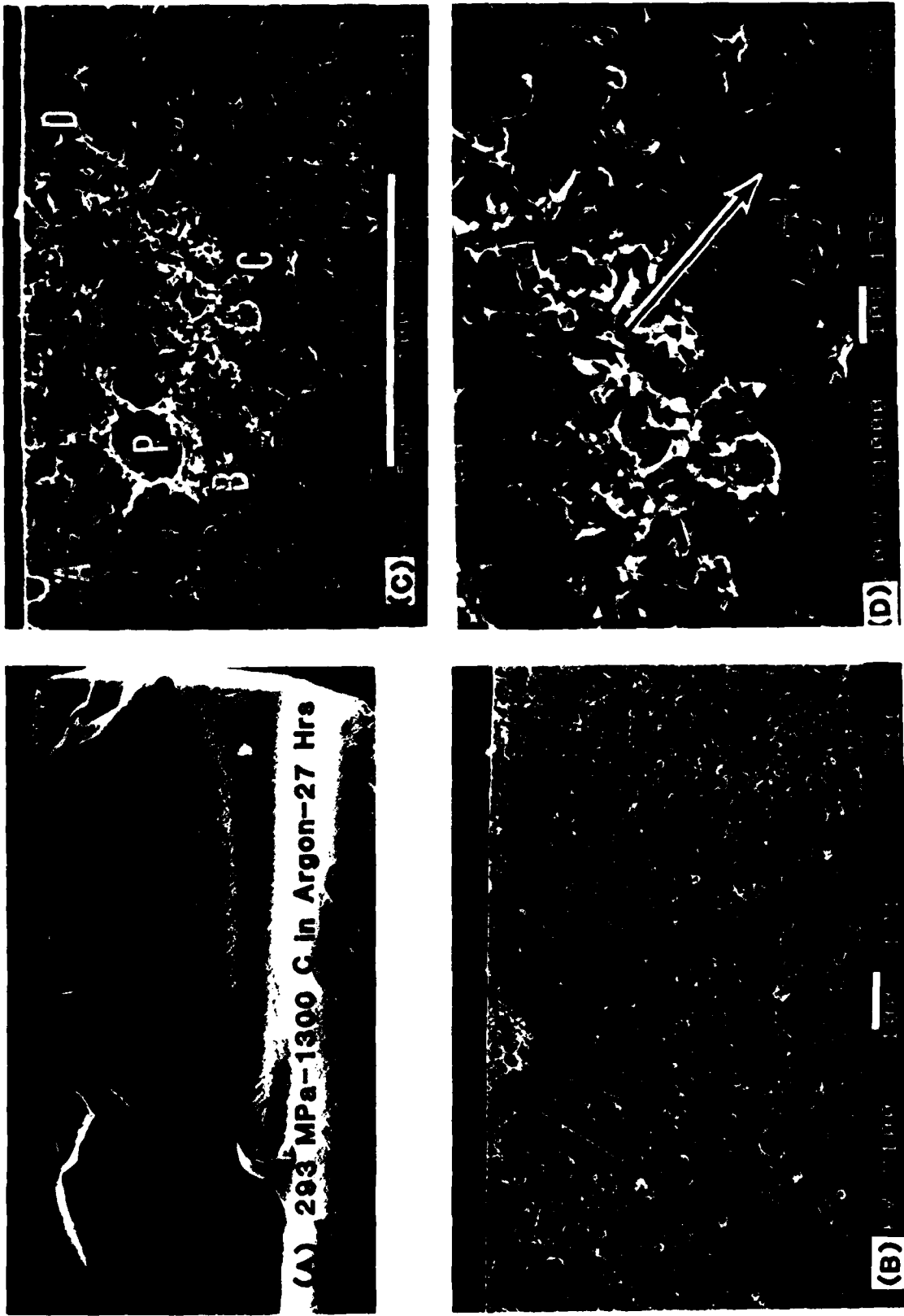


Fig. 45 SEM micrographs of the fracture surface of a flexural stress rupture specimen tested at 1300°C in partial Argon gas environment. (A) Overall view of the fracture surface (B) Failure Initiation Region (C) Higher magnification view of the failure site showing that ABCD is the slow crack growth region. Note large porosity (P) inside the SCG region. (D) Arrow indicates the transition for slow crack growth to fast fracture.

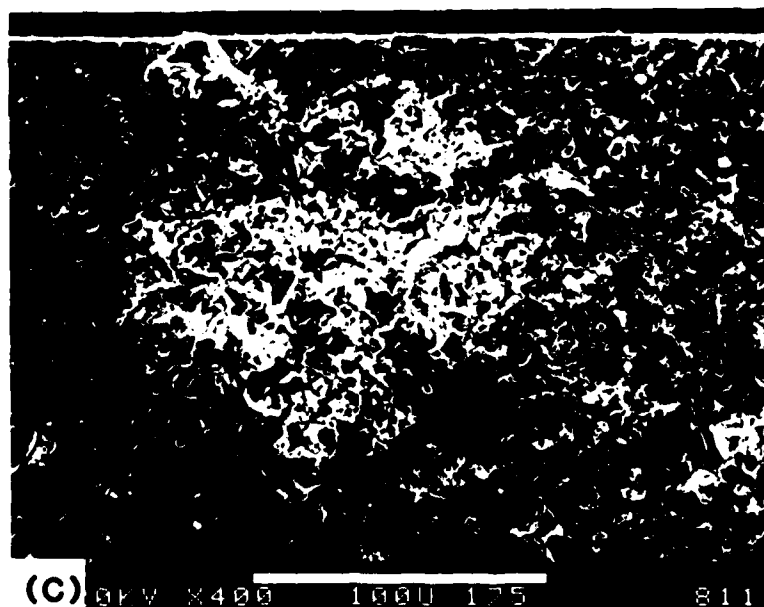
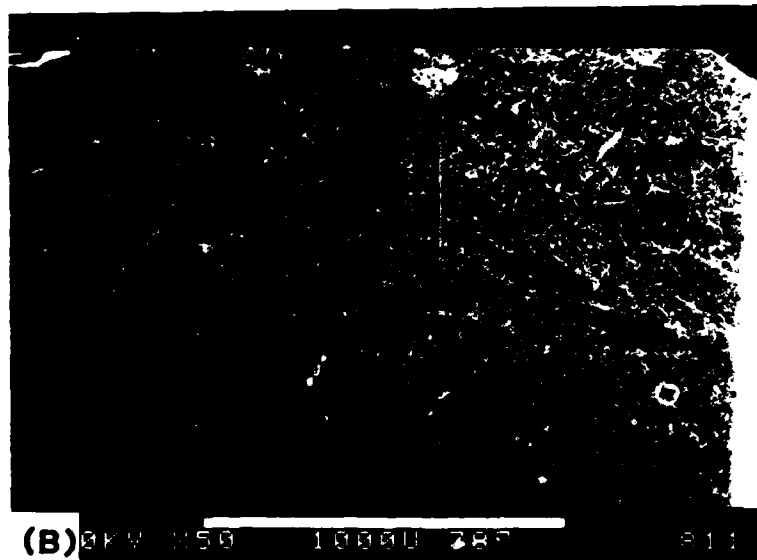
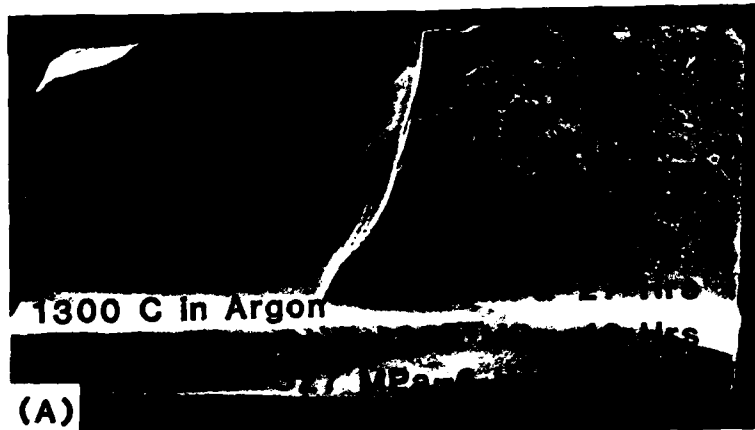


Figure 46

SEM micrographs of the fracture surface of a flexural stepped stress rupture specimen tested at 1300°C in partial Argon gas environment. (A) Overall view of the fracture surface. (B) Arrows indicate the SCG region. (C) Higher magnification view of the SCG region.

TABLE V. FLEXURAL STRESS RUPTURE DATA AT 1200°C FOR SINTERED α -SiC (CARBORUNDUM 1978*) AS SUPPLIED BY GEORGE QUINN[†]

Specimen No.	Applied Stress MPa	Time-to-Failure (hours)
1	414	Failed on loading
2	345	" " "
3	340	" " "
4	"	45 seconds
5	330	24 minutes
6	"	22 seconds
7	"	Failed on loading
8	320	25 minutes
9	"	2.12 hours
10	"	Failed on loading
11	"	" " "
12	310	8.3 hours
13	"	0.9 hours
14	"	3 minutes
15	"	19.7 hours
16	300	Failed on loading
17	"	" " "
18	"	0.8 hour
19	"	2 minutes
20	"	32 seconds
21	290	2.4 hours
22	"	0.9 hours
23	"	6.9 hours
24	"	Failed on loading
25	280	19.3 hours
26	"	2.8 hours
27	270	12 hours
28	"	280.7 hours
29	260	314.9 hours
30	"	3.8 hours
31	250	110 hours
32	"	720 hours
33	"	506.3 hours

Sample Size: width - 0.110" thickness - 0.085" and length - 2".

[†] Army Materials and Mechanics Research Center, Watertown, Mass. 02172.

* Average Fracture Strength at 20°C = 363 MPa with a Standard Deviation = 45 MPa. Weibull modulus = 10.6.

Quinn^{2,9} investigated the 1978 sintered α -SiC material and the data are given in Table V. The average flexural strength (four-point bending) at 20°C was 363 MPa with a standard deviation of 45 MPa. The Weibull modulus was 10.6. Assuming that the material obeys a simple power law crack velocity-stress intensity relation ($V = A K_I^n$), one can analyze the data in terms of log stress-log time curve and the slope is 1/n as shown in Fig. 47. The value of the exponent, $n = 40.8$. Considerable scatter in the data (two orders of magnitude, Table V and Fig. 47) is self evident. All fracture surfaces were examined but none revealed the presence of SCG at 1200°C. Almost all failure origins were associated with surface porosity.

Quinn¹ has recently also investigated the 1980 sintered α -SiC material, the data showed an extreme scatter (four orders of magnitude) as given in Table VI and Fig. 48, respectively. A value of the exponent, $n=24.6$ was obtained from the plot, Fig. 48. The large scatter in stress rupture data can only be partly attributed to low Weibull modulus ($m=5.2$). Again, examination of the fracture surfaces did not reveal the presence of SCG in tests made at 1200°C. All fracture surfaces showed fast fracture appearance similar to that observed at 20°C and majority of the failure origins were associated with surface porosity.

3.5 Crack Velocity Exponent

The uniaxial tensile and flexural stress rupture results were also analyzed to estimate the values of the crack velocity exponent, n , in the crack velocity stress intensity relation, $V = AK_I^n$ (assuming that the material obeys this simple power law), for subcritical crack growth following the work of Davidge et al.¹³ and others^{9,14}. Under delayed fracture conditions, the ratio of failure times t_1 and t_2 under constant applied stresses σ_1 and σ_2 at a given temperature for a given environment is approximately given by^{9,13,14}:

$$\frac{\sigma_1}{\sigma_2} = \left(\frac{t_2}{t_1} \right)^{1/n} \quad (1)$$

A plot of $\log \sigma$ vs $\log t$ would result in a straight line with a slope of 1/n. The results for uniaxial tensile stress rupture testing of sintered α -SiC at 1200°C and 1300°C are shown in Fig. 49. Because of scatter and limited experimental data points, no least-squares analysis was done for curve fitting. At 1200°C and 1300°C, the values of n obtained from the plot (Fig. 49) were about 27 and 21,

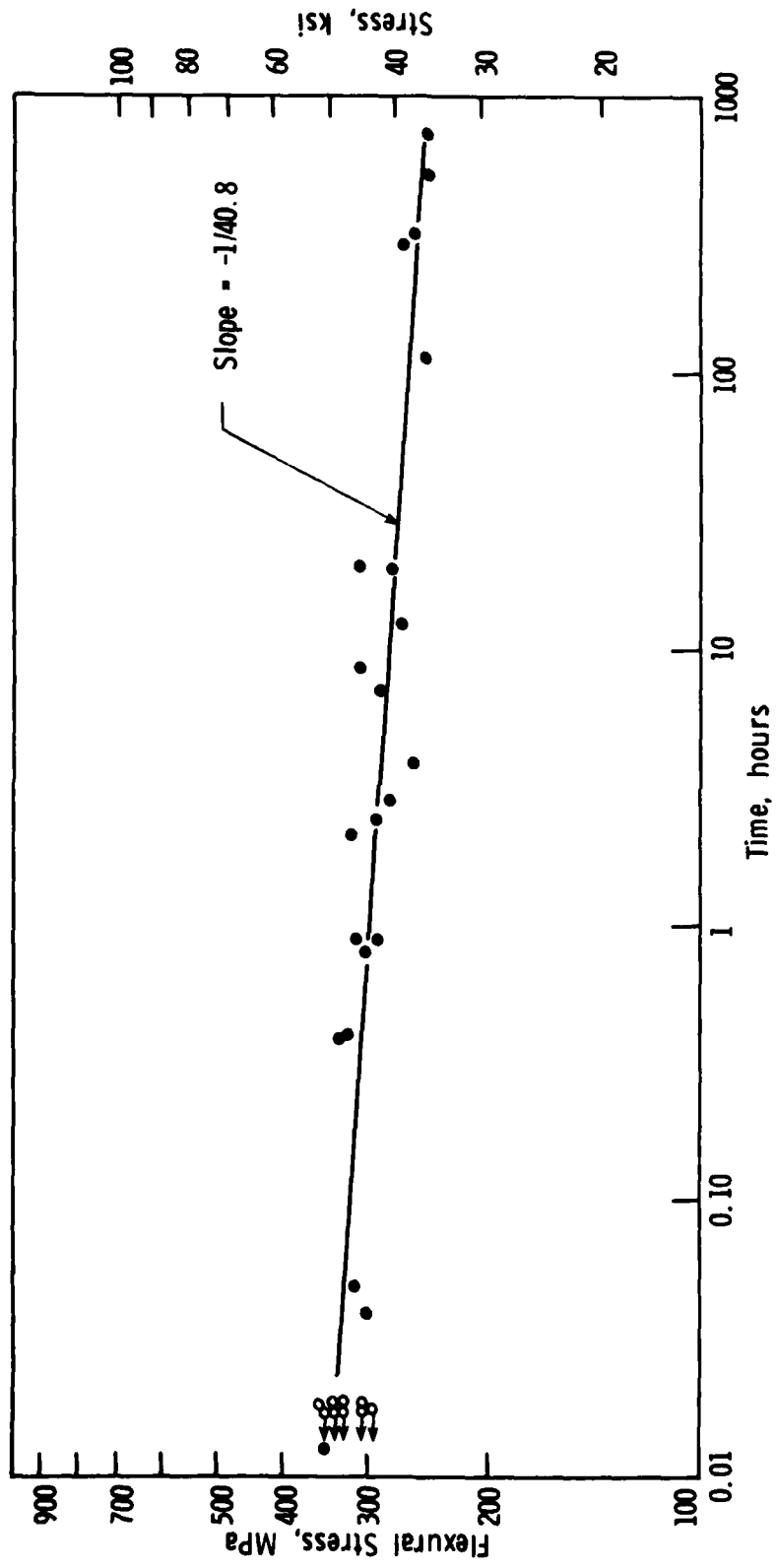


Fig. 47 Flexural stress rupture at 1200°C for Carborundum sintered alpha SiC (1978).
Courtesy of G. Quinn, AMMRC.

TABLE VI. FLEXURAL STRESS RUPTURE DATA AT 1200°C FOR SINTERED α -SiC (CARBORUNDUM 1980*) AS SUPPLIED BY GEORGE QUINN⁺

Specimen No.	Applied Stress MPa	Time-to-Failure (hours)
1	550	Failed on loading
2	"	" " "
3	"	0.018
4	500	0.422
5	"	Failed on loading
6	"	" " "
7	"	" " "
8	"	" " "
9	450	" " "
10	"	" " "
11	"	0.037
12	"	0.18
13	"	0.52
14	400	Failed on loading
15	"	" " "
16	"	13.6
17	"	0.072
18	"	1.07
19	"	0.21
20	"	3.4
21	350	0.033
22	"	87.3
23	"	383.0
24	"	Failed on loading
25	"	1.07
26	"	138.5
27	300	Failed on loading
28	"	19.9
29	"	9.1
30	"	584.7
31	"	13.9
32	280	1461.0
33	"	863.0
34	260	3.6
35	"	Over 4000
36	200	Survived 1005
37	"	" "

Sample size: width - 0.110", thickness - 0.085" and length - 2".

⁺ Army Materials & Mechanics Research Center, Watertown, Mass. 02172.

* Average Fracture Strength at 20°C = 407 MPa with a Standard Deviation = 82 MPa. Weibull modulus = 5.2.

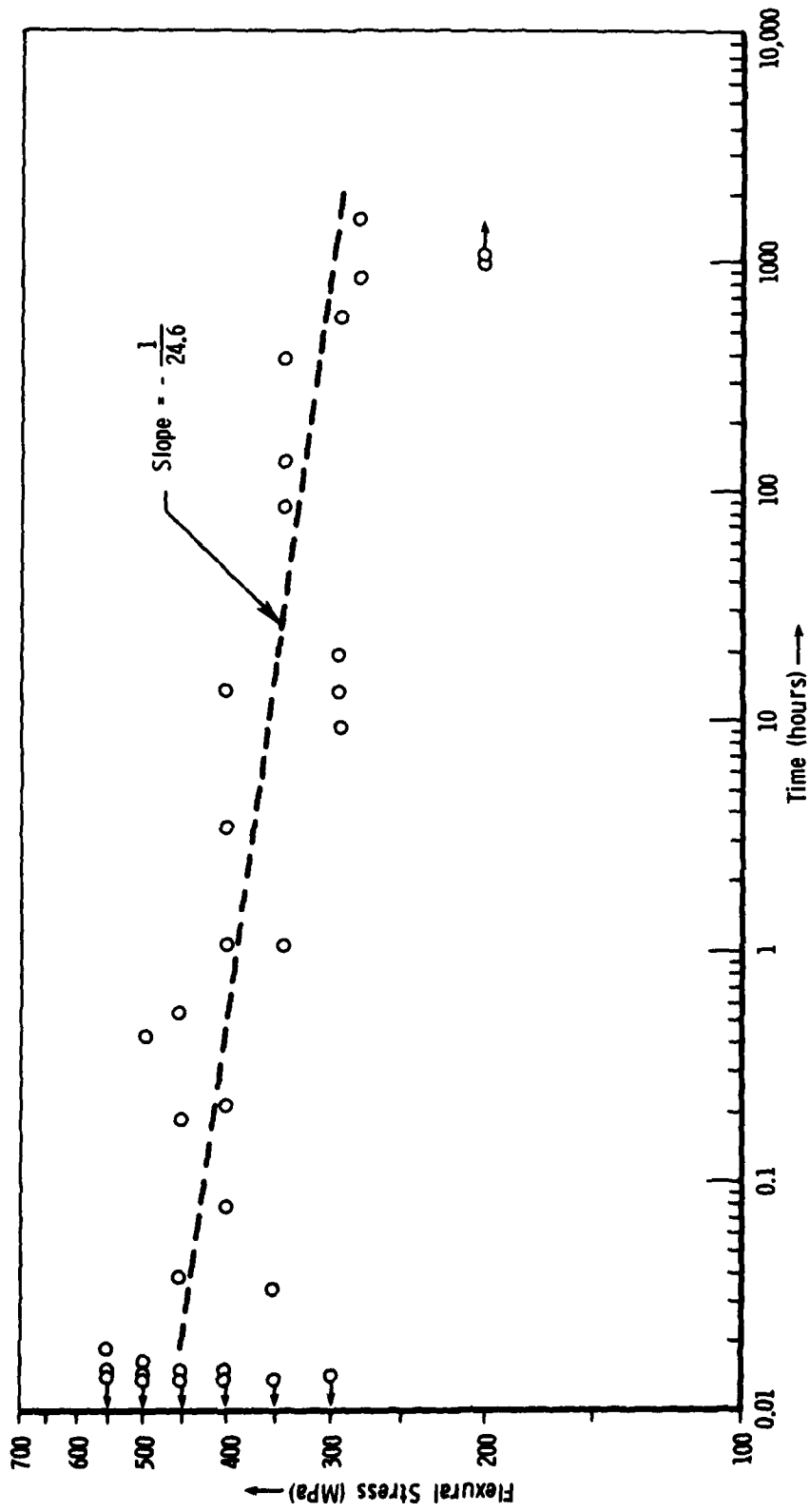


Fig. 48 Flexural stress rupture at 1200°C for Carborundum sintered alpha SiC (1980).
 Courtesy of G. Quinn, AMMRC.

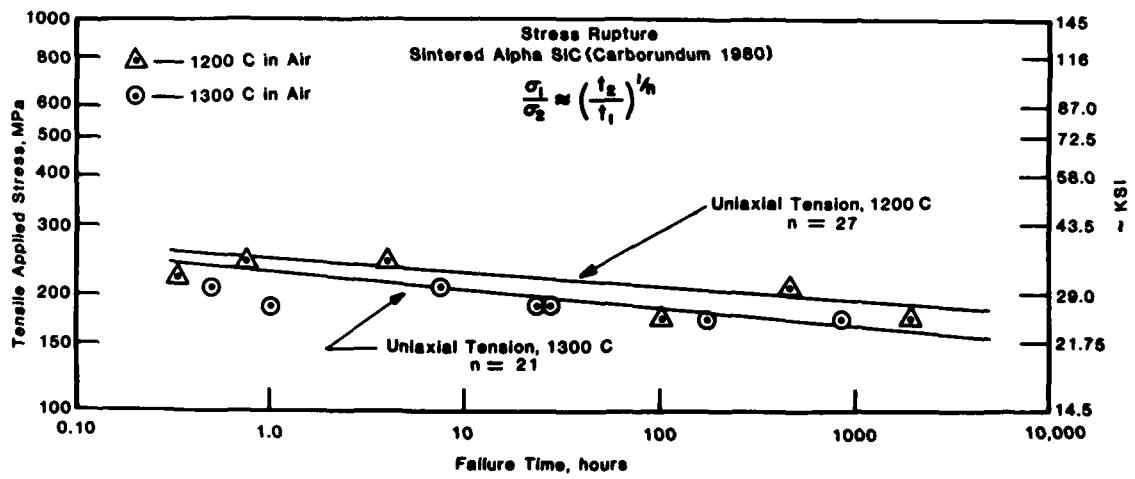


Fig. 49 Uniaxial tensile stress rupture results.

respectively. Both values are comparable in magnitude but the trend is clearly indicated towards a lower n value at the higher temperature suggesting the presence of slow crack growth. This was confirmed by the fracture surfaces of specimens tested at the higher temperature of 1300°C in air which showed clearly the large regions of slow crack growth (Figs. 28-29, 31, 32 and 34). Only restricted and limited evidence for the presence of slow crack growth was observed in tensile stress rupture tests at 1200°C after the specimen sustained the stress for a significant length of time (see Figs. 17, 18 and 22). It should be pointed out that flexural stress rupture tests carried out at 1200°C in air by Quinn at high applied stress levels which sustained the stress for a significantly long time (e.g. 350 MPa-383 h, 300 MPa-585 h, 280 MPa-1461 h, Table VI) failed to show the presence of slow crack growth on the fracture surfaces. This illustrates the importance of uniaxial tensile stress rupture testing in revealing the presence of slow crack growth compared to flexural stress rupture testing.

The results for flexural stress rupture testing at 1300° and 1400°C in air for sintered α -SiC are shown in Fig. 50, and the values of n obtained were 16 and 13, respectively. Again, the value of the crack growth exponent, ' n ', decreases as the temperature and the extent of slow crack growth increases. Quinn^{9,2,1} reported values of n at 1200°C in air to be around 41 for 1978 α -SiC and 25 for 1980 α -SiC, respectively, using flexural stress rupture testing method. Both groups of material (1978 α -SiC & 1980 α -SiC) showed large variations in time-to-failure for a given applied stress. It should be pointed out that greater emphasis should be given on actual observations of fracture surfaces of test specimens in regard to the presence of subcritical or slow crack growth rather than on quantitative data points.

3.6 High temperature Annealing Effects

In order to determine the influence of annealing at high temperatures ($\geq 1000^{\circ}\text{C}$) in air on the fracture strength of sintered α -SiC, a series of bend bar type specimens was precracked at room temperature using Knoop Indenter with 4000 gm indentation load. The Knoop indenter introduces a

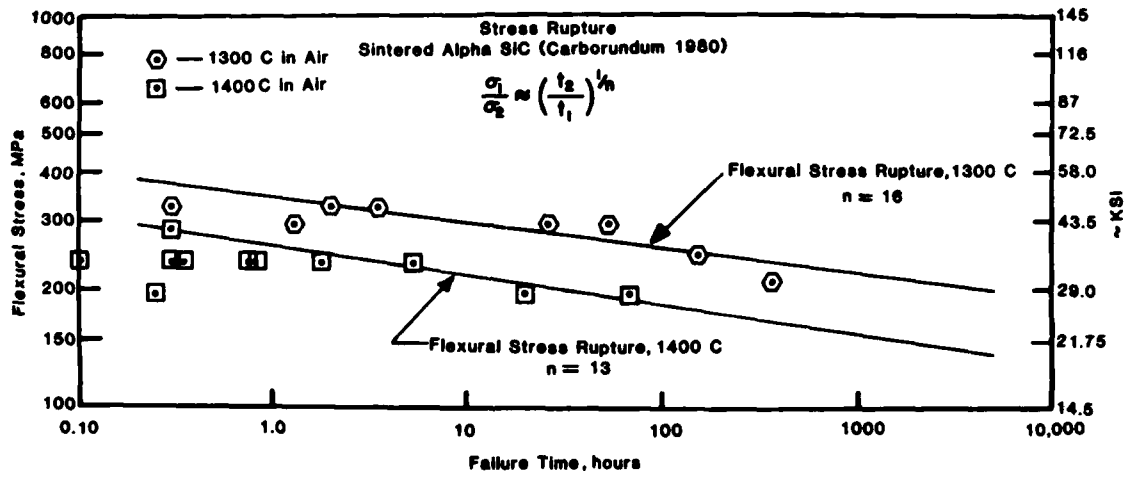


Fig. 50 Flexural stress rupture results.

surface flaw whose size (length on the surface and depth) can be controlled by choice of the indenter load. Complete details regarding the introduction of flaws have been given elsewhere³.

Precracking sintered α -SiC specimens with a 4000 gm Knoop indenter introduces a semi-circular or elliptical type crack whose depth varies from 0.145 to 0.155 mm. The precracked specimens were annealed in air at 1000^o and 1200^oC for 4 hrs. and subsequently tested in 4-point bending at 20^oC. The room temperature fracture stress, σ_F , variation as a function of annealing temperature is given in Table VII. In order to compare the increase in magnitude of σ_F for annealed specimens relative to room temperature fracture strength, two precracked specimens were tested at 20^oC and failed at the precrack site at 149 and 159 MPa. Specimens annealed at 1000^oC failed at the precrack site and σ_F varied from 209 to 317 MPa with an average value of 271 MPa showing an increase of over 50% compared to σ_F at 20^oC. The two specimens annealed at 1200^oC showed a significant increase in σ_F (average σ_F =324 MPa) relative to room temperature strength (154 MPa) of precracked samples. Furthermore, these annealed specimens did not break at the precrack site and failed at a site some distance from the Knoop indentation. A typical fracture surface for one of these specimens (σ_F =292 MPa) is shown in Fig. 51. The fact that precracked specimens had a flaw close to twice the size of inherent (processing) flaws and still did not fail at the precrack site suggests the possibility of crack tip blunting or healing which results in high values of fracture strength. It is possible that oxidation could also be assisting the crack tip blunting process.

4. SUMMARY

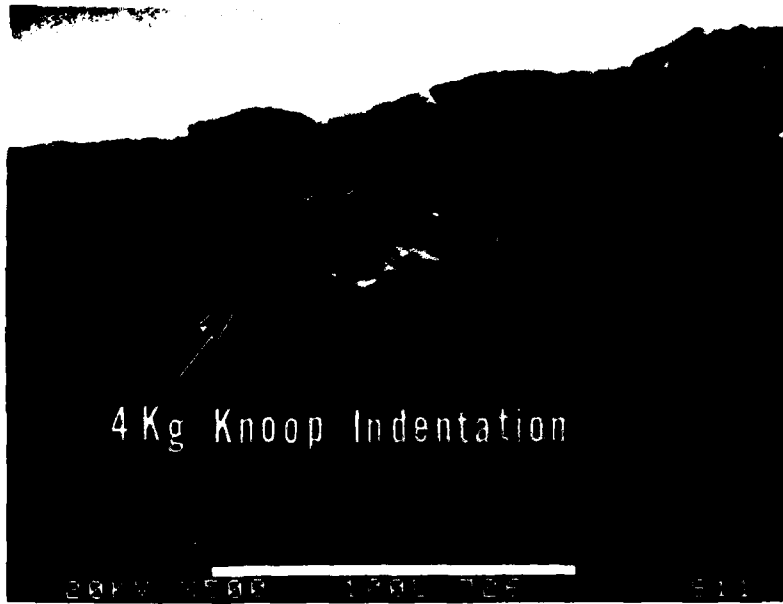
Detailed and careful uniaxial tensile stress rupture tests were made at 1200^o and 1300^oC in air on sintered α -SiC (Carborundum 1980) to investigate the presence of subcritical crack growth. At 1200^oC, limited fractographic evidence showed the presence of slow crack growth. In a majority of the failures, fractographic evidence showed the presence of a large pore (combination of interconnecting pores) as the failure site. The material could sustain applied stress of 175 MPa for a reasonable time (>100 hrs.) without

TABLE VII. FLEXURAL (4-POINT BEND) STRENGTH VS. ANNEALING TEMPERATURE
 DATA FOR SINTERED α -SiC SPECIMENS PRECRACKED WITH 4000 g
 KNOOP IDENTATION

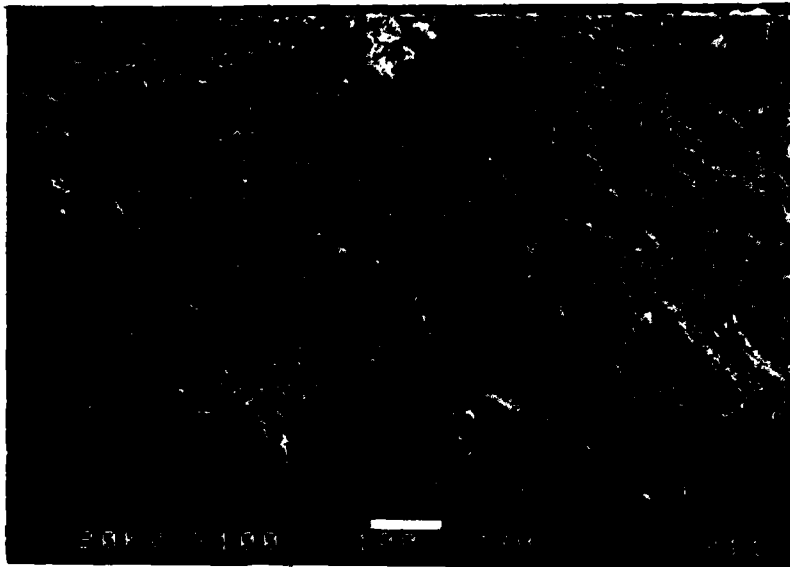
Specimen No.	Annealing Temp.	Fracture Stress at 20°C, MPa	Remarks
1	1000°C	317	Failed at the crack
2	"	305	" " " "
3	"	243	" " " "
4	"	209	" " " "
5	"	281	" " " "
6	1200°C	292	Did not fail at the crack
7	"	356	" " " " " "
8	20°C	149	Failed at the crack
9	"	159	" " " "

Average strength for the as received sintered α -SiC = 337 MPa at 20°C. Depth of crack due to 4000 g Knoop identification is approximately 150 μ m.

(A)



(B)



(C)

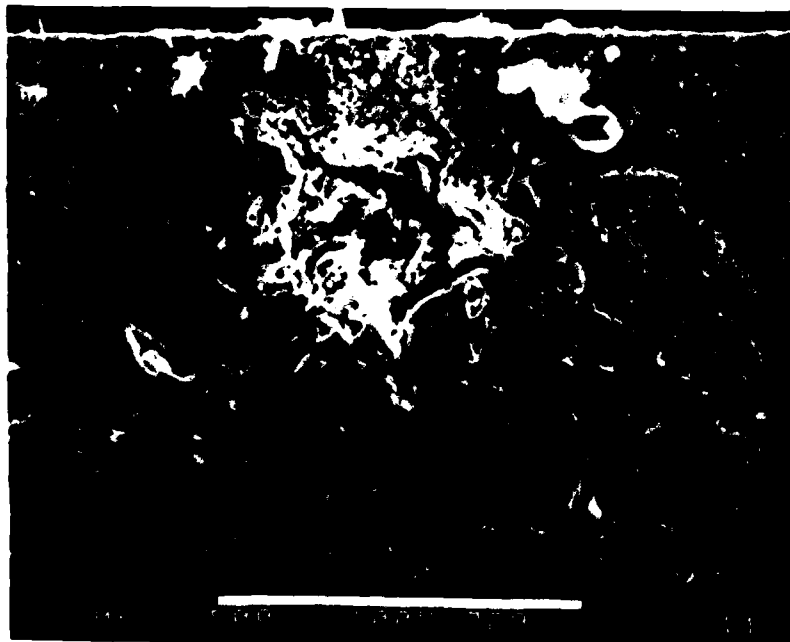


Figure 51

SEM micrographs of a pre-cracked specimen, annealed at 1200°C in air for 4 hrs. and subsequently tested in 4-pt. bending at 20°C. (A) Failure did not occur at the precrack site (Knoop indentation) but away from it. (B) Failure occurring at a subsurface porosity. (C) High magnification view of the failure site.

showing signs of degradation in strength. The nature of crack propagation during slow crack growth and fast fracture is primarily intergranular and transgranular, respectively. Fractographic evidence showed the presence of porosity in promoting the initiation of slow crack growth.

Flexural stress rupture tests performed at 1300° and 1400°C clearly showed the presence of slow crack growth. The amount of slow crack growth increased with increasing temperature and stress. Flexural stress rupture tests carried out at 1200°C in air by several investigators^{1,2,8-10} on essentially similar type sintered α -SiC failed to show fractographically the presence of slow crack growth similar to that seen in uniaxial tensile stress rupture tests at the same temperature. Values of the crack velocity exponent, n , were measured using flexural and tensile stress rupture methods and were found to be comparable.

The average fracture strength (in 4-point bending) of sintered α -SiC at 20°C is about 337 MPa with a Weibull modulus of 10.9. The material contains a uniform distribution of fine porosity of 0.5 μm to 3 μm along grain boundaries and randomly occurring large flaws usually in size ranging from 20 μm to 80 μm (interconnected pores). These large pores are the most common site for surface initiated failures. The flexural strength is independent of temperature from 20° to 1400°C. The flexural strength evaluation technique is not sensitive enough to reveal the presence of subcritical or slow crack growth at temperatures of 1200°C and lower.

The uniaxial tensile stress rupture testing is more sensitive in revealing the presence of slow crack growth fractographically compared to flexural stress rupture testing.

Acknowledgement

The author is thankful to R. Elder for helping partly in doing the tensile stress rupture testing, and to R. Goss for doing SEM work. Thanks are due to Dr. E. M. Lenoë, AMMRC, for suggestions from time-to-time in carrying out the program. Finally, it is a pleasure to thank T. J. Whalen and A. F. McLean for reviewing the report.

References

1. G. Quinn, "Stress Rupture of Sintered Alpha SiC," Tech. Rept. AMMRC TN81-4, Dec., 1981.
2. G. Quinn and R. N. Katz, "Time-Dependent High Temperature Strength of Sintered Alpha SiC," J. Amer. Ceram. Soc. 63 [1-2], 117 (1980).
3. R. K. Govila, "Ceramic Life Prediction Parameters," Tech. Rept. AMMRC TR 80-18, May, 1980.
4. A. F. McLean and R. R. Baker, "Brittle Materials Design, High Temperature Gas Turbine, Vol. 2 Ceramic Turbine Rotor Technology," AMMRC TR 78-14, Interim Report No. 12, March, 1978.
5. R. L. Allor, R. K. Govila and T. J. Whalen, "Influence of Machining on Strength Properties of Ceramic Turbine Materials," Presented at the 10th Automotive Materials Conference, University of Michigan, Ann Arbor, Mich., on Nov. 12, 1981.
6. E. H. Kraft and J. A. Coppola, "Thermo-Mechanical Properties of Sintered α -SiC," pp. 1023-1037 in *Ceramics for High Performance Applications II*, edited by J. J. Burke, E. M. Lenoë and R. N. Katz, Brook Hill Publishing Co., Chestnut Hill, Mass., 1977.
7. R. K. Govila, "Uniaxial Tensile and Flexural Stress Rupture Strength of Hot-Pressed Si_3N_4 ," J. Amer. Ceram. Soc., 65 [1] 15-21 (1982).
8. J. Coppola, M. Srinivasan, K. Faber, and R. Smoak, "High Temperature Properties of Sintered Alpha SiC," Presented at the International Symposium on Factors in Densification and Sintering of Oxide and Non-Oxide Ceramics, Hakme, Japan, Oct., 1978.
9. G. Quinn, "Characterization of Turbine Ceramics After Long-Term Environmental Exposure," Tech. Rept. AMMRC TR 80-15, April, 1980.

10. M. Srinivasan, "Elevated Temperature Stress Rupture Response of Sintered Alpha SiC," presented at the 81st Annual Meeting of the American Ceram. Soc., Cincinnati, Ohio, 1979.
11. J. A. Costello and R. E. Tressler, "Oxidation Kinetics of Hot-Pressed and Sintered α -SiC," J. Amer. Ceram. Soc., 64 [6] 327-31 (1981).
12. K. D. McHenry and R. E. Tressler, "High Temperature Dynamic Fatigue of Hot-Pressed SiC and Sintered α -SiC," Amer. Ceram. Soc. Bullet., 59 [4] 459-61 (1980).
13. R. W. Davidge, J. R. McLaren and G. Tappin, "Strength-Probability-Time (SPT) Relationships in Ceramics," J. Mater. sci., 8 [12] 1699 (1973).
14. J. E. Ritter, pp. 667-86 in Fracture Mechanics of Ceramics, Vol. 4, edited by R. C. Bradt, D. P. H. Hasselman, and F. F. Lange, Plenum, New York, 1978.

UNCLASSIFIED

SECURITY CLASSIFICATION OF THIS PAGE (When Data Entered)

REPORT DOCUMENTATION PAGE		READ INSTRUCTIONS BEFORE COMPLETING FORM						
1. REPORT NUMBER	2. GOVT ACCESSION NO.	3. RECIPIENT'S CATALOG NUMBER						
	-	-						
4. TITLE (and Subtitle)		5. TYPE OF REPORT & PERIOD COVERED						
High Temperature Strength Characterization of Sintered Alpha Silicon Carbide		April 1, 1980 - December 31, 1981						
		6. PERFORMING ORG. REPORT NUMBER						
7. AUTHOR(s)		8. CONTRACT OR GRANT NUMBER(s)						
R. K. Govila		DAAG 46-77-C-0028						
9. PERFORMING ORGANIZATION NAME AND ADDRESS		10. PROGRAM ELEMENT, PROJECT, TASK AREA & WORK UNIT NUMBERS						
Ford Motor Company - Scientific Research Lab. Ceramic Materials Department, Room E-3172 P. O. Box 2053, Dearborn, Michigan 48121		D/A Project: AMCMS Code: - Agency Accession:						
11. CONTROLLING OFFICE NAME AND ADDRESS		12. REPORT DATE						
Army Materials and Mechanics Research Center Watertown, Massachusetts 02172		October, 1982						
14. MONITORING AGENCY NAME & ADDRESS (if different from Controlling Office)		13. NUMBER OF PAGES						
-		78						
		15. SECURITY CLASS. (of this report)						
		Unclassified						
		15a. DECLASSIFICATION/DOWNGRADING SCHEDULE						
16. DISTRIBUTION STATEMENT (of this Report)								
Approved for public release; distribution unlimited.								
17. DISTRIBUTION STATEMENT (of the abstract entered in Block 20, if different from Report)								
-								
18. SUPPLEMENTARY NOTES								
-								
19. KEY WORDS (Continue on reverse side if necessary and identify by block number)								
<table> <tr> <td>Silicon Carbide</td> <td>Mechanical Properties</td> </tr> <tr> <td>Creep</td> <td>Fractography</td> </tr> <tr> <td>Ceramic Materials</td> <td>High Temperature</td> </tr> </table>			Silicon Carbide	Mechanical Properties	Creep	Fractography	Ceramic Materials	High Temperature
Silicon Carbide	Mechanical Properties							
Creep	Fractography							
Ceramic Materials	High Temperature							
20. ABSTRACT (Continue on reverse side if necessary and identify by block number)								
-see next page-								

UNCLASSIFIED

SECURITY CLASSIFICATION OF THIS PAGE(When Data Entered)

ABSTRACT

Uniaxial tensile and flexural stress rupture testing of sintered α -SiC (Carborundum 1980 material) was carried out at 1200° to 1400°C in air at various applied stress levels and the corresponding times-to-failure were measured. Fractographic evidence from uniaxial tensile stress rupture testing at 1200°C revealed limited presence of slow crack growth associated with surface connected porosity failure sites. The extent of slow crack growth increased with increasing temperature and large regions of SCG were observed in tests made at 1300°C. These observations were supported by flexural stress rupture testing at 1300° and 1400°C. Slow crack growth is characterized primarily by intergranular crack propagation while fast fracture (brittle failure) occurs transgranularly. The uniaxial tensile stress rupture testing is much more sensitive in revealing the time-dependent crack growth behavior, especially at lower temperatures such as 1200°C in air, than flexural stress rupture testing.

UNCLASSIFIED

SECURITY CLASSIFICATION OF THIS PAGE(When Data Entered)